Titre: Title:	Response of Composite Panels with Conductive Coatings Submitted to Emulated Lightning Strikes
Auteur: Author:	Sri Markandeya Rajesh Ponnada
Date:	2017
Type:	Mémoire ou thèse / Dissertation or Thesis
Référence: Citation:	Ponnada, S. M. R. (2017). Response of Composite Panels with Conductive Coatings Submitted to Emulated Lightning Strikes [Thèse de doctorat, École Polytechnique de Montréal]. PolyPublie. https://publications.polymtl.ca/2751/

URL de PolyPublie: PolyPublie URL:	https://publications.polymtl.ca/2751/
Directeurs de recherche: Advisors:	Daniel Therriault
Programme: Program:	Génie mécanique

UNIVERSITÉ DE MONTRÉAL

RESPONSE OF COMPOSITE PANELS WITH CONDUCTIVE COATINGS SUBMITTED TO EMULATED LIGHTNING STRIKES

SRI MARKANDEYA RAJESH PONNADA
DÉPARTEMENT DE GÉNIE MÉCANIQUE
ÉCOLE POLYTECHNIQUE DE MONTRÉAL

THÈSE PRÉSENTÉE EN VUE DE L'OBTENTION
DU DIPLÔME DE PHILOSOPHIAE DOCTOR
(GÉNIE MÉCANIQUE)
AOÛT 2017

UNIVERSITÉ DE MONTRÉAL

ÉCOLE POLYTECHNIQUE DE MONTRÉAL

Cette thèse intitulée :

RESPONSE OF COMPOSITE PANELS WITH CONDUCTIVE COATINGS SUBMITTED TO EMULATED LIGHTNING STRIKES

présentée par : PONNADA Sri Markandeya Rajesh

en vue de l'obtention du diplôme de : Philosophiae Doctor

a été dûment acceptée par le jury d'examen constitué de :

M. BOUKHILI Rachid, Ph. D., président

M. THERRIAULT Daniel, Ph. D., membre et directeur de recherche

M. SIROIS Frédéric, Ph. D., membre et codirecteur de recherche

M. SHESHYEKANI Keyhan, Ph. D., membre

Mme DUBÉ Martine, Ph. D., membre externe

DEDICATION

To everyone who has made this thesis possible

ACNKOWLEDGEMENT

This journey has only been possible because of the advice of experienced professors & industrial partners, the assistance of knowledgeable colleagues, the workmanship of many skilled personnel, the company of many good colleagues & friends and support of the funding agencies. A big "thank you" to each and everyone.

I thank the CRIAQ COMP-502 team for having initiated such an interesting project and my doctoral advisors Prof. Daniel Therriault and Prof. Frédéric Sirois for giving me the opportunity to be part of this learning experience. Thank you for your advice, encouragement and patience.

This thesis would not have been complete without the selfless technical inputs and assistance of Lucile Moret and Sampada Bodkhe. I also wish to convey my sincere appreciation to David Fecteau, Isabelle Nowlan, Martin Gagne, Maxime Tousignant, Nicholas Veerabadren, Rouhollah Farahani, Samir Khalfaun, and Xavier Cauchy.

I would specially like to compliment the workmanship of the personnel from the building services: carpentry, electrical and plumbing, whose help was critical in building the lightning impulse emulator.

I will cherish the great time I had with friends from both the laboratory of multi-mechanics (LM^2) and laboratory of electrical energy and outside for a long time to come and wish them all the very best in their endeavors.

Sincerely,

Sri Markandeya Rajesh Ponnada

RÉSUMÉ

De nouvelles méthodes de conception et de fabrication pour obtenir des matériaux conducteurs électriquement sont régulièrement développées. L'évaluation de la performance d'un matériau conducteur pour la protection contre la foudre (LCF) repose habituellement sur des essais et des analyses approfondis nécessitant l'accès à une infrastructure imposante. Cela peut entraîner des retards considérables dans le programme de recherche et / ou des dépenses déraisonnablement élevées. Cependant, lors de recherche exploratoire portant sur le développement de matériaux conducteurs pour LCF, il n'est financièrement pas viable ou techniquement productif de passer à travers la gamme complète de tests de foudre standardisés qui produisent des résultats binaires «go no-go». Le temps nécessaire pour de telles études approfondies est également difficile à justifier. Une étape de pré-qualification est donc souhaitable car elle peut servir de mécanisme de rétroaction pour améliorer la préparation/conception de matériaux avancés avant qu'ils ne soient soumis à des tests à grande échelle plus dispendieux et longs. Il est donc nécessaire de développer des équipements abordables et de nouveaux protocoles de test / analyse qui permettent une évaluation préliminaire mais holistique de nouveaux matériaux pour LCF. Cette nécessité est la principale motivation de cette thèse de doctorat.

Le premier objectif de cette thèse porte sur la conception de montages expérimentaux à faible coût en divisant le test de foudre standard en deux parties distinctes. Un nouveau circuit d'émulateur d'impulsions capable de produire une amplitude de crête de 40 kA a été conçu et fabriqué, tandis que des alimentations commerciales pouvant produire jusqu'à 500 A DC ont été utilisées pour tester les matériaux LSP contre des courants continus. Cet arrangement réduit la complexité et maximise la sécurité des circuits respectifs, menant à une meilleure rentabilité. Les émulateurs ont également été conçus avec une grande flexibilité afin d'accommoder des échantillons avec une large gamme de conductivités et pour reproduire diverses formes d'ondes. Les signaux d'onde émulés ici sont conformes aux normes SAE.

Le deuxième objectif porte sur la caractérisation et l'analyse des matériaux conducteurs. Différents matériaux conducteurs, chacun avec leurs propres méthodes de fabrication, ont été étudiés comme revêtements pour LCF de l'avion. Il s'agissait de différents métaux (argent, étain et un mélange cuivre-étain) et des matériaux hybrides (i.e., polymère carbone-argent et composite

à base d'argent). Une série d'essais a été effectuée en utilisant les émulateurs conçus lors du premier objectif. L'analyse des dommages reposait sur des techniques non destructives telles que les tests par ultrasons et la thermographie. La performance d'un panneau en composite non protégé renforcé par des fibres de carbone (substrat) et un autre substrat protégé à l'aide d'un grillage expansé en cuivre ont servi de référence à des fins de comparaison. On a observé que les matériaux composites avec des revêtements hybrides présentaient plus de dégâts que ceux avec revêtements métalliques. Il est intéressant de noter que le dommage dans la catégorie des revêtements hybrides était plus sévère que pour le cas de panneau composite non protégé. La méthodologie proposée dans cette thèse a permis une étude systématique des matériaux conducteurs pour LCF. Ces résultats aideront à améliorer la conception du matériau et finalement identifier les technologies les plus prometteuses pour les tests standards de protection contre la foudre.

Cette évaluation peut également servir d'inspiration comme tests et analyses pour d'autres applications. À titre d'exemple, les matériaux considérés pour la protection contre la foudre des appareils aériens pourraient aussi répondre aux exigences demandées par d'autres applications conductrices en aéronautiques comme les antennes, les capteurs de blindage électromagnétique, etc. La protection contre la foudre est reconnue comme l'un des paramètres les plus sévères pour la performance électrique. Aussi, il y a un grand intérêt par l'industrie aérospatiale pour des matériaux performants et légers. Afin de fabriquer quelques prototypes pour des applications telles que celles mentionnées ci-dessus, un procédé basé sur la combinaison des techniques de l'écriture directe, du masquage hydrophobe et du placage d'argent sans courant a été développé. Cette méthode consiste à limiter le placage d'argent à une zone préalablement délimitée avec l'impression d'un polymère sacrificiel et avec l'utilisation d'un revêtement hydrophobe. Des configurations conductrices avec une résolution de l'ordre de quelques centaines de microns ont être réalisées avec cette méthode. Les revêtements conducteurs ont été appliqués sur différentes surfaces selon les applications choisies.

En résumé, le montage expérimental et la méthodologie de recherche ont été développés pour mener des expériences contrôlées pour l'évaluation de la protection contre la foudre offerte par différents revêtements conducteurs appliqués sur des structures en composites. Ce travail contribue aux efforts de la communauté scientifique portant sur le développement de matériaux

avancés pour LCF. Ces découvertes mèneront à un transport aérien plus sécuritaire et plus écologique. La faisabilité d'étendre l'utilisation de revêtements conducteurs à d'autres applications aérospatiales au-delà de LCF a également été démontrée.

ABSTRACT

New design and manufacturing schemes to produce electrically conductive materials are regularly devised. The evolution of an electrically conductive material into a solution for lightning strike protection (LSP) relies on extensive testing and analysis requiring access to heavy infrastructure. This can lead to substantial delays in the research program and/or unreasonably high expenses. However, when exploring such conducting materials for LSP, neither is it financially viable nor technically productive to put them through the full battery of sophisticated lightning tests utilizing standard protocols that yield binary "go - no go" results. The time spent on such extensive studies is also difficult to justify. A pre-qualification program is thus desired. Such a program, if designed appropriately, can also serve as a feedback mechanism to improve on the materials' technology readiness before they are subjected to full-scale tests. There is a need to develop low-cost equipment and associated test/analysis protocols that allow for a preliminary but holistic evaluation of new materials for LSP, which serves as the motivation for this PhD thesis.

The first objective of this thesis relating to the establishment of low-cost test equipment was achieved by dividing the standard lightning test into two separate parts of reduced severity. A new impulse emulator circuit capable of producing a 40 kA peak amplitude was designed and transformed into a physical structure, while commercial power supplies that could produce up to 500 A DC were used to test the LSP materials against continuous currents. This arrangement lowers complexity and safety demands on the respective circuits, hence leading to cost-effectiveness. The emulators were also designed with a flexibility to both accommodate samples with a wide range of conductivities, and reproduce current waveforms with chosen test parameters, leading to wider application. The emulated lightning waveforms were shown to conform to SAE standards.

The second objective concerns testing and analysis of conductive materials. Different conducting materials, each with their own manufacturing methods, were investigated as coatings for aircraft LSP. These included different metals (silver, tin and copper-tin) and hybrid materials (silver-carbon and silver-conducting polymer). A series of tests were conducted utilizing the designed emulators. Damage analysis relied on non-destructive techniques such as ultrasonic testing and

thermography. The performance of unprotected carbon fiber-reinforced polymer (substrate) and an expanded copper mesh-protected substrate formed the basis for comparison and evaluation. It was observed that the composites with hybrid coatings witnessed more damage compared to those with metallic coatings. Interestingly, the damage in the former category was even severe than that in unprotected CFRP. The proposed methodology allows for a systematic study of the conductive materials to aid in improving material design and ultimately identifying the most promising technologies for advanced lightning tests.

A “holistic” evaluation must also share a utilitarian view of research, i.e. the extension of the materials, tests, and analysis for other applications must also be inquired into. As an example, materials considered for aircraft lightning protection could meet the requirements of various other conducting aerospace applications like antennae, EMI shielding, sensors and so on. This is because lightning presents one of the harshest parameters for electrical duress while low density materials are a key demand of the aerospace industry. In order to realize designs of varied sizes and shapes with a useful degree of automation for applications such as those mentioned above, a method based on the fusion of direct-write techniques, hydrophobic masking and electroless plating of silver was developed. This method works by restricting the electroless wet chemistry (deposition) to an area that is previously printed with a sacrificial polymer and the surroundings masked with a hydrophobic coating. A resolution on the order of hundreds of microns can be realized with this method. Selective area coatings with different fabrication schemes and designs were demonstrated to illustrate the scope of application.

In summary, equipment and methodology was developed to conduct controlled experiments for the assessment of lightning strike protection offered by different conductive coatings to polymer composites. This work is believed to support the scientific community in its research on LSP materials for polymer aircraft, ultimately enabling greener and safer air travel. The feasibility to extend the utility of conductive coatings to other aerospace applications beyond LSP was also demonstrated, adding to the value of research .

TABLE OF CONTENTS

LIST OF TABLES

LIST OF FIGURES

LIST OF SYMBOLS AND ABBREVIATIONS

a	Radius of the wire
A	Area
ARP	Aerospace Recommended Practice
C	Capacitance
CFRP	Carbon Fiber-Reinforced Polymer
CNC	Computer Numerical Control
CRIAQ	Consortium for Research and Innovation in Aerospace in Quebec
δ	Skin depth
Δ	Electrical quantity defined as: $\sqrt{R^2 - 4(L/C}$
DMA	Dynamic Mechanical Analysis
e	Mathematical constant:2.71
EDS	Energy Dispersive X-ray Spectroscopy
EMI	Electro-Magnetic Interference
EUT	Equipment Under Test
FAA	Federal Aviation Administration
FEM	Finite Element Method
FRP	Fiber-Reinforced Polymer
GFRP	Glass Fiber-Reinforced Polymer
ICP-MS	Inductively Coupled Plasma - Mass Spectroscopy
IGBT	Insulated Gate Bipolar Transistor
i, I	Current
i_0	Initial current
i_{peak}	Peak current

IR	Infra-Red
ITO	Indium Tin Oxide
k	Probe correction factor
l	Length
L	Inductance
L_G	Variable inductance
L_V	Variable inductance
LSP	Lightning Strike Protection
μ_0	Magnetic permeability of air
NASA	National Aeronautics and Space Administration
NDE/T	Non-Destructive Evaluation/Testing
NSERC	Natural Sciences and Engineering Research Council of Canada
π	Mathematical constant:3.14
PEDOT:PSS	Poly(3,4-ethylenedidxythiophene) polystyrene sulfonate
PLA	Polylactide
q	Charge
Q	Heat
ρ	Resistivity
r	Radius of the *RL* loop
R	(Bulk) Resistance
R_D	Damping Resistance
R_S	Sheet Resistance, Sample Resistance
RLC	Resistance-Inductance-Capacitance
RL	Resistance-Inductance

σ	Standard deviation
SAE	Society of Automotive Engineers
SEM	Scanning Electron Microscopy
SHM	Structural Health Monitoring
SWNT	Single-Walled Nanotube
τ_{RL}	Time constant of *RL* circuit
t	Thickness, Time
t_1/t_2	Impulse form
t_d	Pulse duration
t_t	Total duration
TGA	Thermo-Gravimetric Analysis
USAF	United States AirForce
V	Voltage
V_0	Initial voltage
V_{C0}	Initial voltage in the capacitors
w	Width
W	Power
WiFi	Wireless Fidelity
XRD	X-Ray Diffraction

CHAPTER 1 INTRODUCTION

On an average, aircrafts are struck by lightning once an year [1, 2]; a dramatic discharge of electrical charges can have serious consequences to the structure, electronics, and also cause fuel-related accidents [1]. Fortunately, such mishaps have been rare owing to the excellent conductivity of the all-metal (usually aluminum alloys) bodies which form a Faraday cage and restrict the electrical currents to the exterior of the aircraft. Today's polymer composite aircraft predominantly utilize metallic meshes and foils to compensate for their inferior electrical conductivity. Integration challenges (i.e. both during fabrication and repair), possibility of galvanic corrosion at carbon fiber-mesh interface [3] and increased weight (metal plus the accompanying resin/isolation layers for corrosion mitigation) are all issues associated with the above-mentioned lightning strike protection (LSP) materials. For these reasons, the aerospace industry is looking towards alternative materials and methodologies to achieve light-weight, externally applied conductive aircraft surfaces, a promising avenue being conductive films and coatings.

To realize a similar goal, industries and research groups from universities in and around the province of Quebec, Canada, collaborated through the COMP-502 project 'Conductive surface films or coatings for composite structures' to explore different electrically conductive materials for application as light-weight LSP technologies. This project was coordinated by the Consortium for Research and Innovation in Aerospace in Quebec (CRIAQ) and the Natural Sciences and Engineering Research Council of Canada (NSERC), and comprised of Bombardier Inc. (Aerospace), Bell Helicopter Textron Canada Ltd. and 3M Canada Company as industry partners and Polytechnique Montreal, McGill University and the Université du Québec à Montréal as partners for academic research. The project was structured to contain:

- Three MATerial design and fabrication groups,
- A mechanical INTegrity and environmental testing group, and
- An ELEctrical design and fabrication group.

This thesis appertains to the ELE group where the candidate's research goal was to identify the most promising surface materials for their ability to effectively protect composite materials

against lightning strikes. This being the initial phase of the project, many different ideas for surface materials have been explored in parallel by the MAT groups. Lightning interaction with materials is a multi-physics phenomenon and thus electrical conductivity alone is insufficient to provide a complete picture pertaining to damage resistance. Simulation-based techniques cannot provide accurate results, especially when the material systems themselves are not well defined. Therefore, emulated lightning tests are continuously needed to evaluate and support the process of materials development. However, there are not adequate testing facilities, which, even otherwise is a very expensive. In this initial phase, testing with a moderately strong strike able to emulate the main characteristics of a lightning waveform is warranted and will suffice for comparison and development purposes within a practical time envelope. Test protocols involving characterization of lightning damage to coatings/substrate materials along one or several axes: visual, structural, thermal and so on, are required. This information will help tailor remedial measures to improve materials design and manufacturing (as/if required).

Thus, the candidate's broad responsibilities consisted of:

- Establishing low-cost test facilities to emulate lightning current waveforms in the laboratory, and
- Testing and evaluating (damage analysis via non-destructive methods) the conductive coatings.

In addition to the above accomplishments, the candidate also pursued:

- Extension of the application of the conducting coatings in the aerospace sector, beyond LSP.

The work carried out to realize the above goals is presented in this thesis, which is divided into 8 chapters commencing with this introduction. Chapter 2 comprises of a review of pertinent literature. Chapter 3 defines the research objectives and the methodology employed to realize the same. It also briefly discusses the presented research articles and their coherence with the objectives. The key findings of this thesis were submitted to suitable peer-reviewed journals as three research articles. These are presented as Chapters 4, 5 and 6, and respectively report the lightning test equipment developed, lightning test results, and extended applications developed based on the principal research work. A general discussion summarizing the results of this research work is included in Chapter 7. Concluding remarks and recommendations are made in Chapter 8.

CHAPTER 2 LITERATURE REVIEW

Until recently, aircrafts were manufactured out of lightweight aluminum alloys. Now, the civil-aviation industry has been imbibing composite technologies for additional weight reduction and improved mechanical properties. A composite material "is a macroscopic combination of two or more distinct materials, having a recognizable interface between them" [4]. This entails that the constituents must be chemically distinct and physically separable in such materials. Composites can be designed so that one of the constituent materials forms a continuous phase and contains the other materials, then the continuous phase is called a matrix and discontinuous phase the reinforcement. The resulting engineering properties of the composite are intermediate between the absolute properties of the component materials and depend on the design of the combination. A well-known example of composites are fiber-reinforced polymers (FRP) employed in the aerospace industry. The fibers could be glass, carbon or aramid and so on and employed as reinforcements while polymers such as epoxy or polyurethane the binding matrix [5]. The adoption of composite technology, especially carbon-fiber reinforced polymer (CFRP) and glass-fiber reinforced polymer (GFRP), can be clearly witnessed in a number of structural components for the Boeing 787 aircraft [6]. Up to 50% of the 787's structure is made up of composites.

On an average, every aircraft is struck by lightning once a year [1, 2]. Several accidents instill that safety in terms of lightning strikes cannot be compromised [1]. Aluminum and its alloys are excellent electrical conductors and form a Faraday cage protecting the structure and critical electronics from lightning effects for a safe journey. The electrical conductivity of polymer composites is far inferior to that of metals. For example, carbon fibers have a 1000 times higher electrical resistivity compared to metals [5] and epoxy is further resistant by many orders of magnitude. This means that in the event of a lightning strike, the enormous energy of the lightning arc cannot be dissipated or rerouted to a lower potential zone without serious damage to the structural material. From around 5% in 70s, the utilization of composites has today risen to over 50%. The percentage utilization of composites has witnessed a steep hike in the last decade. Thus, lightning protection is garnering special attention in the aerospace community.

Today, long-distance services are improving, however in parallel, with increased passenger numbers and new airports, a lot of airlines operate their fleet so that there are multiple stops on a given route. Frequent landings and take-offs imply that aircraft today spend more time at altitudes

with high probability of strike [1]. With the above reasoning coupled with the fact that it is the aircraft that trigger lightning 90% of the times [1, 7], one can expect the strike statistics to change. Secondly, the number of natural lightning strikes is also increasing due to global warming. A 12% increase in lightning events is expected for every 1 °C rise in temperature [8]. Lastly, today's aircraft rely heavily on various technologies such as fly-by-wire, electronically controlled fuel systems, computer-based navigation, advanced digital avionics and so on. This reliance on electrical automation and technology increases the risk with indirect effects of lightning [9].

2.1 Lightning strikes to aircraft

2.1.1 Aircraft in lightning environment

Lightning is a sudden, high intensity electrical discharge that occurs as atmospheric charges try and neutralize. Lightning occurs approximately 8 million times per day [10]. The most common source of lightning are the Cumulonimbus clouds. The works of Benjamin Franklin [11], C T R Wilson [12] and many others have contributed in unraveling the nature of this phenomenon. But even today, the exact mechanism behind cloud electrification is unclear. References [13, 14] discuss the key theories for charge generation - collisions between ice crystals and graupels (snow pellets or "soft hail"), ion capture by falling "hydrometeors" in an electric field, etc. It has been found that clouds can have multiple discrete charge centers whose positions are above an altitude required for attaining freezing temperatures. Generally, clouds may exist from an altitude of 1 km from the earth surface, but the center of the negative charges found in the lower regions of the cloud will exist at around 3 km or above [15]. The three main kinds of lightning flashes [16] associated with clouds are cloud to earth lightning, inter-cloud lightning and intra-cloud lightning. Others include the cloud to sky sprites and ball lightning [17].

An aircraft can be a part of any of the three above-stated kinds of lightning, and in such a case the event is called "aircraft-intercepted lightning". However, this is only a rarity and as often as 90% of the times, it is the aircraft that initiates the lightning [1, 7]. Based on aircraft design, points of extremities such as the nose or wing tips enhance the ambient electric fields around them [2]. This field intensification may lead to the formation of bidirectional leaders (see Figure 2.1(b), frame 2) thereby triggering a lightning [18]. Statistics compiled in the US Department of Transport sponsored 'General Aviation Lightning Strike Report and Protection Level Study' [19]

reveal that most of the lightning strikes occur during rain, however lightning in the absence of rain was also reported. With regard to aircraft position in the cloud environment, statistics state that the aircraft is prone to a maximum risk of lightning strike within the clouds. It has also been observed that it is during climb or descent that the frequency of strike is higher [1]. Usually, the air temperature between -5 to 0 °C and the altitude 9144 feet above mean sea level have been statistically prominent for lightning strikes to modern commercial jets [20].

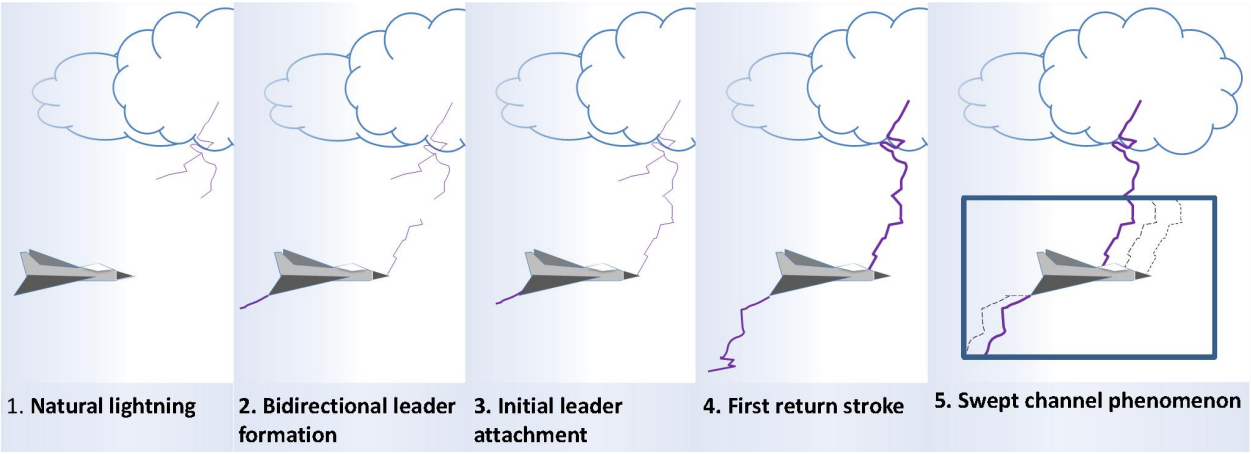

Figure 2.1: A time-lapse schematic explaining the mechanism of aircraft intercepted lightning: 1. A natural lightning occurs in the vicinity of an aircraft, 2. bi-directional leaders are generated from the extremities of the aircraft in response to the aggravated electric field, 3. initial leader attachment occurs, thereby establishing a conductive path, 4. the charge stored in the clouds is transferred through the conductive channel as what we see as a bright flash, and 5. as multiple charge centers in a cloud or near-by clouds are discharged, subsequent strokes occur. As the aircraft is moving, these strokes result in swept channel which show up as a series of hits over the surface of the aircraft

2.1.2 Lightning interaction with materials

The physical effects of lightning due to current injection are called direct effects while exposure to electromagnetic fields results in indirect effects. These effects are listed in Table 2.1.

According to Kind and Feser [21], lightning strokes are “single, unidirectional impulse currents of short duration,” they “reach a peak value i_{peak} rapidly without oscillation and then decrease to zero”. The main characteristics of the waveform may be explained via the following terms.

Table 2.1: Direct [22] and indirect [23] lightning effects

Direct effects	*Indirect effects*
Shockwave ▪ over-pressures leading to matrix cracking and fiber damage	Electromagnetic coupling ▪ transient current and voltage inducement
Arcing and sparking ▪ fuel ignition & other fires ▪ welding and roughening of movable parts	Structural IR voltages
Resistive heating ▪ melting and welding ▪ resin evaporation & charring leading to burnouts, ply delamination	Bound charge ▪ secondary arcing
Dielectric breakdowns ▪ puncturing, splintering	Electrostatic pulses
Magnetic force effects ▪ deformations	
Electrical shocks	

(i) Peak current, i_{peak}: The maximum value of current that is generated in a given stroke. The enormous currents (i) of lightning will also produce large voltages (V) unless their paths provide for low resistance (R). According to Ohm's law:

$$V = iR. \tag{2.1}$$

These large voltages can then result in "flashes" between their paths and other objects, and must be considered with the same caution as the actual lightning strike.

(ii) (Maximum) rate of change of current, di/dt: The peak voltage produced in objects with inductive impedance (L) is different from that of those having resistive impedance. The governing law is then a combination of Oersted's law, Faraday's law of induction and the Lenz's law. This case will see the voltage, V as:

$$V = L\left(\frac{di}{dt}\right). \tag{2.2}$$

The steepness of the curve is critical to the generation of an accurate test waveform.

(iii) Total charge, $\int i\mathrm{d}t$: The amount of charge that each of the lightning components can transfer during a strike; particularly the C-component can amount to 200 C [24]. Power input, W, can be calculated as:

$$W = Vi = \frac{Vq}{t}, \tag{2.3}$$

where q is the charge. This power input which determines the extent of heating and associated phenomena is proportional to the total charge transfer at the first approximation [13].

(iv) Action integral, $\int i^2\mathrm{d}t$: This integral of current squared over time, with units A^2s or J/Ω, is connected to resistive or joule heating, which is the phenomenon of generation of heat in a (resistive) material when electric current passes through it. The amount of heat generated, Q:

$$Q = i^2 R. \tag{2.4}$$

In addition to the above, impulse form, t_1/t_2, time period, t_d, and total duration, t_t, are also used to define waveforms.

It is seen that electrical resistance (measure of opposition to flow of electric current) is a dominant electrical property governing the lightning interaction with materials. While electrical resistance depends on the shape and size of the material under consideration, it is the electrical resistivity (ρ) which is inherent to materials, and for simple geometries is measured indirectly from the resistance of the specimen as:

$$\rho = R \times \frac{A}{l} = \left(\frac{V}{i}\right) \times \frac{A}{l}, \tag{2.5}$$

where, R is the bulk resistance of the specimen, A is the area of cross section of the specimen, and l is the length. The resistance itself is deduced from current (i) and voltage (V) measurements across the specimen.

The value of resistance for a bulk material can be obtained either from two-probe or the four-probe method. In the two probe method, the same electrodes are used to both inject a known value of current and measure the developed voltage, while separate sets of electrodes are used for these purposes in the four-probe method. The advantage of the four-probe approach is that the contact resistance is discarded from the measurements. When greater precision is required,

resistivity is measured using collinear, equally-spaced, 4-point probe system and consequently calculated as:

$$\rho = R_S \times t = \left(\frac{\pi}{\ln(2)} \times \frac{V}{I} \times k \right) \times t, \tag{2.6}$$

where, R_S is the sheet resistance of the sample, which is equivalent to the bulk resistance of a square sample, i.e., sample length is equal to its width. t and k are respectively the sample thickness and a correction factor that takes multiple parameters such as probe geometry and spacing, and sample thickness into consideration.

Resistivity also varies as a function of temperature. For metals, resistivity increases with temperature; this increase is taken as a linear function when away from the melting point.

Direct currents flow through the bulk of the material, however with increasing frequency, alternating current density shifts towards the surface of the conductor. Skin-depth, δ, of a material is defined as the distance from the surface where the value of current density falls to 1/e of that at the surface. In addition to frequency, skin-depth is influenced by permittivity and magnetic permeability of the material.

On the other hand, non-conducting materials such as GFRP are unable to transfer electric current and undergo dielectric breakdown. Dielectric strength is the minimum voltage at which dielectric breakdown occurs in the material [25]. For materials that may be exposed to lightning or other high voltage transients, a voltage impulse (1.2 μs/50 μs) may be used to test specimens. The impulse dielectric breakdown voltage is "the peak voltage that the wave causing breakdown would have reached had breakdown not occurred" [26].

2.1.3 Conductive materials for aircraft lightning protection

In order to build a Faraday cage for today's composite aircraft, manufacturers employ either one or a combination of the following material technologies:

Metallic meshes and foils: Almost all meshes/foils available today take the form of stretched / expanded products. This allows them to achieve a higher degree of protection in one direction which during layup is matched with the direction of airflow during flight. The order of thickness is many tens of microns for both classes of materials; although unlike meshes, foils require no

weaving and thus have lower projected thickness. More importantly, the absence of weaving stresses permits the use of very high purity materials (no alloying for strength) which translates into higher conductivity. Materials include: copper, bronze, nickel and phosphoric acid anodized aluminum. Wires made of these materials can also be woven into the standard fiber mat to make inter-woven wire fabrics for use in less-critical zones [27, 28]. Furthermore, prepregs incorporating metallic meshes are also available. The conductivity of the matrix of such prepregs has also witnessed an improvement due to the modification with certain additives.

Metalized fibers and fabrics: This list of products consists of carbon, graphite, glass, polyester and other synthetic fibers coated with any one of nickel, copper, silver, gold, palladium, platinum or ITO (indium tin oxide) [29]. Further, hybrids in the form of multi-layered coating are also possible. Product range includes – chopped fibers, veils, and mats or even in the form of prepregs. The advantages of this class of materials are in easier handling and time-saving during fabrication.

Surfacing films and tapes: Surfacing films/tapes incorporate metallic screens and foils. The advantage is the ease in handling, layup and improved quality of surface both before and after painting. The latest of classes is the 'sprayable' LSP materials, made by loading one-part epoxies with conductive particles. When nanoparticles are used standalone, without a binder, their coatings can also lead to better dispersion and coverage on the (ply) surface, and limitations with respect to matrix viscosity, reinforcement content and their distribution will no longer hold relevance [30]. Many new materials are under investigation: advanced materials such as carbon nanotubes [31, 32] and graphene [3] with their exceptionally high theoretical conductivity on one hand and equally competitive hybrids, for example, silver [33] and nickel-coated [30] carbon nanotubes, nickel and copper coated chopped carbon fiber [34] and so on are being investigated for potential application in LSP materials.

Lightning diverter strips: Diverter strips may be continuous metallic strips or segmented [35] whose one end is grounded. Segmented strips take the form of a series of continuously-placed metallic buttons, bonded or riveted to a long plastic strip . The buttons could be round or take an elongated shape, but are separated by a short distance (hundreds of microns) so that they don't form a electrical path under normal conditions. However when a strong-enough electric field is applied, the gaps between the buttons break down and help guide the lightning currents between

the point of strike and a conducting zone. Diverter strips are applied in regions of aircraft such as radome that cannot be covered in continuous conducting materials.

2.2 Laboratory emulation of lightning

The characteristics of lightning and the nature of its interaction with aircraft have largely been derived via areal experiments (i.e., in the sky) [36]. The NASA storms hazard program (1980-86,) the USAF-FAA lighting characterization program (1984-85, '87) and the French Transall program (1984, '88) were the major research efforts where natural lightning was intercepted with special aircraft fitted with sensors and other processors. Today our understanding of aircraft-lightning interaction is developed enough that "in-service flight testing" like that applied to the first instances of composite application in the aerospace industry [37] are not required. Various ground-based testing methods have been devised that can ensure accessible, less expensive (compared to areal experiments), repeatable and safe emulation of lightning on custom samples.

2.2.1 Test standards and procedures

Aircraft need to meet stringent requirements in terms of quality and performance of their systems. On the lightning front, these requirements are set forth to mitigate both direct and indirect effects. Table 2.2 lists the recommended practices for testing to meet different government regulations.

Table 2.2: Recommended practices for aircraft lightning protection from SAE

Pub.	*Title*	*Content*	*Ref.*
ARP5412	Aircraft lightning environment and relative test waveforms	Characteristics of lightning encountered by aircraft and resultant transients at electrical/electronic system interfaces	[38]
ARP5414	Aircraft lightning zoning	Definitions and guidelines for location of lightning strike zones on aircraft	[39]
ARP5416	Aircraft lightning test methods	Techniques for testing of aircraft and their systems for simulated direct and indirect lightning effects	[40]

LSP (direct effects) testing of aircraft can be categorized into two kinds. The first concerns the identification of lightning attachment points and thus establishing the zoning for the aircraft. This is achieved via high-voltage attachment testing on small aircraft or scaled down models of large aircraft/sections [40]. High voltage facilities are also used for the swept channel attachment tests.

The second category is the high current testing to study physical damage, and verify the ability of the material/component to withstand the large lightning currents. It is indeed important to consider zoning for this case because, the different current components or their combinations need to be utilized for testing different zones. Structural and component-level tests also utilize high-current facilities.

Different material types and or compositions may be employed based on threat level. Figure 2.2 and Table 2.3, from ARP 5412, describe the standard waveform of lightning. For lightning tests on materials, the current components are, as a standard, emulated sequentially in a single run. It can be observed that the A/D (peak) and C (rectangular) component are the two most distinct regions of the typical current component and thus are often used to study LSP materials for preliminary investigations [41-43].

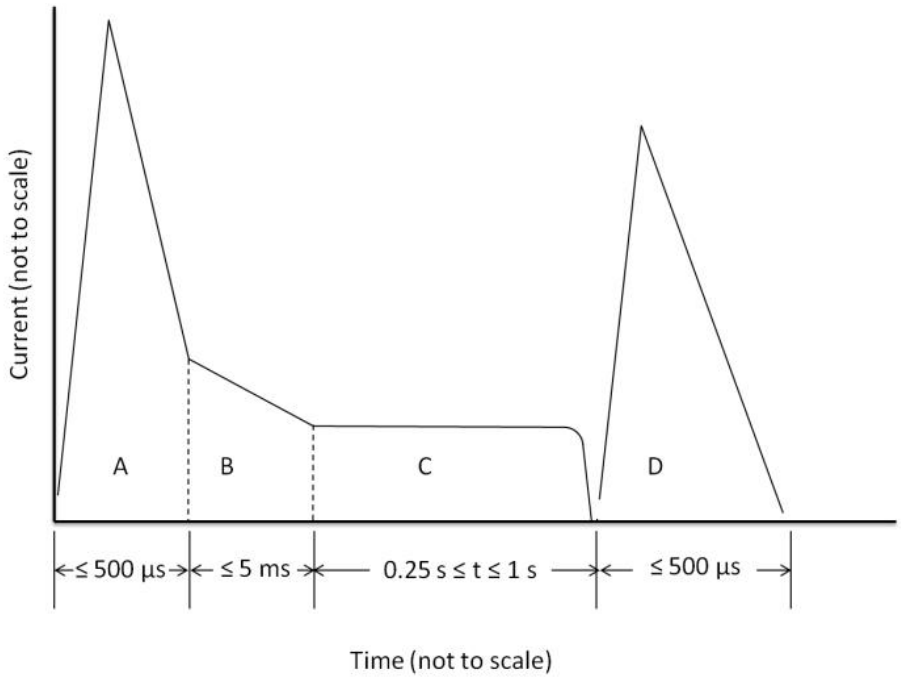

Figure 2.2: Typical current components of the standardized lightning waveform [38]

Table 2.3: Details of lightning current components, A through D [38]

Comp.	*Mathematical definition, t is time (s)*	*Charge transfer (C) or action integral (A^2s)*	*Duration*
A	$I(t)=I_0(e^{-\alpha t} - e^{-\beta t})$; $I_0 = 218810$ A,	2×10^6 $A^2s \pm 20\%$	≤ 500 µs

Table 2.3 (continued) : Details of lightning current components, A through D [38]

	$\alpha = 11354\ s^{-1}, \beta = 647265\ s^{-1}$	(in 500 µs)	
B	$I(t)=I_0(e^{-\alpha t} - e^{-\beta t})$; $I_0 = 11300$ A, $\alpha = 700\ s^{-1}, \beta = 2000\ s^{-1}$	10 C ± 10%	≤ 5 ms
C	Squared waveform	200 C ± 20%	0.25 – 1 s
D	$I(t)=I_0(e^{-\alpha t} - e^{-\beta t})$; $I_0 = 109405$ A, $\alpha = 22708\ s^{-1}, \beta = 1294530\ s^{-1}$	0.25×10^6 A^2s ± 20% (in 500 µs)	≤ 500 µs

2.2.2 Design of lightning current emulators

The resistance (R), inductance (L) and capacitance (C) - *RLC* circuits are the established circuits for impulse generators [22]. A typical *RLC* circuit shown in Figure 2.3(a) could produce different types of waveforms as shown in Figure 2.3(b).

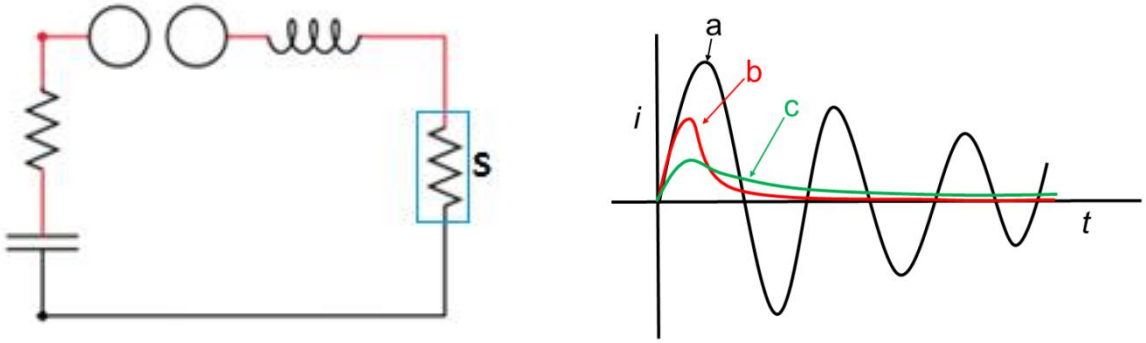

(a) **(b)**

Figure 2.3: (a) Typical RLC circuit [44], and (b) Generated waveforms [45]: (a) under-critically damped, (b) critically-damped, and (c) over-critically damped

The conditions for producing each of these types of waveforms can be defined as follows [45]:

a. Under-damped (oscillatory): $0 < R < 2\sqrt{L/C}$,

b. Critically-damped (unipolar): $R = 2\sqrt{L/C}$, and

c. Over-damped (unipolar): $R > 2\sqrt{L/C}$.

The unipolar waveform produced in an under-damped circuit however comes with disadvantage of low peak currents. Crow bar circuits such as the one shown in Figure 2.4(a) are utilized to overcome this disadvantage [44, 45]. During the operation of this circuit, the crow bar switch is engaged at the moment when the peak current is reached (voltage across crow bar is zero) to

short out the capacitors. As the energy from the capacitors at that moment would be stored in the (sample and crowbar) inductance, the decay times are increased and a unipolar pulse is produced.

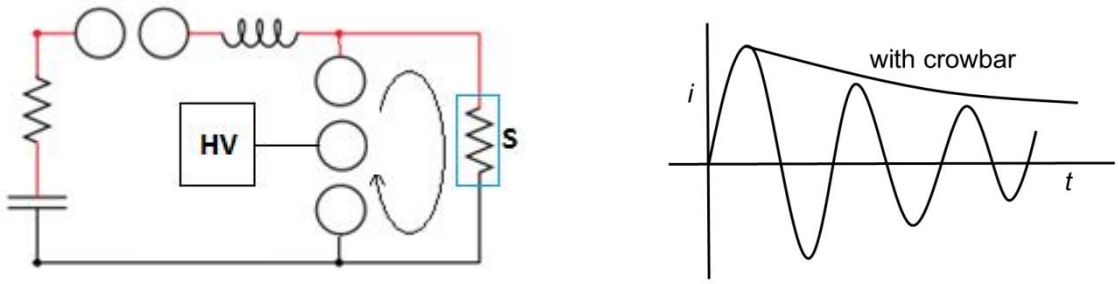

(a) **(b)**

Figure 2.4: (a) A crow bar circuit [44], and (b) Typical generated waveform [45]

Energy for the lightning emulators can come either from capacitive or inductive storage systems, transmission line based storage devices, mechanical machines and accumulator batteries are other available sources. Large capacitor banks are the energy source in many emulator designs whether for full-scale testing [46] of the aircraft or laboratory tests on smaller components and test samples. While capacitors are known for their suitability for low-power charging, power amplification and long-term storage, inductive storage facilities have also been utilized in certain studies [47]. They can attain larger energy densities compared to capacitors. The switch usually takes the form of one of the following: (i) spark gap (air-gap) consisting of two conductive spheres/rods etc. (ii) a laser-induced trigger, or (iii) high-power diodes or even thyristors. A spark gap or diodes/thyristors, for instance connected to a capacitor bank can also have a say on the latter's maximum voltage. The requirement for multiple pulses in a single test can be achieved by using multiple sources triggered by individual spark gaps [48] or a rail gap switch. Next, although the choice of sample depends on the experiment, as the resistance/load in the electrical circuit, it has a strong influence on the test waveform and pre-calibration of input circuit parameters may be required each time the sample type changes. Concerning the physical form of the generators, it is crucial to maintain a symmetric, coaxial configuration in order to maintain the high currents. As the current and voltage levels of test facilities increase, superior quality of materials and design, rating of individual components and insulating materials between such

coaxial lines and components would be required [42, 48]. Some emulators are illustrated in Figure 2.5

The lightning C-component is produced using a direct current (DC) source such as batteries [49]. The source can be operated individually or connected to the impulse emulator. Discharging techniques can be based on switches or insulated gate bipolar transistor (IGBT); this must be carefully executed from a hardware point of view so that these two emulators do not damage each other. Charging the DC source with the impulse emulator has been shown while using an IGBT [49].

Electrical parameters are measured/monitored via measuring resistors, Rogowski coils (induction effects), Hall generators, magneto-optic methods based on Faraday effect, photo-luminescent diodes and so on. Of these, the measuring resistors and Rogowski coils are popular in this field. Additional apparatus such as those to measure heating [50], luminescence/radiation during heating/explosions [47], mechanical impulse [51] to the samples may also be employed.

2.3 Characterization of lightning damage in the laboratory

Broadly, physical testing and modeling/simulation are the two approaches to study and understand lightning-induced direct damage in aircraft. Most commonly, physical testing involves emulating a lightning strike on composite panels with/without LSP materials. The extent of damage is then inversely proportional to the protection offered by the LSP material. In general, physical testing requires large investments of qualified personnel, money and time. This encourages many industries/agencies to adopt computer-aided modeling and simulation at various levels of product development. However, the complexity of understanding lightning material interactions limits the application of these techniques for direct effects evaluation and is not discussed further.

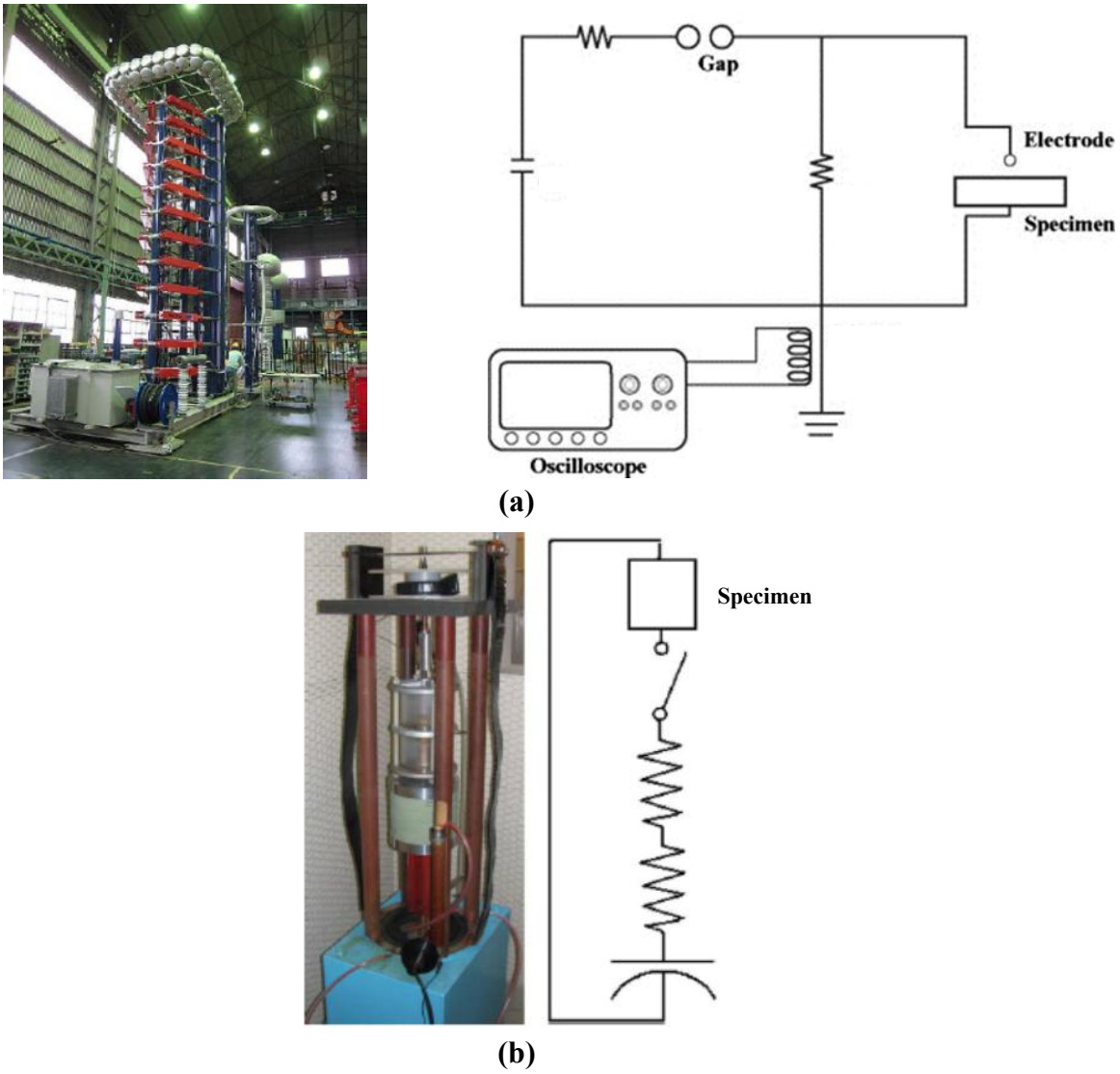

Figure 2.5: Photographs and circuit diagrams of (a) Lightning impulse generator, Haefely Test AG. [52, 53], and (b) Lightning strike generator, University of Washington [52, 53] (Only non-standard components are identified for clarity)

At present, a hybrid of both approaches is more optimal in terms of utility and viability e.g., incorporating information from lightning tests into finite element method (FEM) models to verify mechanical integrity [54], acoustic shockwave parameters validations via instrumented impact tests [51] and so on.

2.3.1 Lightning damage to composite materials

Lightning interaction with materials manifests in a combination of electrical, mechanical and thermal effects among others. This interaction is complex, and three major modes of damage are usually observed in composite materials (see Figure 2.6).

Resin deterioration: When large amount of energy is injected into the composite system, the bonds of the polymers undergo homolytic cleavage (which essentially is composed of single-electron reactions) [55]. Depending on the materials and their chemical surroundings two events can occur: (i) these decomposed products quickly react with other chemical species forming char, or (ii) vaporization preceded by quick loss in polymerization. Other aspects to be considered in this case are that of heat which is produced in the process of dielectric breakdown of air and Joule heating (of fibers and conducting matrices). Such a thermal decomposition of the polymer (resin) material has deleterious effects. Primarily, the resin is burned off and often the heat can damage the fibers also. In worst of cases, this can lead to a burn through. Another issue that worries engineers and safety experts is the noxious fumes that can emanate during such events [56, 57] .

Fiber damage: Three major reasons can be cited to explain fiber damage: (i) shockwaves due to supersonic expansion of air around the lightning arc, (ii) Joule heating of the carbon fibers as they conduct the large lightning currents, (iii) the pressure exerted by hot pyrolysis gases which are entrapped between lamellae.

Delamination: Resin degradation results in the emanation of hot gases. The high pressure can lead two events. One of them, as mentioned above, is the fracture of fibers. In the other case, the hot gases push through the ply lamellae and augment delamination. The area of delamination is thus usually larger than the area of resin deterioration. It has been shown that the pattern generated by the delaminations in the composites resembles the shape of “pairs of fans” propagating along the fiber direction in each of the lamellae [52].

2.3.2 Visual, non-destructive, mechanical and spectroscopic analysis of damage

Once a lightning strike has been emulated on the material under evaluation, the next step is to characterize the damage. Multi-technique characterization is often required for a complete understanding of the damage. Caution must be exercised to understand direct effects in view of factors such as the texture, surface features and even the finishing of the surface. Rough textures

may influence the attachment of lightning channel via dispersing its root at the material surface [58]. Similarly, even perforated structures may witness a distributed arc spread over an area, as it attaches to the ends of the fibers generated in the holes [59]. Painting the test component better mimics the real scenario [60].

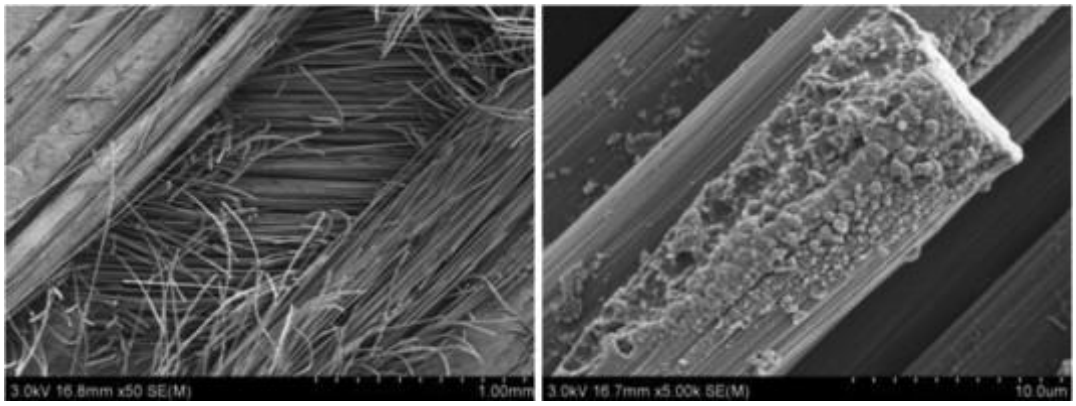

(a) (b)

Figure 2.6: Scanning electron microscopy (SEM) images showing two key modes of lightning damage in CFRP: (a) fiber fracture and (b) resin pyrolysis [61]

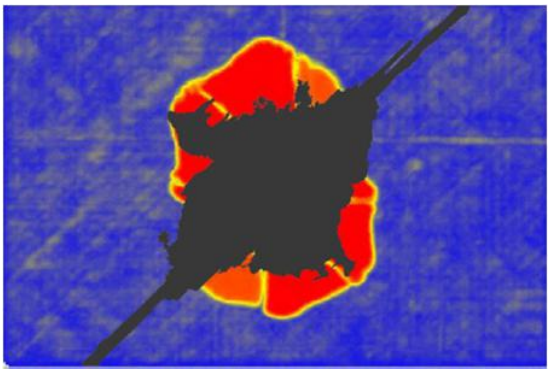

Figure 2.7: Damage analysis results obtained through hybrid techniques: Resin deterioration area (binary image) is overlaid on an ultrasonic C-scan image of internal damage in a graphite/epoxy composite after an artificial lightning test (image rotated by 90°) [52]

Advanced visual techniques

Photography is possible at two instances, the first while testing the sample and secondly while studying damage. High-speed or long exposure modes of photography (with neutral density or polarized lenses) [62] are used in the first case. Such photography is used to study zoning, identification of specific lightning attachment points on a given sub-system [63] and direct effects such as arcing/sparking, an aspect critical to fuel tanks and allied systems [46, 64]. High-resolution cameras are applied to both record and study lightning-induced damage. The dual nature of the data, which is both qualitative (e.g., identification of damage modes) and allows extraction useful quantitative data (e.g. damage area), makes photography the key step in any characterization campaign.

Optical microscopy, categorized into dark/bright field, fluorescence and polarized light microscopy depending on the characteristics of the light source, is regularly employed for studying lightning strike damage in composites. Electron microscopy is used where high magnification and resolution are required. Spectrometric and/or diffractometry data from specific locations on the sample can also be obtained. For damage analysis via microscopy, it is suggested to 'freeze' the damage so that its characteristics are not altered due to handling or aging and to allow studies to be carried out at any point of time. Polymer encapsulation is commonly used for mounting specimens, sections/cut-outs of interest are encased in transparent epoxies. However, differentiation between the polymer matrices of the composites and that used for encapsulation may be taxing and result in errors. This issue can be resolved via introduction of fluorescent dyes into the encapsulating polymers. The result then will be similar to those presented by a liquid penetrant test, albeit inverted in contrast. Such a use of dyes comes handy in attempts to identify inter- and intra-ply arcing, matrix cracking etc. Some other kinds of defects may require the polarized light or the contrast differences provided by bright or dark fields to identify both their physical existence and origin. Ideas, for example, comparing scanning electron microscopy (SEM) images of the sample at position of arc strike and those of thermogravimetry (TGA) residue can hint the source of damage, which in this case is thermal degradation [30]. Other tools and techniques include photomultipliers for radiation measurement [47], profilometry to study surface roughness etc.

Non-destructive evaluation

Visual inspection (and the conventional coin-tap [65]) helps locate damages and defects while microscopic examination reveals microstructural details. Non-destructive tests (NDT), on the other hand, are useful for macro and sub-macro-scale investigations. Non-destructive evaluation (NDE) ensures minimum alteration to the samples in the course of testing. It allows for the generation of a visual record or use ancillary systems to convert the outputs into one. This combined with advancement in electronics and computer science has led to data portability, application of artificial intelligence [66] for defect identification [67] & classification [68], pattern recognition, and so on, facilitating even the less-experienced practitioners.

Key non-destructive tests include ultrasonic testing, acoustic emission, thermography, radiography, X-ray computer tomography scan and so on. Almost all of these techniques are multi-purpose. For example, eddy current testing, which is based on electromagnetic induction can not only identify defects originating from impacts [69] but also help in measuring characteristics of materials such as coating thickness during wet spraying or the electrical conductivities of materials aimed at lightning strike protection [70]. Nonetheless, they all also have their limitations, which for eddy current testing is that it is applicable to conductive materials only.

NDT techniques applied to studying lightning damage in composites are focused on four aspects:

- Profile – shape and directionality: define failure mode in composites
- Penetration – number of plies damaged: estimation of residual strength
- Location – distinguish between damaged and undamaged (baseline) regions: choose samples for post-lightning characterization
- Extent – differentiate surface and internal damage: handy during repair.

Different combinations of lightning strike parameters and test materials yield equally different test results. One can compare and correlate specific damages in the material system to other changes such as mechanical properties [60]. For example, correlation of damage progression with impact-damage area and impulse currents through acoustic emission monitoring during compression tests [71] makes stress-strain curves even more information worthy.

Mechanical testing

Mechanical testing is a very useful concept in lightning strike evaluation since, post-strike, it can:

(i) Determine the extent of damage in terms of changes in mechanical properties, and
(ii) Estimate useful residual life for a given application.

Mechanical testing provides useful data in the form of stress-strain curves from which moduli, ultimate strengths, resilience or toughness can be derived and compared. However, proper normalization of data is important, e.g., impact depth with sample thickness or post-strike strength with pre-strike strength or that of the edge (unaffected zone) samples. Such a normalization must come from a scientific analysis of the data; data fitting (linear or power-law etc) must be carried out to decide on the best correlations presented by the data sets [60].

Mechanical impacts have a strong say on the compressive properties of the composites; residual strength may be reduced by up to 50% [72]. This makes compression-after-impact tests a more sensitive parameter to gauge the extent of such damage [29]. Flexural characteristics are ascertained through bending tests performed on rectangular coupons in the 3-point or 4-point configurations. Interestingly, these tests feature tensile and compressive forces on opposite sides of the test specimen. The lightning struck face is maintained in tension probably so that the test is as severe as possible with the damaged fibers in tension providing stress concentration (notch-effects) [73]. Some authors have also employed dynamic mechanical analysis (DMA) focusing on various parameters such as glass transition temperature related to the resin cross-link density [74]. The key advantage of DMA is its ability to detect low intensity thermal damage (degradation,) which cannot be easily detected by conventional non-destructive techniques.

Hybrid techniques are the current trend in the industry. In literature, one such technique was based on the use of built-in optic fiber strain sensors embedded into the material/components of the aircraft (for example, “the main spar of a test wing”) to monitor their behavior with respect to load. Further, information on the impulse and other forces exerted due the lightning arc may be computed. Such information can then be used during modeling and simulation assignments and also in the development of equivalent mechanical tests [64]. In another interesting set of studies, Chen et al. [75] investigated if an artificially damaged rudder could function effectively given the rigid structure principle applied to its manufacture. They fixed the rudder into an actual fin and, and conducted static tests with a network of actuators and sensors that confirmed the rudder was able to sustain their design loads

Spectroscopic tools

Spectroscopic tools yield valuable information on the chemistry and stability of materials. In the context of lightning strikes, changes in the chemical make-up of the coatings both in terms of composition and structure may be detected and cause-effect relationships derived. For example, while studying carbon fiber-bismaleimide composites that were filled with nickel-coated single wall nanotubes [30], the authors employed inductively-couples plasma - mass spectroscopy (ICP-MS), to study the affects of high currents and associated heating on the metallized nanotubes. In the same study, special attention was paid to the strain-sensitive G-band of the nanotubes through Raman spectroscopy. The authors compared positions of the G-bands before and after lightning strikes and found a peak shift which they attributed to the strain possibly generated as the "resin pulverizes and pulls the nanotubes along with it." In another study involving nanotubes [76], it was observed from the EDS data, that nucleation of iron and titanium took place after carrying high current tests on composites. This was attributed to the destruction of the nanotubes at high temperatures that left behind the catalysts and abraded products from the sonicator tips.

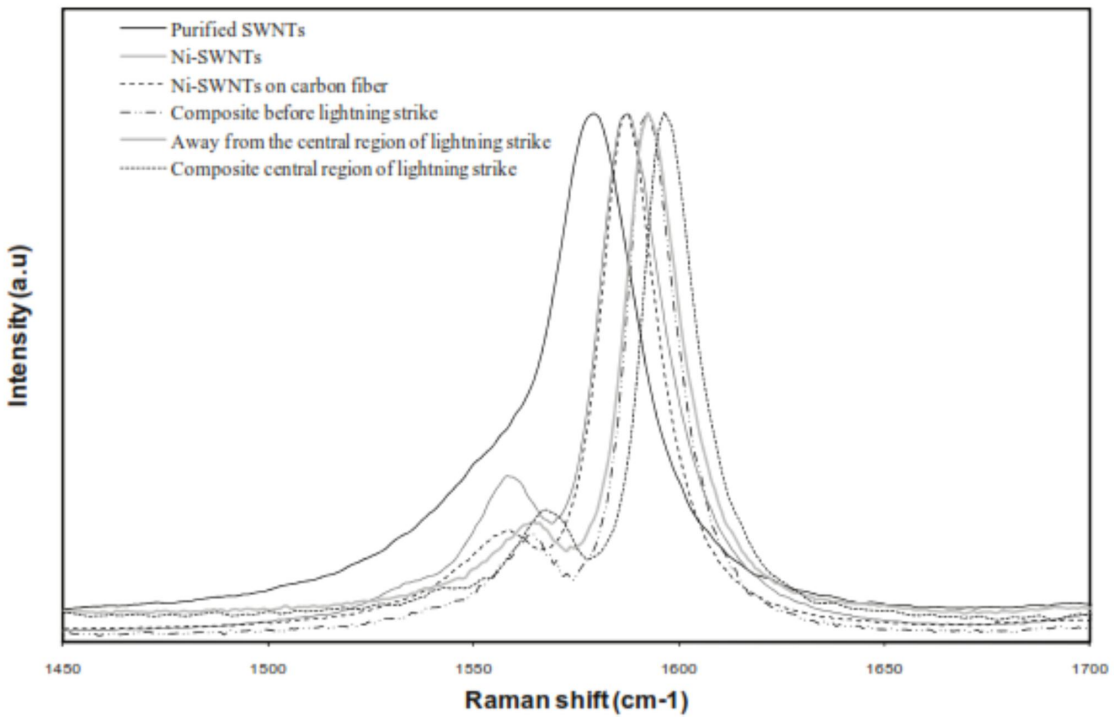

Figure 2.8: Raman spectroscopy study of nickel-coated SWNTs used as conductive fillers in bismaleimide–carbon fiber composites subjected to lightning strikes [30]

2.4 Summary of literature

Present day LSP research is shifting towards conductive coatings. The major advantage of the externally applied conductive solutions is that any shape and size can be easily covered with these materials. Further, lightning-induced damage will be confined to the exteriors of the structural material enabling quick and easy repair. However, two critical challenges remain to be resolved before these materials undergo a transition from laboratory technologies to commercial products. They are (i) good dispersion and homogeneity, and (ii) lower contact resistances between conducting particles. Therefore, metallic meshes and foils still form the benchmark in terms of overall sheet resistance. Testing of direct effects of lightning is critical to the certification of aircraft for protection against lightning strikes. The high current tests damage both the LSP material and the composite it is protecting. Photography and non-destructive testing are common damage analysis techniques. A study of the type and extent of damage can provide feedback on fabrication flaws and other high current material properties. While in the aircraft industry, such results are used to evaluate LSP materials and make choices depending on aircraft zoning, in the laboratory, this feedback serves for improving the process methodology of conducting materials under development. As for lightning emulation, separate systems to emulate lightning impulse and continuous currents have been used in many studies. Most impulse emulators are based on crow bar circuits, while batteries are used for emulating lightning continuous currents.

CHAPTER 3 RESEARCH OBJECTIVES, METHODS AND RESULTS

This doctoral research is part of a larger effort of the COMP-502 project to develop conductive films or coatings for aircraft lightning protection. This thesis work is directed at designing and building experimental test facilities. Necessary test protocols would be developed in order to employ these facilities to carry out a preliminary investigation into the potential of the newly designed coatings to offer lightning strike protection to aircraft structures. The test equipment and protocols conceived must allow for carrying out scientific studies on the interaction of the materials with experimental lightning in a time-bound and cost-effective manner. At the same time, it is also envisaged to explore other applications of the test facilities/methods and materials by expanding upon the research efforts and available laboratory infrastructure.

3.1 Research objectives

The specific primary objectives of this thesis work are:

Objective 1: To establish screening-level lightning test facilities

Conceive, design and build an 'impulse strike emulator' to generate micro-second-range currents of up to 40,000 A, and a 'continuous current emulator' to generate sub-second-range steady currents of up to 500 A conforming to the SAE standards [38], and demonstrate their functionality.

Objective 2: To execute lightning strike tests on conductive coatings and damage analysis thereof

Subject conductive coatings realized within the scope of COMP-502 project to lightning currents using the impulse and continuous current emulators realized through Objective 1, and study the damage protection that the conducting coatings (material design schemes) offer to underlying CFRP through non-destructive methods.

In addition to these, a secondary objective was pursued:

Objective 3: To explore ideas to expand the application of test facilities, methods and/or materials

Devise and demonstrate a selective material deposition/coating technique to extend the use of conducting materials to other aerospace applications.

3.2 Thesis chapters, research articles and their coherence with the objectives

The methods adopted to accomplish each of the objectives and the main scientific findings from the studies are presented in chapters 4 through 6 and form the core of this thesis. These were submitted as research articles to peer-reviewed journals. Given the multi-disciplinary and experimental nature of the work, journals with a wide topical scope and emphasis on practical application were selected for the submitted articles. Each of these journals enjoys a large readership within the research community and provides an effective platform for publication and dissemination of knowledge.

Establishment of screening-level lightning test facilities

The first article 4 titled '*Development of a 50 kA Lightning Impulse Emulator*' was submitted to Review of Scientific Instruments, AIP Publishing on 23 August 2017. It describes the procedure adopted for the design, development and demonstration of a lightning impulse emulator. Catia® was used for structural design. Different materials such as acrylic, aluminum, copper, fiberglass, wood etc. were chosen for fabrication based on requirement and merit. This RLC circuit-based emulator produces a peak amplitude of 40 kA. The impulse emulator offers variable current amplitude, variable circuit inductance, conducted-current and arc-entry test modes. The effect of each of these features on the impulse waveforms is studied via short circuit tests and lightning strikes to aluminum panels and unprotected (bare) CFRP. Additionally, the possibility to produce oscillatory pulses is theoretically demonstrated. Through these experiments, the waveform that best conforms to the requirements of the SAE standards is revealed. This paper, along with Lightning C-component emulation realized using commercial power supplies capable of producing up to 500 A DC (discussed in Chapter 5), fulfill Objective 1. It is anticipated that these low-cost electrical circuit and physical design schemes will further drive the development of similar or improved lightning emulators, thereby fostering research in the area of high current engineering.

Execution of lightning strike tests on conductive coatings and damage analysis thereof

The second article titled '*Damage Response of Composites Coated with Conducting Materials Subjected to Emulated Lightning Strikes*' was submitted to Materials & Design, Elsevier B. V. on 13 July 2017. The damage characteristics of the composite protected by different conductive coatings developed as a part of the COMP 502 project are discussed in this paper. Silver-carbon and silver-conducting polymer hybrids, silver, and copper-tin composite-protected CFRP were tested against lightning impulse currents of 40 kA peak. The tested specimens were subjected to ultrasonic non-destructive evaluation to study the damage characteristics. Furthermore, the performance of metallic materials: copper-tin and tin-protected CFRP was evaluated against 1 s pulses of 200 A continuous current. Resistance data supplemented by real-time thermal monitoring was used to characterize the behavior of the coatings against the continuous currents. Materials design and processing challenges that limit the performance of the coatings are identified and suitable remedies are proposed. The unprotected (bare) and expanded copper foil (ECF)-protected CFRP form the lower and upper performance thresholds for the study. This article fulfills the requirements of Objective 2. The analysis of different material design/manufacturing strategies studied in this work can support various materials research groups to better analyze their products before proceeding to the more demanding test phase. Furthermore, the 2-step test protocol and analysis methods presented herein complement Objective 1 and are expected to widen the platform for investigation of LSP materials, forming the basis for development of greener and safer aircrafts.

Exploration of ideas to expand the application of test facilities, methods and/or materials

The third article titled '*Continuous and Selective-Area Coating of Silver on Fiber-Reinforced Polymer Composites for Aerospace Applications*' was submitted to the Langmuir, ACS Publications on 13 July 2017. Firstly, the Tollen's process for electroless plating of silver was adapted to coat CFRP. The process chemistry for both pre-processing (sensitization) and coating steps was optimized to attain improved deposition mass with a low resistivity. Sintering temperature and time were also studied. In order to produce selective area coatings of silver, a two-stage masking process was utilized. In the first stage, the requisite design for the conducting selective-area coating was printed in a fast-drying polymer. Secondly, a hybrophobic coating was sprayed onto the polymer; the polymer was peeled off as the hydrophobic coating was drying up. The remnant hydrophobic coating now functions as a mask to restrict the electroless silver chemistry to the requisite design. Designs for electrical connections, electromagnetic

shielding, antennae and sensors were demonstrated as possible applications of the selective area coatings. This article caters to Objective 3. The resourcefulness of a technique to produce selective area coating of a metal is undeniable. The integration of economical hardware and commonly available materials to devise a novel selective-area deposition technique results in a highly accessible technology. In particular, the engagement of computer numerical control (CNC) / three-dimensional (3D) printing equipment enables both custom and serial fabrication of conductive designs. It is believed that when this technology is scaled appropriately on the lines of resolution/speed/economy, it will hold potential to cater to the industrial needs.

CHAPTER 4 ARTICLE 1: DEVELOPMENT OF A 50 KA LIGHTNING CURRENT EMULATOR

P. S. M. Rajesh, Maxime Tousignant, Samir Khalfaun, Daniel Therriault, Frédéric Sirois*

Submitted to Review of Scientific Instruments, August 2017

4.1 Abstract

In this paper, we describe the development of a lightning impulse emulator with a view to producing peak currents up to 50 kA as per the waveforms described in SAE ARP 5412. The goal is to devise a modular screening setup for evaluating the efficacy of various new developmental conductive coatings for lightning strike protection of aerospace polymer composites. This system incorporates a damping resistance and a variable inductance as degrees of freedom to control the waveform. It also features a modular design for portability. Additionally, the test fixtures allow for conducted current or arc-entry tests. The emulator is realized in three stages: circuit conceptualization, mechanical design and fabrication, and technology demonstration. Conceptualization involves the drafting and verification of the electrical circuit of the emulator via analytical and simulation routes. After this, the circuit is translated into a physical structure through computer-aided design and constructed using a careful choice of materials. Control and data recording facilities are discussed. Ultimately, the functionality of the emulator is demonstrated via tests in short circuit configuration and strikes to aluminium and carbon fiber reinforced polymer panels. This paper presents the key aspects of each stage and discusses the characteristics of the emulator.

Keywords: Lightning; Emulator; Direct Effects; Electrical conductivity; Carbon-fiber composite

4.2 Introduction

Lightning strike emulators are usually restricted to specialized test centers or advanced laboratories owing to their sophisticated construction, high costs and expertise required for operation. Services of such centers or laboratories are sought for certification purposes or to perform specialized experiments. However, there arise cases where frequent testing may be required even if it is at reduced amplitude. An example could be a project to investigate the

feasibility of using different electrically conductive materials as coating technologies for lightning strike protection (LSP) of aircraft built from fiber-reinforced polymer [1]. A low-cost, easy-to-use lightning emulator is sought for local use for such industrial or academic projects due to limitations in budget, technical support or time. Direct and continuous feedback to the research teams is a major advantage of such accessible equipment as it facilitates the fine tuning of the designs, the materials and the manufacturing processes of the equipment under test (EUT) in an efficient manner, and it utilizes the research efforts to their fullest potential.

The standardized current waveform [2] of lightning shown in Figure 4.1 can be visualized to be composed of two distinct components – a peak impulse, A, and continuous current, C; Component B can be considered as a transition between A and C components. This is usually followed by another impulse component, D. Although a test waveform comprising components A through C or D would be needed consecutively for an actual simulation of lightning, it is not rare that emulators for individual waveforms to be built and operated [3-5]. Such single component emulators, while being comparatively simple and cheap, allow for the study of specific properties required to withstand the individual current components and better understand the material characteristics of interest.

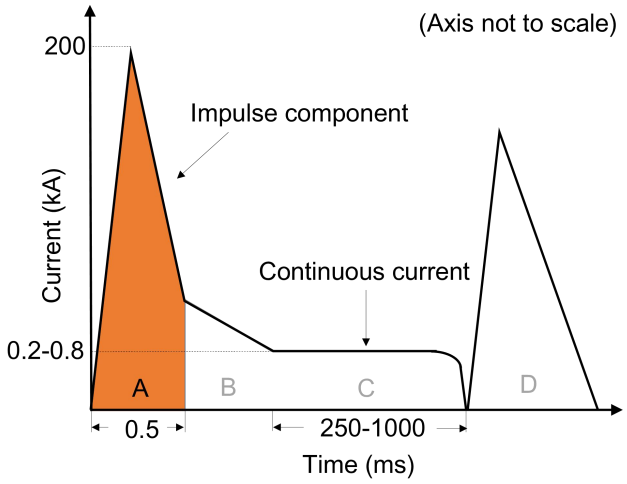

Figure 4.1: Standardized lightning current waveform as described in SAE ARP 5412 [2]

This paper describes the design and development of a 20 kJ (max. stored energy) lightning impulse emulator capable of producing peak currents between 10 and 40 kA. The various operational features and flexibility of the emulator has been demonstrated through tests in short-

circuit configuration and on aerospace materials. Once the EUT has passed the screening tests of reduced current amplitudes with this emulator, it is then possible to send the EUT to high-tech facilities to perform full certification tests based on standard waveforms and methods.

4.3 Conceptualization of the circuit

The first step in the realization of a working impulse emulator was to draft the basic electrical circuit to produce the requisite lightning impulse waveform shown in Figure 4.2(a). Applications of this nature typically use RLC circuits with pre-charged capacitors [6], as shown in Figure 4.2(b), although inductors may also be used in place of capacitors for energy storage [7].

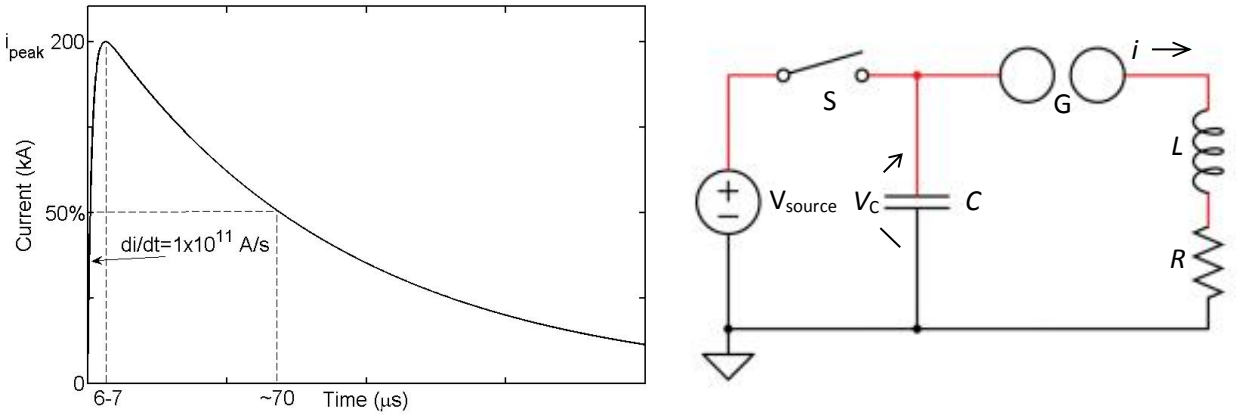

(a) **(b)**

Figure 4.2: (a) A-component test waveform as described in SAE ARP 1512 [2] and (b) Typical RLC circuit for emulation of lightning impulse; V_{source}: high voltage (DC) source, S: charging switch, V_C: voltage across capacitors, C: capacitance, G: sparkgap (trigger), L: circuit inductance, R: circuit resistance

A circuit as shown in Figure 4.2(b) gives only 3 degrees of freedom to design the system, i.e. the values of the electrical parameters R, L and C. In fact, there is a fourth degree of freedom, which is the initial voltage in the capacitor, $V_{C0}=V_C$ @ $t=0$, and has an impact on the peak value of the current, but does not affect the time constants of the system. The nominal operating voltage in our case was limited to 70 kV for safety reasons, mainly because our test setup was located in a small room that was not a high-voltage facility. However, it is technically possible to charge the capacitors up to 90 kV in case it is really needed.

The A-component impulse waveform defined in the SAE ARP5412 [2] standard was chosen for emulation, although the current value was scaled down by a factor of 4 (i.e. from 200 kA to 50 kA). Thus, according to Figure 4.2(a), the target parameters for the emulated waveform were:

1. A peak current of 50 kA
2. An initial rate of current rise d*i*/d*t* of about 35 kA/μs
3. A time to peak of about 6-7 μs
4. A time decay to 50% of about 70 μs

This impulse waveform *i(t)* is quite well described in the SAE standard with a double exponential formula, which reads:

$$i(t) = i_0(e^{-\alpha t} - e^{-\beta t}), \tag{4.1}$$

where, i_0 is 218810 A, α=11354 $s^{-1}$and β=647265 s^{-1}.

The mathematical solution of damped *RLC* circuit with zero initial current and a capacitor initially charged at V_{C0} has a mathematical solution that takes exactly the form of (4.1), i.e.,

$$i(t) = \frac{V_{C0}}{\Delta}(e^{-\alpha t} - e^{-\beta t}), \tag{4.2}$$

with

$$\Delta = \sqrt{R^2 - 4\left(\frac{L}{C}\right)}, \tag{4.3}$$

and the exponent are given by:

$$\alpha = \frac{R - \Delta}{2L} \text{ and } \beta = \frac{R + \Delta}{2L}.$$

The initial *di*/*dt* of the current pulse at *t*=0 is given by:

$$\frac{di}{dt} = \frac{V_{C0}}{L}. \tag{4.4}$$

The time t_p to reach the peak value of the current is given by:

$$t_p = \frac{L}{\Delta}\ln\left(\frac{R + \Delta}{R - \Delta}\right). \tag{4.5}$$

The inductance of the circuit is composed of two parts; the inductance associated to the sample, L_S, and the rest of the inductance of the setup, L_G. In order to start the design process, the

minimum inductance of the loop containing the sample under test was estimated using the formula [8]:

$$L = \mu_0 N^2 r \ln\left(\frac{8r}{a-2}\right), \tag{4.6}$$

where, μ_0 is the magnetic permeability of air ($4\pi\times10^{-7}$), N is the number of turns (one turn in the present case), r is the radius of the loop, and a is the radius of the wire forming the loop that carries the current into the sample. Since the samples we want to test here are square panels with sides of ~25 cm, this dimension was used as the radius r of a single-turn loop. A cable radius a=1 cm was also assumed, which is large enough to avoid excessive corona discharges at 70 kV. This resulted in an inductance L_S in the range of 1 μH for the sample.

The inductance ensuing from the employment of the sparkgap (purchased as is) and its current return path form another loop that add an additional inductance L_G that was temporarily fixed equal to Ls as a first estimate. Therefore, in the preliminary design, a value of $L=L_S+L_G$=2 μH was used. This was sufficient to verify the target in terms of the initial di/dt, since it depends only on the ratio V_{C0}/L, i.e. di/dt = 35 kA/μs if the capacitor is charged at 70 kV, which turns out to be exactly what was targeted.

Next, the remaining two degrees of freedom, i.e. R and C, needed to be fixed. The value of the resistance R is the most natural one to fix next, because it roughly determines the peak current in the circuit, according to (4.2) and (4.3). Let us assume that R mainly consists of the sum of R_{damp}, a damping resistance, and R_s, the sample resistance. In order for the current in the emulator to be as independent as possible of the sample resistance R_S, we must chose $R_{damp}>>R_S$, so that $R=R_{damp}+R_S\approx R_R$. The sample resistance is readily known to be in the range of 25 mΩ or less for composite panels coated with a conducting material. Therefore, a damping resistance value in the range of R=1 Ω was targeted in order to make sure it dominates the dynamics of the current waveform.

Finally, in order to make sure that the final RLC circuit is damped and corresponds to (4.2), one must make sure that Δ in (4.3) is real, which means $R^2>4L/C$, i.e. C>8 μF. In this work, C=10 μF is chosen as a first guess.

Therefore, for the choices made above, i.e. $R \approx 1\ \Omega$, L=2 μH, C=10 μF and V_{C0}=70 kV, the analytic expressions above give:

1. A peak current of 53.4 kA (target = 50 kA ➔ OK)
2. An initial di/dt of 35 kA/μs (target = 35 kA/μs ➔ OK)
3. A time to peak of 4.3 μs (target = 6-7 μs ➔ faster but roughly OK)
4. A time decay to 50% of 12.3 μs (target = ~70 μs ➔ NOT OK)

Clearly, the peak current and initial rate of current rise closely matches the target values, while the time to peak is shorter but still acceptable. However, it is impossible to meet the time decay requirement with the present amount of energy stored in the system without increasing substantially the value C of the capacitor, while simultaneously adjusting the damping resistance to avoid overshooting the desired peak current. Keeping the choices V_{C0}=70 kV and L=2 μH, one can choose C=70 μF and R=1.3 Ω in order to find an almost perfect match with the initial targets, i.e.:

1. A peak current of 51.0 kA (target = 50 kA ➔ OK)
2. An initial di/dt of 35 kA/μs (target = 35 kA ➔ OK)
3. A time to peak of 6.5 μs (target = 6-7 μs ➔ OK)
4. A time decay to 50% of 70 μs (target = ~70 μs ➔ OK)

However, a value of 70 μF for the high voltage capacitors is way too high to be realized practically. In fact, at such high voltage, and especially for generating fast rising current pulses, very few types of capacitors can be used, and they are bulky in size. For the 2.6 μF Scyllac capacitors [9] chosen later in this design (see Table 4.1 and associated text), it was barely possible to physically assemble more than 4 units in the setup, whereas one would need 27 capacitors of 2.6 μF in parallel to achieve 70 μF. Another issue with using so many large capacitors is that it represents a lot of stored energy (170 kJ), and 93% of this energy must be dissipated in the damping resistor of 1.3 Ω, which requires a substantial thermal over-rating. Therefore, the time decay criteria had to be either sacrificed or achieved by changing dynamically the circuit topology.

An option to improve the situation is to add a free-wheeling diode to the initial circuit shown in Figure 4.3(a). This changes the behavior of the *RLC* circuit to that of a first order *RL* circuit when it reaches the last part of the decay phase, as illustrated in Figure 4.3(b). Indeed, as soon as the

voltage at the cathode of the diode *D* becomes negative, which happens slightly after the current peak in the *RLC* circuit, the diode starts to conduct the full current carried by the sample, and shortly after the spark gap opens (due to lack of voltage between the electrodes). The sample current thus flows in a *RL* circuit whose time constant is $\tau_{RL} = L_S / R_S$. This time constant is greater than that of the initial *RLC* circuit, as shown in Figure 4.4, which was produced assuming that the diode behaved as an ideal switch.

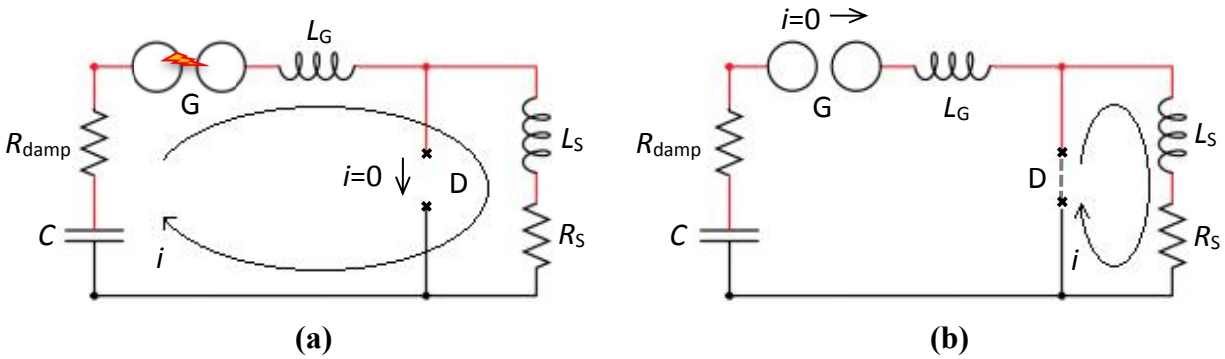

Figure 4.3: (a) *RLC* circuit behavior: operation with diode in blocking mode, and (b) *RL* circuit behavior: operation with diode in conduction mode

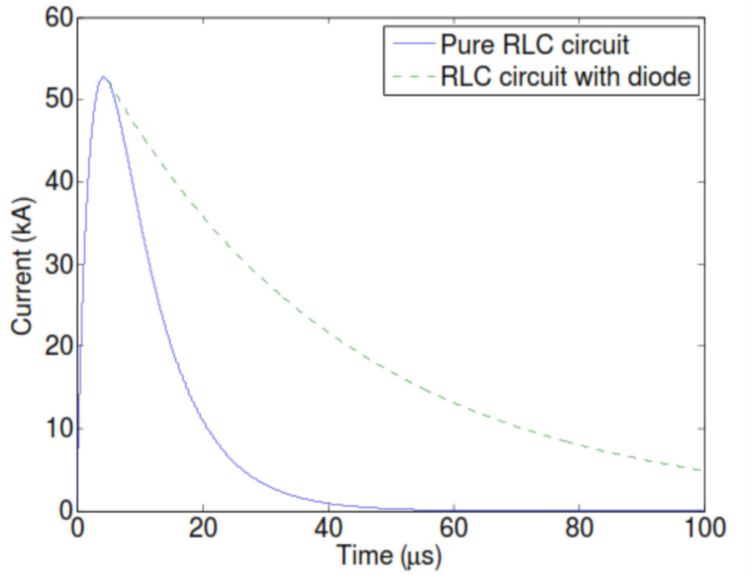

Figure 4.4: Effect of the diode on the waveform produced by the RLC circuit

R_R=1.0 Ω, R_S=0.25 Ω, L_G=1 μH, L_S=1 μH, C=10.4 μF, V_{C0}=70 kV and ideal diode

The presence of the diode thus decouples the two meshes of the circuit during the decay of the current and allows increasing substantially the decay time. One must note though that the decay time then becomes very dependent on the sample resistance R_S, as will be shown in the next section. Finally, one can then make inductance L_S in the sample loop adjustable in order to fine tune the final waveform. This is discussed in the next section.

4.4 Mechanical and electrical design

Given the satisfactory analytical results for the conceptualized circuit, a small prototype (not shown) was finally built for validation before proceeding with the design of the actual emulator.

The guiding principles for the emulator design and fabrication were aimed at effectively mimicking the waveform parameters of the standardized lightning impulse while maintaining requisite factor for safety. As seen in the previous section, the circuit inductance plays an important role in deciding the shape of the waveform. It is well known that parasitic inductance can be minimized by decreasing the loop area between two wires. We can further reduce the inductance if using a co-axial arrangement of the wires. Thus, compactness and co-axial construction were emphasized. However, it must be noted that in a practical scenario, these aspects cannot be indefinitely realized. While the need for portability and modularity limits the compactness of the emulator, the separating distances between the electrical conductors in the co-axial system must be chosen appropriately so not to adversely affect the electrical insulation. Moreover, being in a high voltage environment, the possible presence of partial discharges must be considered. Simultaneously, given the substantial amount of energy stored in the capacitors and the fast-rising current (and hence voltage) values, the structure needs to be rugged and safe.

4.4.1 Mechanical design

Electrostatic finite element simulations have been used extensively in the initial design phase in order to size each component of the emulator to achieve dielectric safety (simulations not shown here). In parallel, static magnetic finite element simulations (not shown here neither) were also carried out to determine the approximate inductance of the parts, so we could at the end generate an equivalent electric circuit of the emulator. Based on all these finite element simulations, a final geometric model of the emulator (circuit: (Figure 4.5(a)) could be created on computer aided

design (CAD) software as shown in Figure 4.5(b), comprising six principal components, as listed in Table 4.1.

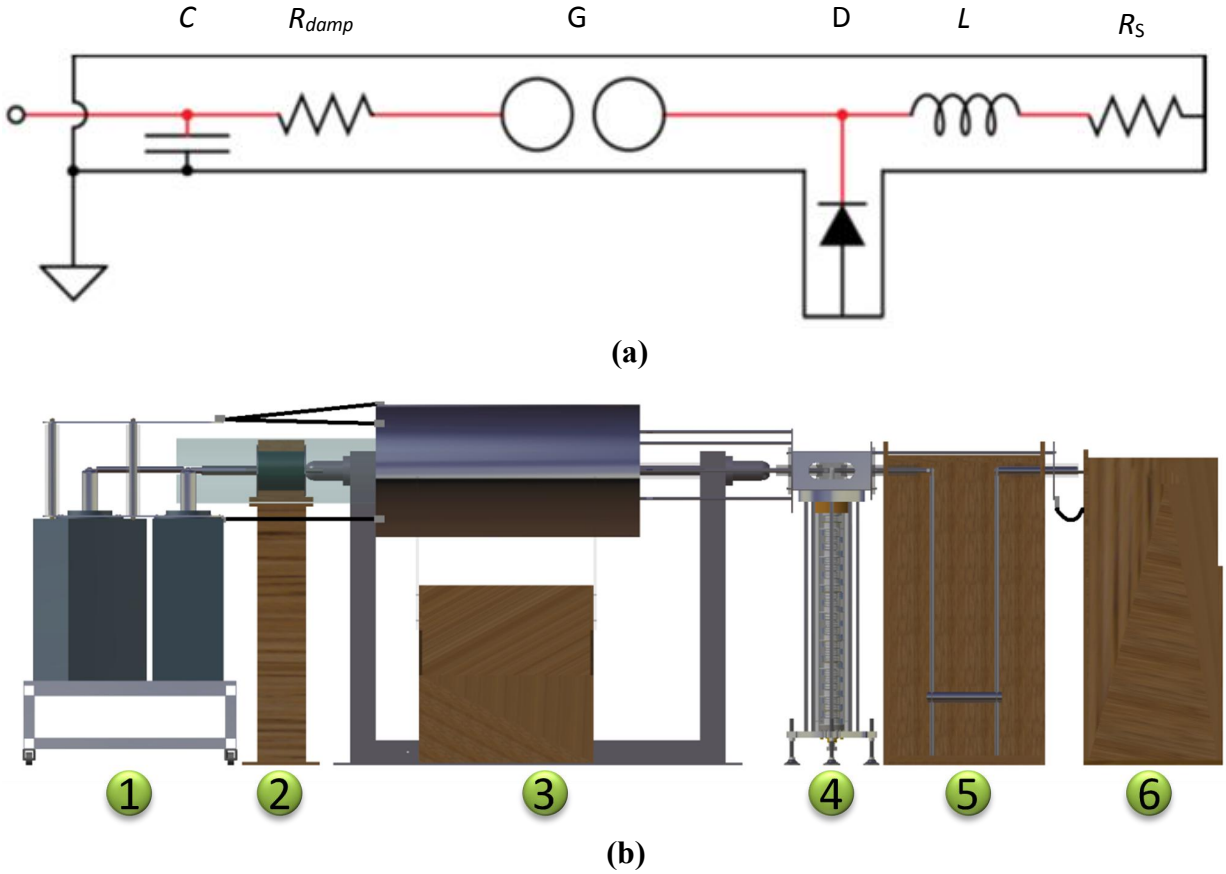

Figure 4.5: (a) Electrical circuit, and (b) CAD model of the emulator; the numbered components are listed in Table 4.1

Table 4.1: The constituents of the electrical circuit and their respective roles and characteristics

No.	*Part*	*Role*	*Characteristics*
1	**Capacitor bank**	Emulator energy source	10.4 μF, 70 kV
2	**Resistance**	Damping resistance for shaping of the current waveform	~1 Ω
3	**Spark gap**	Lightning strike trigger	0-230 kV
4	**Column of diodes**	Convert circuit behavior from *RLC* to *RL* during current decay phase	Insulation designed for at least 150 kV
5	**Variable inductance**	Fine tuning of waveform	0.25 – 2 μH
6	**Test chamber**	Samples fixtures to perform conducted current or arc-entry tests	Arc length up to 1.3 cm

The following is a brief discussion about the each of the constituent:

Capacitor bank: This bank is formed by four Scyllac-type capacitors (2.6 μF each) [9], connected in parallel. The bank can be charged upto 90 kV (limited to 70 kV for safety reasons).

Damping resistance: Two sets of resistors are held in a parallel configuration between metallic electrode plates. Each of these sets if formed by seven high-power resistors connected in series. The resistors (0.2 Ω±10%) were each rated to 8.4 kV (1.2 μs/50 μs) pulse. This assembly can absorb about 12.8 kJ of energy per 1 K of temperature rise.

Spark gap: The spark gap is composed of two conducting spheres (made of graphite in this case) separated by an air gap, and used here as a switch. When the spheres are brought close to each other, the air gap breaks down, triggering the current pulse. In order to produce a homogeneous electric field in this critical region and to contain as much as possible the radiation from the arc, a hollow metallic cylinder is fixed around the spark gap to form the co-axial current return path instead of an arrangement of metallic rods or cables used elsewhere in the emulator.

Column of diodes: The column of diodes is a stack of 31 rectifier diodes, each capable of withstanding a repetitive reverse voltage of 5000 V. The fixture to hold the diodes is designed to perform two functions: (i) hold the diodes in a vertical alignment, and (ii) apply the vendor-stipulated pressure to produce a low-resistance electrical contact.

Variable inductance: This was achieved with a variable size rectangular current loop formed by a movable conducting bar running on two vertical metallic rods, as shown in Figure 4.6. Maximum achievable inductance for the present design is 2 μH.

Test chamber: The sample holder of the chamber can accommodate a maximum test sample size of 30.5 cm × 30.5 cm, and is designed to allow for two kinds of tests (see Figure 4.7):

(i) Arc-entry test: A square frame forming the return electrode clamps the edges of the sample and a striker electrode with a pointed tip (60°) is held at a fixed height (max: 1.3 cm with initiating arc) from the center of the sample; an arc is generated between the electrode tip and the sample.

(ii) Conducted current test: Opposite edges of the sample are clamped under separate electrodes and the impulse current is injected across the width of the sample.

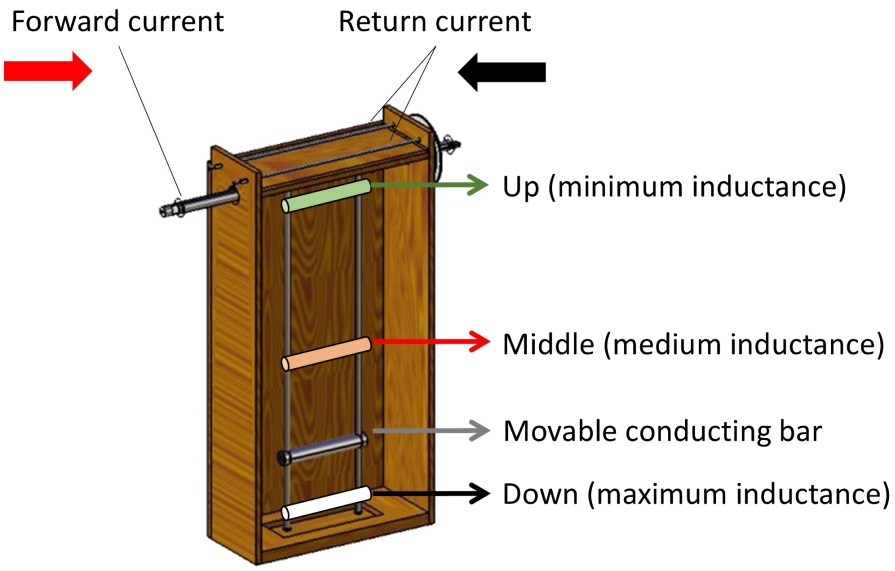

Figure 4.6: Schematic of variable inductance showing different inductance positions used in the study

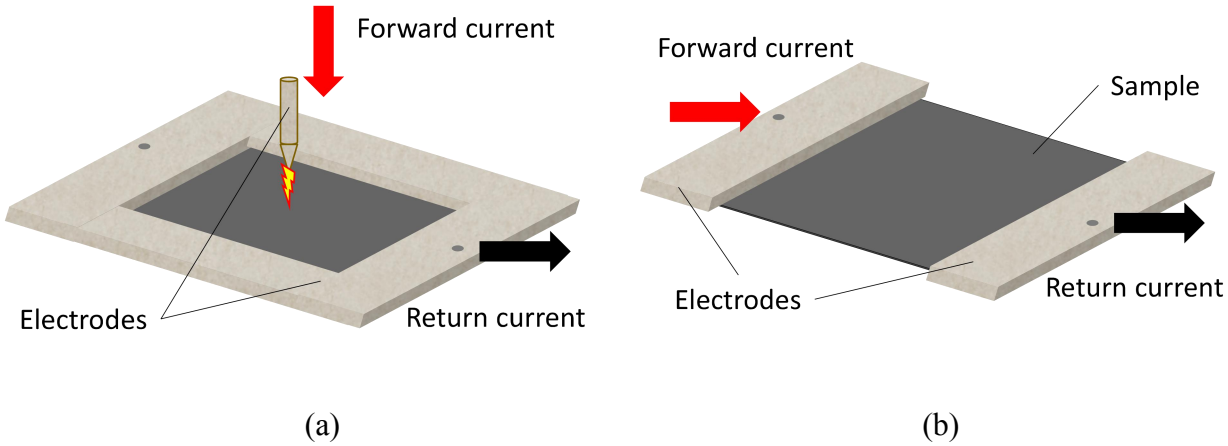

Figure 4.7: Sample configuration for (a) arc-entry, and (b) conducted current tests

4.4.2 Detailed electrical analysis

For this final electrical analysis, a software simulation of the circuit was carried out to verify that it would indeed be able to produce a waveform similar to that in SAE standard with the conceptual 3D design of the emulator. The detailed electric circuit model is shown in Figure 4.8. Values of 25 mΩ resistance and 1 μH inductance were used for the sample and variable inductor respectively. With the simulation parameters shown in Figure 4.8, we obtain a waveform (Figure 4.9) whose shape resembles the impulse waveform in Figure 4.2(a).

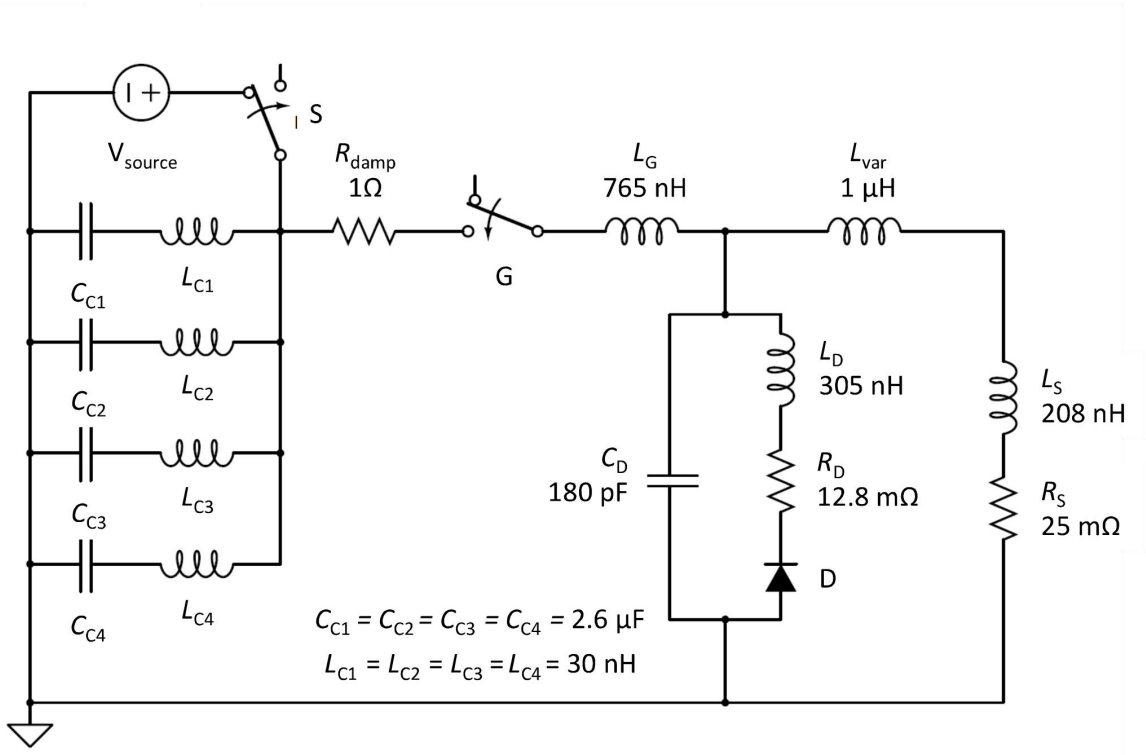

Figure 4.8: Detailed equivalent circuit of the lightning current emulator. V_{source}: high voltage (DC) source, S: charging switch, C: capacitance, R: resistance, G: sparkgap (trigger), L: inductance and D: diode. Subscripts 'C1', 'C2', 'C3' and 'C4' stand for individual capacitors, 'damp' for damping (resistance), 'var' for variable (inductance), and 'S' for sample

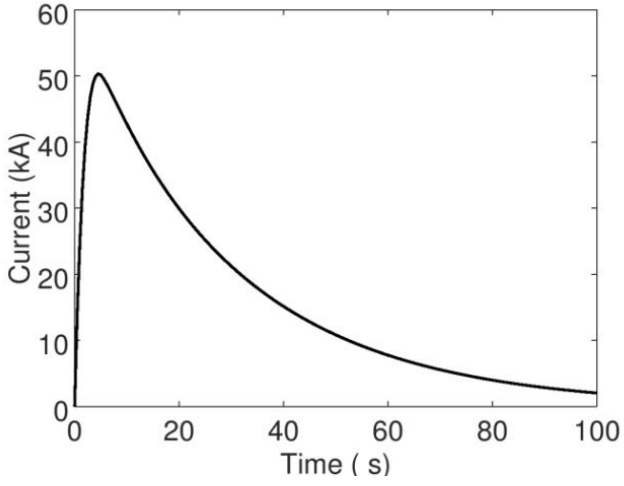

Figure 4.9: Simulated waveform for the detailed circuit (with L_{var}=1 µH and R_S=25 mΩ)

For the waveform shown in Figure 4.9, the following values were obtained for the emulator:

1. A peak current of 50.3 kA (target = 50 kA ➔ OK)
2. An initial di/dt of 24.7 kA/μs (target = 35 kA/μs ➔ slower but roughly OK)
3. A time to peak of about 4.5 μs (target = 6-7 μs ➔ faster but roughly OK)
4. A time decay to 50% of ~25 μs (target of approx 70 μs ➔ faster but acceptable for the purpose)

Furthermore, a parametric study was conducted by changing the values of the variable inductance, L_{var}, between 0.25 – 2.00 μH (Figure 4.10(a)) and of the sample resistance, R_S, between 12.5 – 100 mΩ (Figure 4.10(b)). By varying the inductance, it was shown that the shape of the waveforms could be altered, which allows for better imitation of the standardized impulse waveforms. Similarly, by varying the sample resistance, it was also shown that the emulator could indeed accommodate a variety of tested materials without affecting too much the peak current.

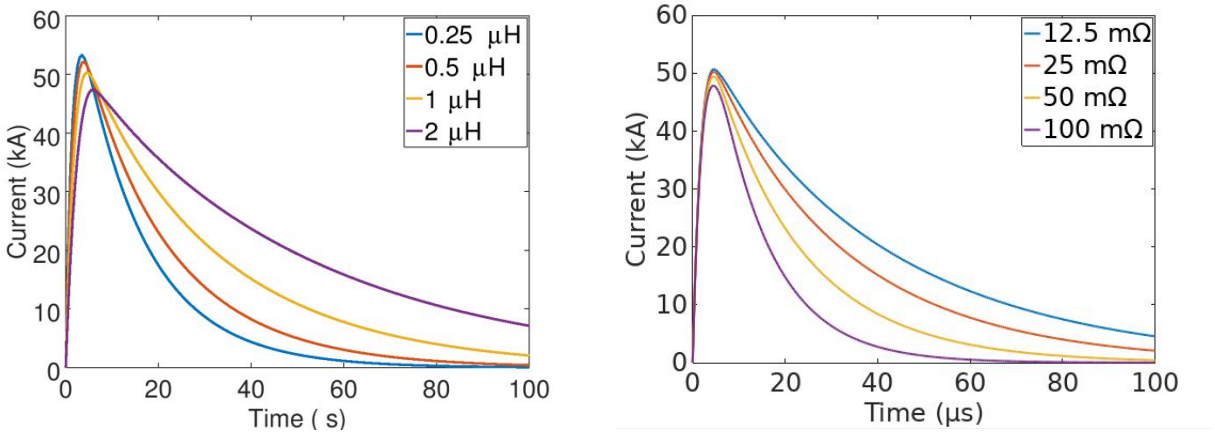

Figure 4.10: Parametric study with variation of (a) L_{var} (with R_S=25 mΩ), and (b) R_S (with L_{var}=1 μH)

The values of R_{damp} or L_S in Figure 4.8 could be further fine-tuned, however it would be very difficult to achieve the objective in terms of decay time. On the other hand, with the addition of a diode, there is no more need to store a lot of energy in the capacitors and waste it in the damping resistance. The action integral is lower by approximately a factor of 2 with respect to the standards, which follows directly from the faster decay time. This is probably the best design that could be achieved with simple and inexpensive means, although the addition of the diode makes the setup much more complicated mechanically than a pure *RLC* circuit, and increases

substantially the realization cost, since in reality, the diode consists of a stack of power diodes pressed together with a controlled pressure. In counterpart, it made it possible to achieve our goal more closely with lower capacitance.

4.5 Construction and operation

Table 4.2 lists the properties of some materials considered for the construction of the impulse emulator. Aluminum and acrylic were largely used to meet the important conducting and insulating requirements, respectively, while providing good mechanical rigidity. The basic construction largely utilized wood due to its low density (for portability), easy fabrication, insulating characteristics and low cost. Whenever possible, off-the-shelf equipment were used; An example being the trolley to place the heavy capacitors. For the designed structural components, once the individual fabricated/machined parts were received, the accuracy of design translation and dimensional tolerances were verified and then the parts were carefully assembled. The final structure is shown in Figure 4.11(a).

Table 4.2: Comparison of different conducting and insulating materials

Property	*Fiberglass*	*Teflon*	*Acrylic*	*Copper*	*Aluminum*
Dielectric Strength (kV/cm) [10]	160	197	197	NA	NA
Electrical resistivity (Ω·m) [10]	NA	NA	NA	1.7×10^{-8}	2.7×10^{-8}
Machinability (qualitative)	+++	+	+	+	+++
Variety in available shapes, size (qualitative)	+	++	+++	++	+++
Price (qualitative)	+	+++	+	+++	+

(a)

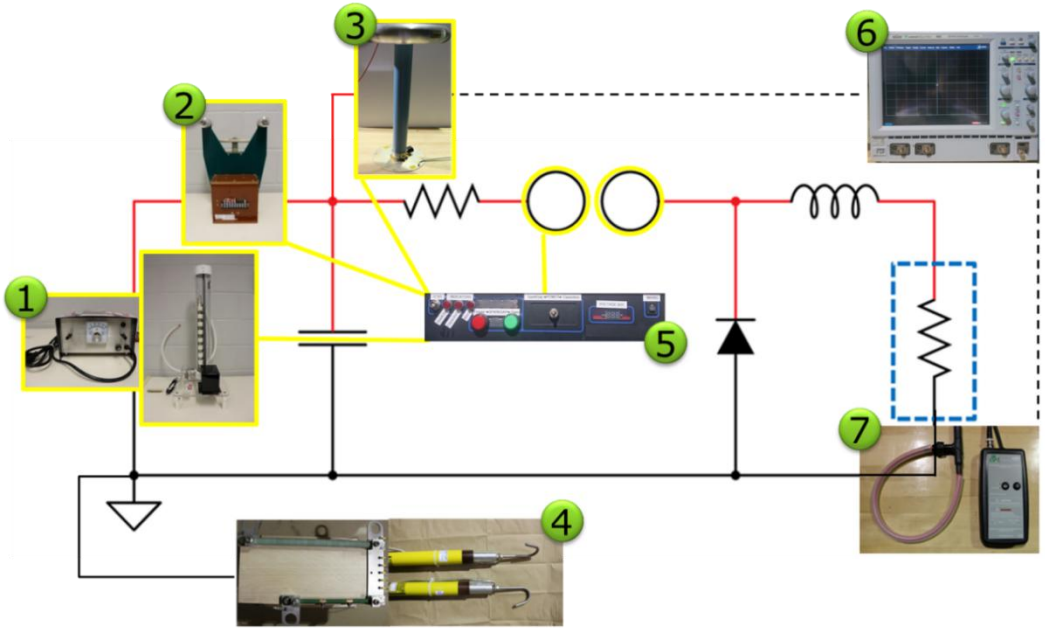

(b)

Figure 4.11: (a) Photograph of the actual emulator with inset showing the electrode configuration in the specimen holder. (b) Electrical circuit of the emulator showing the control and measurement components; 1: high voltage supply (voltage multiplier), 2: high voltage switch, 3: voltage divider (for voltage measurement), 4: grounding rods (with discharge resistance), 5: main control unit, 6: oscilloscope (data acquisition and visualization), and 7: Rogowski coil (current measurement)

The functional circuit of the emulator is shown in Figure 4.11(b); the instrumentation for operation and data recording are seen. At the heart of the control apparatus is a custom-built

control unit that houses the switches and indicators for the high voltage generator, the charging interrupter and the spark gap trigger. The control unit also includes voltage readout from the high voltage divider that is connected to the capacitors. This voltage can also be made available on the oscilloscope, and recorded along with the current monitored by the Rogowski coil for each test. Grounding rods connected to discharge resistors are available to manually discharge the emulator. Separate cameras with neutral-density filters were available to record the test in the form of a high-speed video and a long-exposure photograph. In addition to the standard measures, a number of additional security features were also obviously in place. Most importantly, the emulator is operated from outside the room in which it is housed to prevent any form of risk exposure to the operators; live feed of the emulator from four high definition (HD) video cameras was continually monitored during the entire test period. Exhaust vents were available to withdraw the ozone gas and any other combustion product generated by the electric arcs and partial vaporization of the sample.

To operate the emulator, the sample is clamped into the requisite fixture depending on the type of test, and the variable inductance is set to the required position. Then, the charging interrupter is first engaged and the high voltage supply turned on to charge the capacitors. Once the voltage readout displays the required voltage, the charging interrupter is disengaged and the sparkgap motor is turned on to trigger the arc. The tests waveforms are recorded on an oscilloscope. The capacitors of the emulator are completely discharged from their residual voltage with the help of the grounding rods before the sample is retrieved.

4.6 Demonstration of functionality

Figure 4.12 shows an oscilloscope graph of a ~50 kA current impulse applied on a typical sample of carbon-fiber reinforced polymer (CFRP). The damaged sample along with the ultrasonic and thermal non-destructive test results are seen in the inset, for the purpose of illustrating a typical test for which the emulator was designed. In this particular case, the impulse was produced by charging the capacitors to about 85 kV. However, for safety reasons relative to the small size of our room and following a recent notice from the manufacturer of the Scyllac capacitors used here (General Atomics), it is not recommended to not charge the capacitors above 70 kV, hence the following studies are limited to this maxima.

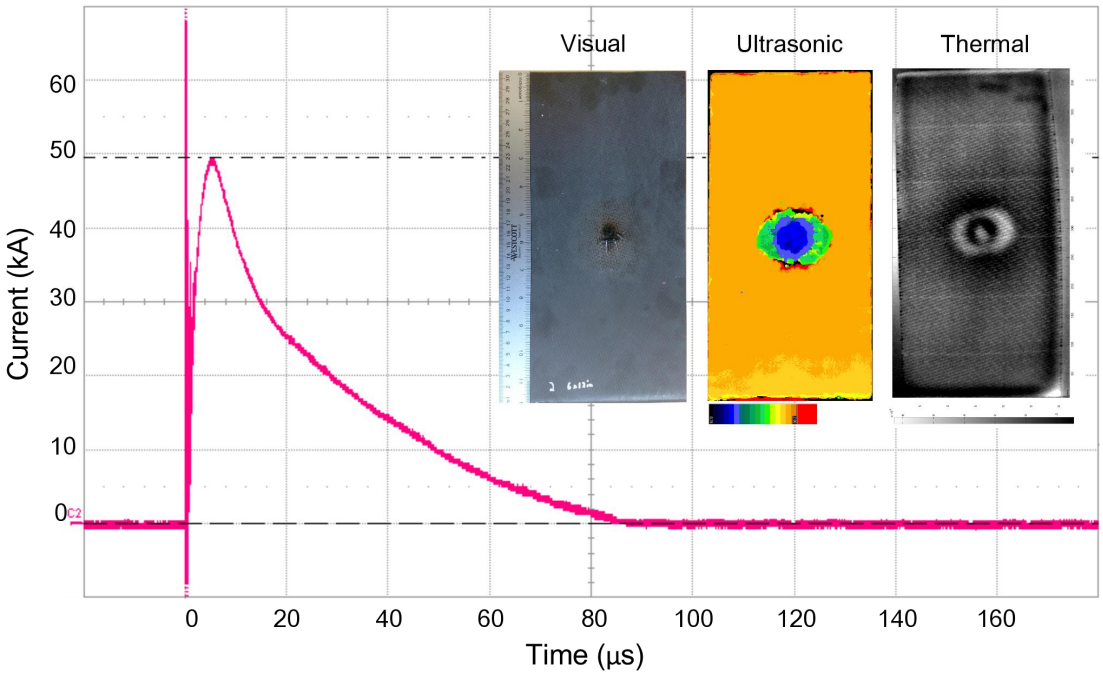

Figure 4.12: The oscilloscope image of a ~50 kA impulse waveform with test specimen subjected to different non-destructive analysis; Sample: CFRP, test type: arc-entry, variable inductance position: middle. (Oscillogram axes were modified for improved clarity)

The following sub-sections discuss the operational flexibility offered by the emulator. Two strategies exist on the emulator to regulate the waveform parameters. The voltage on the capacitors decides the peak current amplitudes. Figure 4.13 shows the short-circuit current (current waveform with no sample) with a peak amplitude of 10, 20 and 40 kA, achieved by varying the initial voltage on the capacitors. As discussed in Section 4.3, the variable inductance can alter the rate of decay and hence the shape of the waveform. This is shown in Figure 4.14. This affects the values of charge and action integral as shown in Table 4.3.

The color-matched data in the Table 4.3 shows that the emulator is capable of imitating the parameters of different lightning components A, A_h and D. When the variable inductance is completely detached from the system, the values of charge and action integral are closer to a scaled-down D-component and these values more than double at the maximum inductance of 2 µH provided by the variable inductance (position: down), where they show a greater resemblance to the scaled A-component. The table also shows that the emulator is more effective at representing the decay times as compared to the rise times.

It is important to deliberate the relevance of lightning tests with at reduced amplitudes. 50% of all lightning events (negative first stroke) have peak amplitude of 30 kA or more and just 5% of the lightning strikes have peak current more than 80 kA [2]. Thus, a capability to produce a peak amplitude of 40 kA makes this emulator highly versatile. In fact, an amplitude of 40 kA was largely employed as the maxima for the studies. Figure 4.15(a) shows a CFRP sample that has undergone an emulated lightning impulse with a peak current of 40 kA; the ultrasonic C-scan of the specimen is also shown. The key damage modes in the sample (fiber fracture, resin deterioration, and delamination) were also seen in other works at similar peak currents [11].

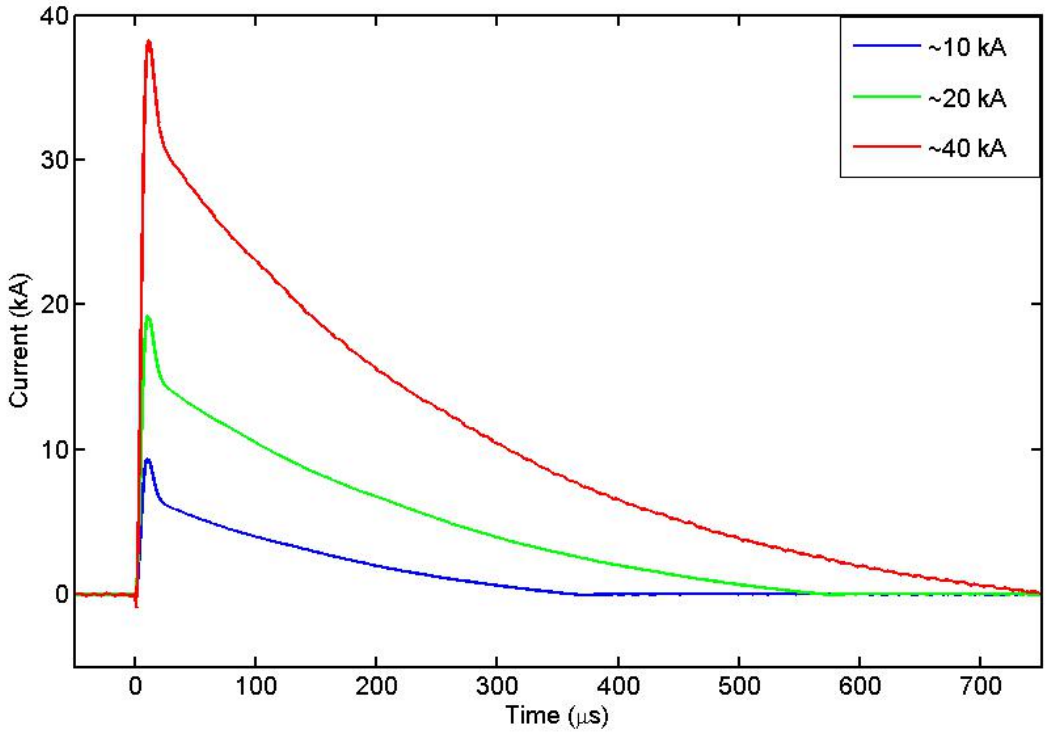

Figure 4.13: Impulse tests in a short-circuit configuration with varying peak amplitudes; Sample: none, test type: short-circuit, variable inductance position: middle

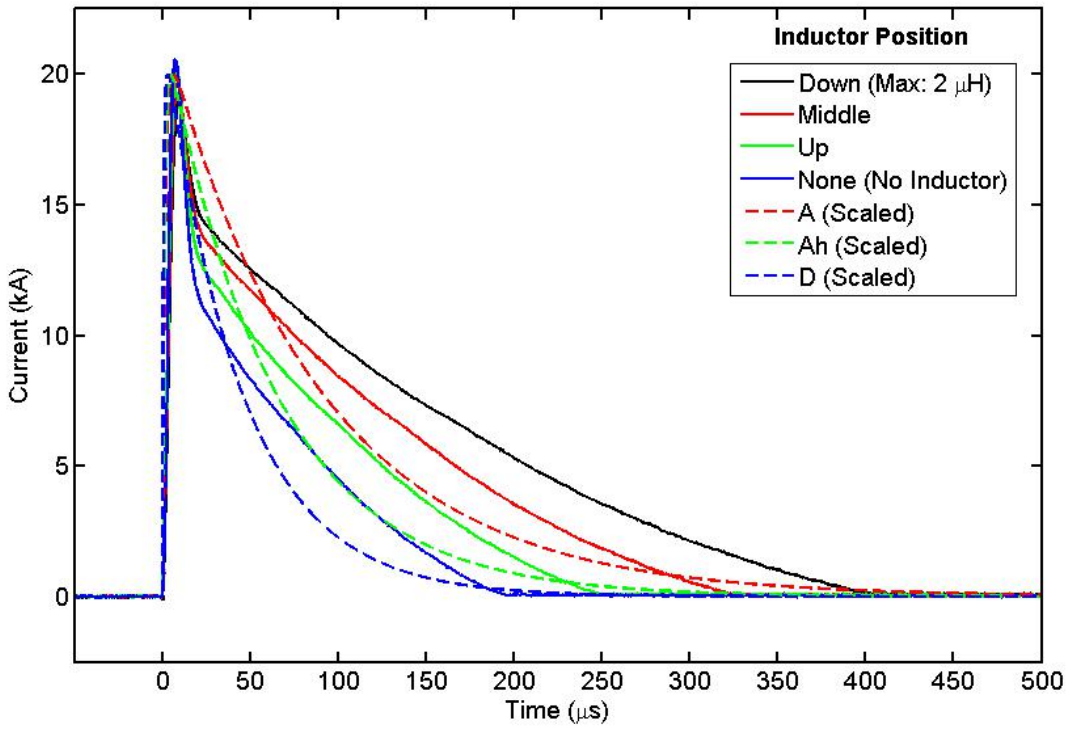

Figure 4.14: Comparison of emulated waveforms with varying values of inductance with scaled-down waveforms defined in SAE ARP 5412; Sample: aluminum plate, test type: arc-entry

Table 4.3: Comparison of waveform parameters achieved by the emulator to those from of standard waveforms

ightning Component/ Variable Inductance	*Peak current*	*Time to peak*	*Time to halve*	*Charge*	*Action integral*
	(i_{peak}) kA	*(t_1) μs*	*(t_2) μs*	*C*	*A^2s*
Maximum (Position: Down)	19.08	8.48	100.97	2.45	23449.67
Medium (Position: Middle)	19.79	7.86	75.70	1.97	18927.45
Minimum (Position: Up)	20.30	7.42	48.61	1.47	13862.53
None (No inductor)	20.74	6.94	29.25	1.09	10023.74
A-Component (Scaled)	20.00	6.36	68.96	1.89	19999.83
A_h-Component (Scaled)	20.00	4.72	49.04	1.34	14222.39
D-Component (Scaled)	20.00	3.18	34.48	0.95	10000.04

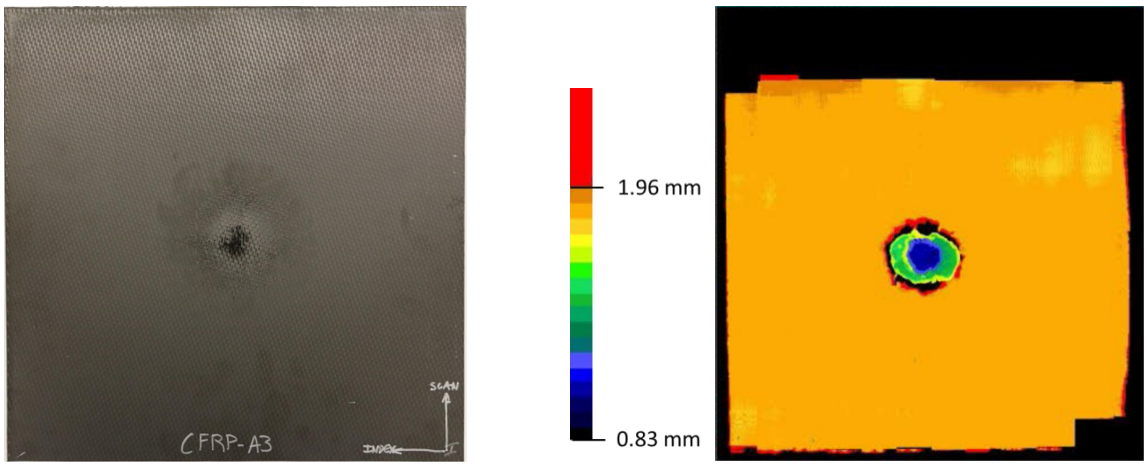

(a)

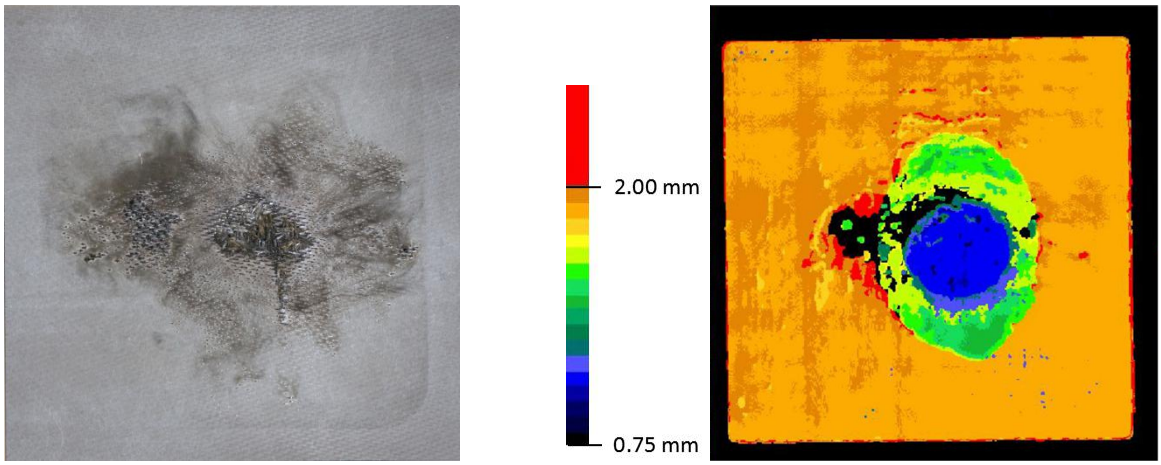

(b)

Figure 4.15: Photographic (left) and ultrasonic C-scan (right) images depicting the damage characteristics of CFRP panels subjected to (a) Scaled A-component impulse stroke of 40 kA (sample size = 30.5 cm × 30.5 cm) and (b) Full scale D, B and C* components in a single stroke (sample size = 22.5 cm × 22.5 cm)

Damage analysis is typically carried out using non-destructive test methods such as ultrasonic C-scans [12] or even eddy current testing [13]. An impulse emulator with the operational flexibility of this kind can not only be used to study conductive coatings, but also be applied to segmented lightning diverter strips [14], lightning arrestors [15], calibration of lightning sensors, and so on. An advantage of this system is that by decoupling the impulse and the continuous components, the users can pay attention to specific characteristics of the materials to tolerate the applied waveform. On the contrary, it is natural for this system to be limited in its ability to deliver a

complete (A-C/D components) or full-scale (up to 200 kA) lightning waveforms. Hence this emulator cannot be used to study the overall damage from lightning for certification tests. However, the retractable sample holder provides the flexibility to subject the sample to subsequent tests (e.g., continuous current tests) without disturbing the damage signature from the impulse test, or conduct damage assessments between repeated strikes.

It is natural to be inquisitive about damage characteristics from a complete lightning waveform. In the course of this research project, such a test was conducted in a certified laboratory (Lightning Technologies Inc., USA) at elevated parameters: full scale D, B, C*-components as defined in SAE ARP 5412 [2]. The result are presented in Figure 4.15(b). Similarly, at this stage, the focus is on lightning protection materials and the effect of geometry or current distribution in/through samples/systems cannot be studied with the equipment without further modifications to the emulator.

4.7 Conclusion

A detailed description of an impulse current emulator from the conceptualization to the testing stages has been provided. The emulator was designed to experimentally study the effects of lightning impulse stokes on protected and unprotected polymer composite panels with a peak amplitude of 50 kA. For this reason, the design greatly emphasized the need to adapt the emulator to test samples of different electrical conductivities and incorporate the flexibility to produce different types of tests (conducted current and arc-entry) and somewhat adjustable waveforms, with the help of a variable inductance in series with the sample under test. The waveform parameters produced with the emulator are in good agreement with the scaled-down values provided for the A-component impulse waveforms in the standards.

4.8 Acknowledgments

This work was funded under the NSERC CRIAQ COMP-502 project. The CFRP panels used in this study were provided by our industrial partner Bombardier (Aerospace) Inc., Canada. The authors thank Nicholas Veerabadren from the Electrical engineering department for his assistance in conducting the emulated lightning tests. The full waveform test at Lightning Technologies Inc., USA was arranged for by our industrial partner 3M Canada Company. The professional services

of Mekanic Inc. (Montreal, Canada) were utilized to verify and improve the mechanical designs of certain components.

4.9 References

1. Gagné, M. and D. Therriault, Lightning strike protection of composites. Progress in Aerospace Sciences, 2014. 64(0): p. 1-16.

2. International, S., ARP 5412 Aircraft lightning environment and relative test waveforms. 2005.

3. Warren, C., et al. Design and implementation of a portable lightning current simulator. in Plasma Science, 2000. ICOPS 2000. IEEE Conference Record - Abstracts. The 27th IEEE International Conference on. 2000.

4. Haryono, T., et al. The Design of A High Amplitude Impulse Current Generator. in High Voltage Engineering and Application, 2008. ICHVE 2008. International Conference on. 2008.

5. Walko, L.C., et al. Full scale lightning generation techniques for aircraft susceptibility evaluations. in Energy Conversion Engineering Conference, 1997. IECEC-97., Proceedings of the 32nd Intersociety. 1997.

6. Kind, D. and K. Feser, High-voltage Test Techniques. 2001: Newnes.

7. Kovalchuk, B.M., et al., Pulse generator with intermediate inductive storage as a lightning simulator. Review of Scientific Instruments, 2016. 87(6): p. 063505.

8. Rosa E.B., The Self and Mutual Inductances of Linear Conductors, Bulletin of the Bureau of Standards, 1908. 4(2): p. 301–344.

9. http://www.ga.com/series-c-high-voltage-energy-storage-capacitor

10. John R. Rumble, CRC Handbook of Chemistry and Physics, 98th Edition (Internet Version 2018), CRC Press/Taylor & Francis, Boca Raton, FL.

11. Hirano, Y., et al., Artificial lightning testing on graphite/epoxy composite laminate. Composites Part A: Applied Science and Manufacturing, 2010. 41(10): p. 1461-1470.

12. Fisher, F.A., J.A. Plumer, and R.A. Perala, Aircraft Lightning Protection Handbook. 1989: Federal Aviation Administration.

13. Szatkowski, G.N., et al., Electrical Characterizations of Lightning Strike Protection Techniques for Composite Materials. 2009.

14. Cline, J.D. (Fort Lauderdale, FL), Lightning diverter strip. 1980, Dayton-Granger, Inc. (Fort Lauderdale, FL): United States.

15. Haryono, T., et al. The Design of A High Amplitude Impulse Current Generator. in High Voltage Engineering and Application, 2008. ICHVE 2008.

CHAPTER 5 ARTICLE 2: DAMAGE RESPONSE OF COMPOSITES COATED WITH CONDUCTING MATERIALS SUBJECTED TO EMULATED LIGHTNING STRIKES

P. S. M. Rajesh, Frederic Sirois and Daniel Therriault*

Submitted to Materials and Design, July 2017

5.1 Abstract

Lightning strike protection (LSP) offered by different classes of conductive coatings deposited on carbon fiber-reinforced polymer (CFRP) panels was studied in three stages: (i) emulated lightning impulse strikes, (ii) conducted continuous currents, and (iii) physical aspects of lightning-coating interaction. Two types of coatings, hybrid and metallic, were studied. For hybrid coatings, composed of multiple material types, two material design schemes were considered: silver nanoparticles dispersed in conducting polymer PEDOT:PSS, and silver-coated carbon-nanofiber transferred onto an epoxy surfacing film. For the category of metallic coatings, continuous coatings of silver, and a composite of 10% copper in tin were considered. We evaluate the material design schemes of these two classes of materials with respect to the degree of protection offered to the composite substrates from the emulated lightning strikes. Two additional cases, CFRP with an epoxy surfacing film and a continuous coating of tin were also studied, while expanded copper foil (ECF)-protected and unprotected CFRP formed the reference materials. Continuous metallic coatings outperformed their hybrid counterparts, although none of the materials was comparable to ECF in terms of LSP performance. This work demonstrates the limitations of electrical resistivity and/or sheet resistance measurements to provide a reliable estimate about the performance of conductive coatings for lightning protection and the clear need for emulated lightning strikes for assessment.

KEYWORDS: Coatings, Composites, Current, Damage Analysis, Lightning, Resistance, Resistivity, Thermography, Ultrasonic.

5.2 Introduction

Traditionally, aircraft structures were mainly made of aluminium alloys — low-density materials that also possesses very low electrical resistivity. This combination of properties referred to as

'low specific resistivity' is measured using the formula: resistivity × density, $\Omega \cdot g \cdot cm^{-2}$. Lately, the aircraft industry is progressively relying more on fiber-reinforced polymer (FRP) to produce lightweight, fuel-efficient aircraft [1]. However, as polymers are electrically resistant, the complete replacement of metals has not been possible. The latter find application in the form of foils and meshes for lightning strike protection (LSP) and shielding from electromagnetic interference (EMI) [2] among others, undermining the very benefit of lower weight offered by FRP. The scientific community has been active in its research for materials with lower specific resistivity [2]. Application of composite/hybrid material strategies to realize superior specific electrical properties is a natural line of thought for the aircraft industry. Replacing foils/meshes that are integrated into the structure during composite manufacturing by externally-applied coatings has practical advantages covering the entire life-cycle of such "green" aircraft structure. Production: Usually the metallic meshes are co-cured with the composite; the absence of the former would simplify the composite cure cycle (manufacturing process). Application: The primary advantage of low specific-resistivity coatings is the weight-saving arising from the replacement of metallic-meshes (and isolation plies where used), leading to increased fuel efficiency and lower emissions. Service: Externally applied coatings improve accessibility which is critical for fast and effective repair/maintenance. Disposal/recycling: This sustainable design of materials allows for easier separation of the metal from the polymer composite. Such segregation is critical for safe disposal and/or effective recycling. Many of these advantages are also true for externally-applied continuous metallic coatings.

Hybrid materials such as nickel-coated single-walled carbon nanotubes [3], carbon nanofiber – nickel nanostrand mixtures [4], carbon fiber coated with indium tin oxide nanoparticles [5], and others have been investigated for LSP. Given the complications involved in modeling and simulation approaches, experimental studies are employed as a means to reliably study the LSP performance of different conductive materials. Usually, the performance of coated FRP against lightning strikes is compared to their unprotected counterparts (substrate FRP) [3] or the same/ similar coating material produced with different process or fabrication parameters [4-5]. Moreover, as test programs do not share the same scope, hardware and/or (damage) evaluation techniques, a comparison of results from different studies cannot be satisfactorily realized. Thus, certain important questions about different conductive materials remain unanswered: (i) What is the reliability of hybrid materials vis-à-vis metals for LSP?, and (ii) How do different materials

design strategies compare? At the same time, given the advancements in manufacturing techniques such as cold-spray and sputtering, it is also interesting to evaluate continuous metallic coatings as a LSP strategy. This know-how can then be transferred to coat other classes of materials. For example, cold spray of hybrid materials or sputtering of metallic composites can be envisaged. With a view to open a scientific discussion on the stated questions while presenting an approach to test the LSP of different conductive materials in the laboratory, eight different conducting materials were subjected to controlled lightning tests and the damage analyzed via non-destructive methods.

Silver has the lowest electrical resistivity among metals (9.53×10^{-8} Ω·m) [2] and offers good corrosion resistance. Thus, silver-based materials were chosen as the primary LSP candidates for this study. Lightning protection offered by two hybrid formulations: (i) silver nanoparticles dispersed in conducting polymer poly(3,4-ethylenedioxythiophene) polystyrene sulfonate abbreviated as PEDOT:PSS (silver-polymer/Ag-P), and (ii) silver-coated carbon nanofiber (silver-carbon/Ag-C), was compared to (iii) pure silver (silver/Ag). These three materials represent the cases of 0D, 1D and 2D metallization respectively at the micro-scale (and discussed in the Results and Discussion section). While the conducting polymer matrix provides electrical continuum in the silver-polymer nanocomposite coating, the employment of high aspect-ratio metallized nanofibers allow for the formation of a percolation network, i.e. a network of electrically conducting pathways in the silver-carbon hybrid. Pure silver was also deposited onto CFRP to produce a continuous metallic coating. On the other hand, the copper-tin (Cu\Sn) composite and tin (Sn) LSP materials were powder coatings of tin consisting 10% and 0% copper, respectively. CFRP (with no lightning protection) and expanded copper foil (ECF)-protected CFRP formed the (lower) baseline and upper protection threshold for this study, i.e, these two materials defined the range of damage/protection possible within the set of specimens chosen for the study.

Lightning protection tests are typically carried out by subjecting the test sample to the standardized lightning current waveform [6]. The standard lightning waveform (Figure 5.1) is divided into 3 components A, B and C, where B can be considered as a transitory component between A and C. This waveform is usually followed by another stroke D, which is akin to component A but with a lower peak current. Each component represents a set of physical

phenomena occurring during the lightning strike. Although in practice, these currents are sequentially applied to the sample in a single pulse, the study presented herein utilizes different systems to separately emulate the lighting impulse (scaled A-component) and continuous current components, C. Lightning impulse damage was studied via ultrasonic non-destructive evaluation (NDE), while the affect of lightning continuous currents was recorded in the form of voltage response of the coatings in addition to performing real-time thermography.

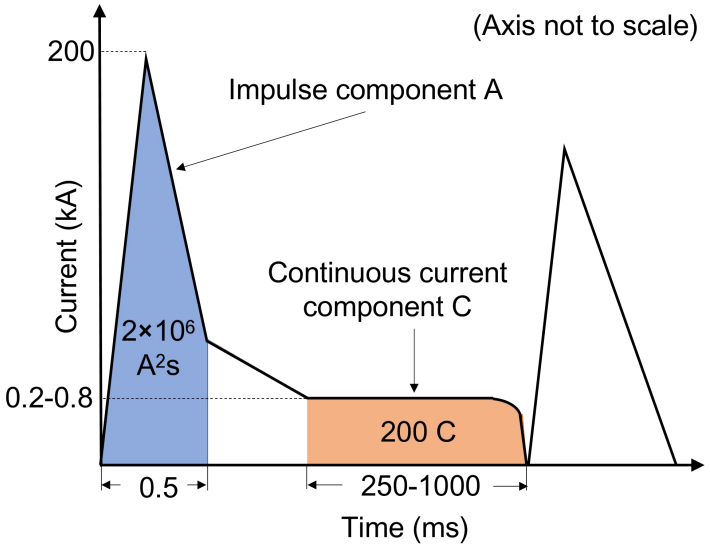

Figure 5.1: Typical current waveform used for lightning direct current effects testing [5]

5.3 Materials and methods

5.3.1 Composite and coating materials

CFRP: The substrate for all the specimens in this study was $(0/90)_{2S}$ carbon-epoxy composite composed of Cycom 5276-1 resin / 8HS carbon fiber weave. The panel was approximately 1.65 mm thick with no coating or surfacing film.

ECF-protected CFRP: ECF (0.020 g/cm^2) overlaid with Cytec Surface Master 905 surfacing film for environmental protection (SF, 0.017 g/cm^2) is co-cured with the CFRP substrate to produce samples that form the upper threshold of performance in this study.

Conductive coatings: Table 1 provides details on the material processing and manufacturing technique coatings that were deposited on the CFRP panels. The coated specimens have no

surfacing film except in the case of Ag-C. The physical and electrical properties of the coatings are also mentioned.

Table 5.1: Manufacturing details and properties [10] of conductive coatings utilized for lightning strike protection

Coating	*Fabrication process*	*Density* ($g \cdot m^{-3}$)	*Avg. 4-point probe resistivity* ($\Omega \cdot m$)
Ag	Electroless plating; sintered in vacuum for 6 h at 120 °C [7]	10.5	0.3
Ag-C	Vacuum-assisted transfer of Ag-C particles onto b-stage epoxy surfacing film. This film is placed over CFRP and cured under vacuum at 150 °C [8]	2.4	0.9
Ag-P	Spray coating of silver nanoparticles dispersed in PEDOT:PSS; annealing at 200 °C for 10 min.[9]	1.7	28.5
Cu\Sn	Cold-spray of 10%copper-tin powder with a gas temperature of 300 °C and a pressure of 60 psi [10]	7.5	(not available)
Sn	Cold-spray tin powder with a gas temperature of 300 °C and a pressure of 70 psi [11]	7.3	0.24 (60 psi)

5.3.2 Testing and damage analysis for assessment of lightning protection

All specimens were tested with no special preparation except for Ag-C and ECF. In order to ensure good contact with the electrode frame (discussed in the following paragraph), the Ag-C specimen was produced with 2.54 cm-wide strips of copper mesh at the four edges of the specimen. Except for a narrow overlapping zone, no conducting material was present under the copper strips. For the ECF specimen, the surfacing film was sanded down for the same width until the ECF became visible. Given the developmental nature of this project within which this study is carried out, the number of samples available for evaluation was limited and thus was distributed between lightning impulse and continuous current tests. A given coating was submitted to continuous current tests only in the event of composite substrate not being damaged during the impulse tests. Although the physical aspects (damage progression) of lightning coating damage were studied in conjunction with the lightning tests, they are discussed separately with the case of Cu\Sn as an example. With respect to test modes, while impulse current tests were performed in the more severe arc-entry mode to accommodate the conditions

of high arc temperatures and shockwaves, continuous current tests were limited to the conduction mode, i.e. the current was distributed through the entire width of the sample with clamped electrodes instead of the center of the specimen via an arc (arc-entry mode) or pointed electrode in contact (injection mode). The severity of the test was downgraded in the continuous current tests for two reasons. It was anticipated that the low-melting point coatings such as Cu\Sn and Sn would not be able to withstand the lightning C-component which is responsible for melting effects in metals. Also, the available power supply was limited in its voltage range of 0 -10 V.

Lightning impulse emulation: The lightning impulse emulator used in this study is based on capacitive storage and was designed and built by the authors [7]. The lightning emulator and the typical impulse waveform (for CFRP) utilized in this study are shown in Figure 5.2(a & b). For the impulse tests, samples were clamped under a metallic frame that formed the negative (ground) electrode and the arc was struck via a pointed striker (positive electrode) fixed above the center of the sample at a height of 6.4 mm (see inset in Figure 5.2(a)). The emulated A-component impulse waveform had a peak amplitude of 40 kA. Specimens of size 30.5 cm × 30.5 cm (effective area after subtracting area under electrodes: 25.4 cm × 25.4 cm) were utilized for the tests.

Ultrasonic inspection: Ultrasonic phased-array pulse-echo technique was employed to characterize the damage in the composite panels subjected to lightning impulse tests. The panels were immersed and clamped in a water tank for scanning. A 5 MHz probe (LM-5MHz, Zetec) with 64 elements (active aperture: 16 elements corresponding to an area of 38.4 mm × 10 mm) mounted in a holder and connected to the ultrasonic test system (Topaz 32/128 PR, Zetec) was used to scan the rear surface (CFRP side) of the panels. The holder separated the probe from the sample surface by a constant distance of 110 mm. The received signal was color-coded according to the echo positions or the amplitude to generate the time-of-flight or amplitude C-scans, respectively.

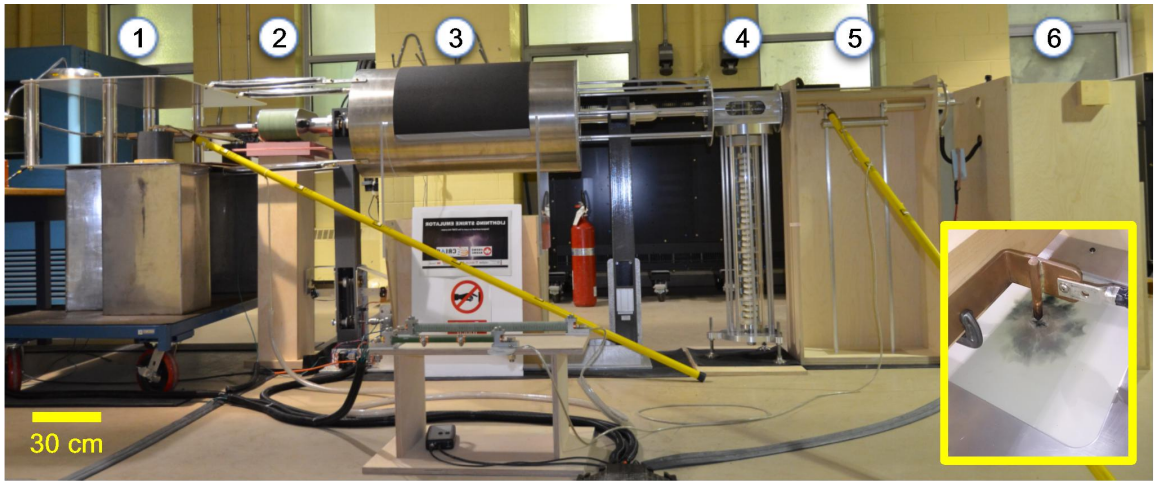

(a)

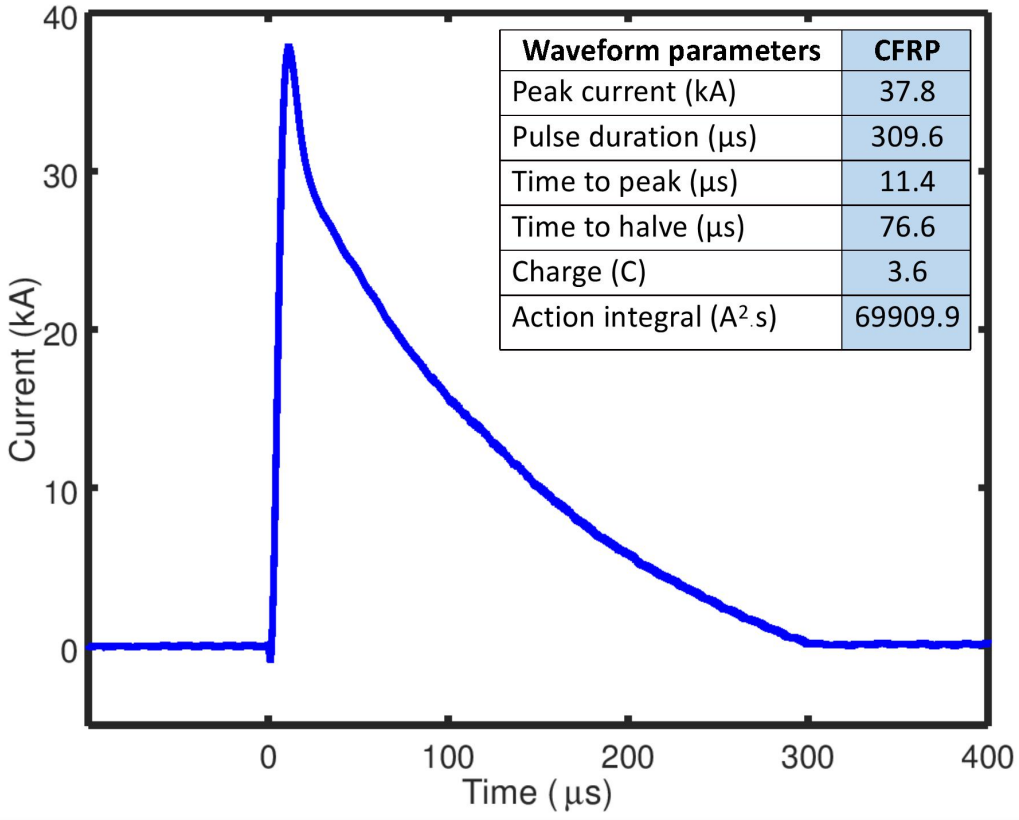

(b)

Figure 5.2: (a) Lightning impulse emulator; 1: capacitor bank, 2: damping resistance, 3: spark gap, 4: column of diodes, 5: variable inductance, 6: test chamber; Inset: Sample holder showing ECF clamped under under an aluminum electrode frame (negative electrode) and copper striker (positive electrode) over its center, and (b) Filtered impulse current waveform for CFRP with estimated parameters

Lightning continuous current emulation: A 5000 W power supply (Lambda EMS 500-10-D-RSTL) was used for the continuous current tests. The schematic of the test setup is shown in Figure 5.3. Composite panels of size 30.5 cm × 12.7 cm (effective area after subtracting area under electrodes: 25.4 cm × 12.7 cm) were subjected to 200 A of current for 1 s to realize a 200 C charge transfer. A LabVIEW® program was used to both control the power supplies and record the current (PR 430 probe) and voltage (voltage taps on specimen, high-frequency noise filtered) data. A National Instruments data acquisition card (NI USB 6211) was used as the interface between the measurement setup and the computer.

Thermography: A thermal camera (T 420, FLIR) was used for real-time thermography during the continuous current emulation. While the coating surface directly faced the camera, thermal reflection of the sample rear (CFRP side) in a protected aluminium mirror (ME8S-G01, Thorlabs Inc.) was used to monitor the heating of the composite substrate. The emissivity of the camera was set to 0.95. Other inputs on local conditions (temperature, humidity, measuring distance and so on) required for the measurements were fed into the camera.

Electrical properties of coating

The sheet resistance of coated coupons were measured. The voltage response was recorded while passing an ambient current (I, A) of 5 A each for 1 s through the specimen coating using a test setup similar to that employed for the lightning continuous current emulation, although a different power supply, Lambda EMS 33-150-D-RSTL), was used. The size of the coupon was 12.7 cm × 1.27 cm (8.9 cm × 1.27 cm subtracting area under electrodes) as shown in the inset of Figure 5.3. Voltage taps were placed symmetrically about the center of the sample separated by a distance, l, equal to the sample width, w, 1.27 cm. The recorded voltage (V, V) in conjunction with the specimen dimensions was used to compute the sheet resistance (R_s, $\Omega \cdot \square^{-1}$) using Equation 5.1:

$$R_s = \left(\frac{V}{I}\right)\left(\frac{w}{l}\right). \tag{5.1}$$

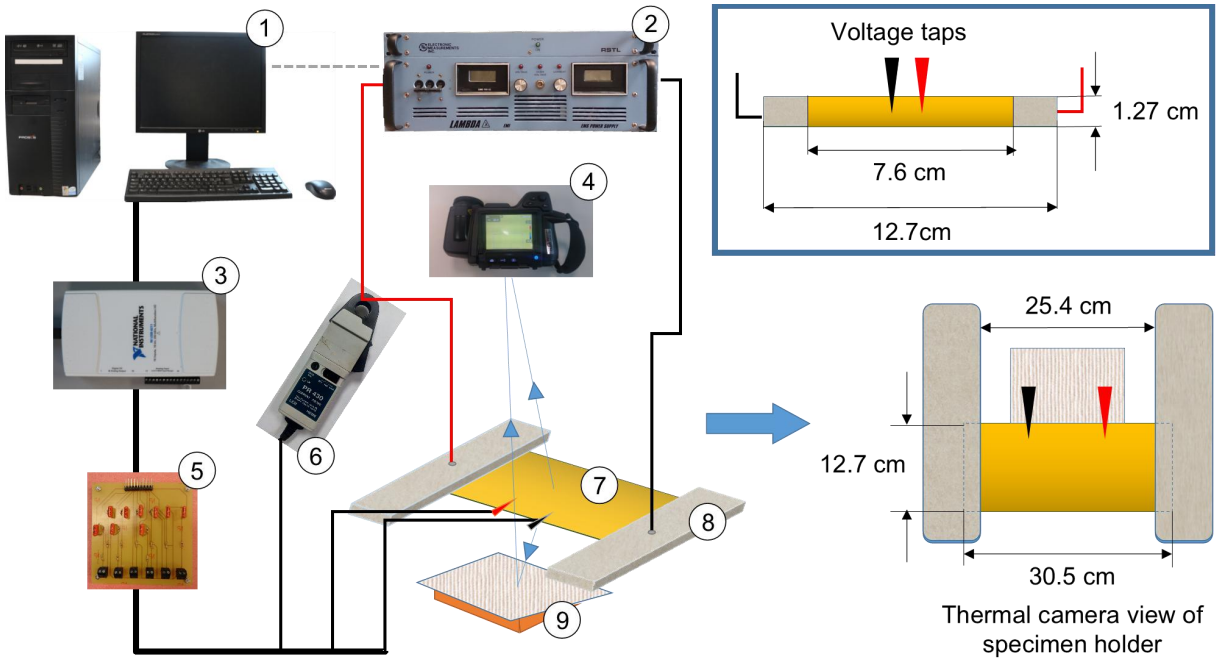

Figure 5.3: Schematic of test setup for lightning continuous current emulation: 1: Computer with LabView® software, 2: Power supply, 3: Data acquisistion card,4: Thermal camera, 5: Signal filters, 6: Current probe, 7: Specimen under test, 8: electrodes, 9: Infrared mirror; Inset: Schematic of test specimen used for ambient-current sheet resistance measurements

5.4 Results and discussion

Six different specimens, Ag, Ag-C, Ag-P, Cu\Sn, CFRP (no coating) and ECF were subjected to emulated impulse strikes corresponding to the A-component waveform with a peak current of approximately 40 kA. The photographs of the specimens post lightning strike tests are presented in Figure 5.4. Based on the type of visible damage, the specimens can be grouped into two categories: (i) Ag-P, Ag-C and CFRP showing damage to the composite substrate in addition to the coating (where applicable), and (ii) Ag, Cu\Sn and ECF showing coating damage only, although Ag shows some resin damage revealing the intact carbon fibers underneath and damage in ECF was almost completely limited to the surfacing film. Ag-P and CFRP samples appeared the most damaged, while the Ag coating was damaged as far as 8 cm from the point of strike, the largest among the tested specimens. While all the specimens had a single central damage zone, the Ag-C specimen showed extra-central damage at four additional locations surrounding the point of strike.

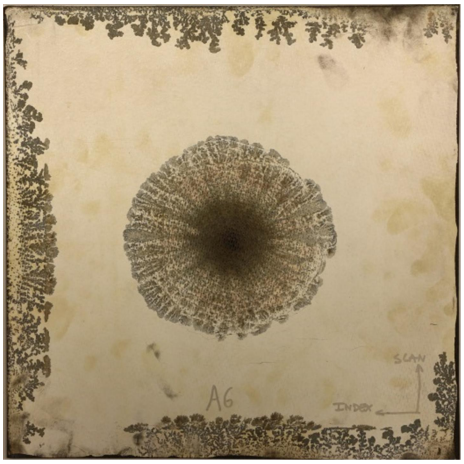

(a) Ag

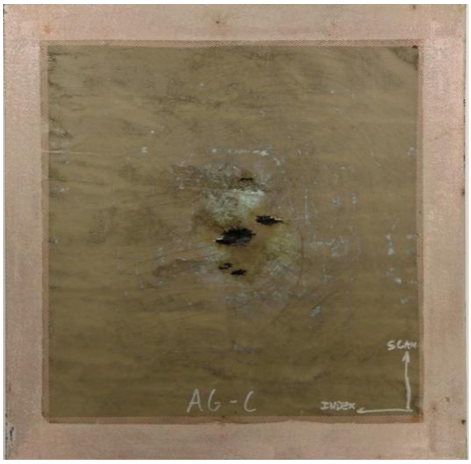

(b) Ag-C

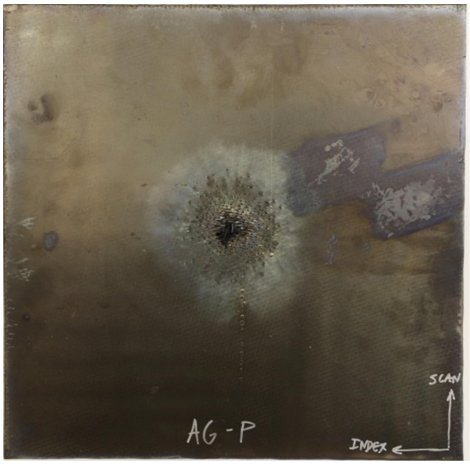

(c) Ag-P

(d) Cu\Sn

(e) CFRP (no coating)

(f) ECF

Figure 5.4: Photographs of the coated composite panels after undergoing 40 kA lightning impulse strike; sample size is 30 cm × 30 cm

Internal damage was studied using ultrasonic inspection. Figure 5.5 shows the time of flight C-scan images of the tested specimens. The time taken for the ultrasound pulse to reflect at a material(-air) interface is utilized to identify the echo positions in the thickness direction, which is then graded into different colors. As the panels are scanned from the rear surface, the farthest echo returns from the undamaged front surface (red color in the scale) while the closest echo from the deepest point within the damage zone (darkest shade of blue in the scale). The estimated maximum damage area and depth are presented in Figure 5.6(a) and (b), respectively. As expected, ECF (max. area: 1886 mm^2 of surfacing film) and Cu\Sn (max. area: 1353 mm^2 of the coating) were limited to surface damage only. However, the Ag specimen showed considerable internal damage to the composite (max. area: 1886 mm^2, depth: 0.75 mm), although lower than of CFRP (max. area: 2139 mm^2, depth: 0.83 mm). Interestingly, Ag-P (max. area: 2142 mm^2, depth: 0.94 mm) and Ag-C (max. area: 2758 mm^2, depth: 1.31 mm) showed more damage than baseline CFRP. While metallic coatings performed better than their hybrid counterparts, two important questions arise: (i) why/why not did each of the material design strategies succeed in offering LSP? and (ii) Why Ag-P and Ag-C were damaged more than the baseline CFRP in spite of their low resistivity?

All three silver-based coatings, Ag, Ag-P and Ag-C possess resistivity values orders of magnitude better than CFRP (see Table 5.1). Schematics of the microstructures (material designs of coatings) of the three specimens are shown in Figure 5.7. Although Ag-P is loaded with silver nanoparticles (Figure 5.7(c)), it is the polymer PEDOT:PSS with a resistivity on the order of 10^{-5} $\Omega \cdot m$ [9] that forms the matrix and is not comparable to metals in terms of electrical resistivity. This leads to Joule heating with higher currents; polymers are easily susceptible to thermal damage and the conducting properties of the coating is quickly degraded. Ag-C uses percolation of 1D fibers to form an electrically conducting network as illustrated in Figure 5.7(b). Such a design strategy can witness weak connections (ineffective sintering) and/or limited percolation (insufficient loading) that degrade performance. Common to both Ag-P and Ag-C composite/hybrid material-based strategies are challenges such as aggregation of the nano-sized particles or fibers. In the Ag coating (Figure 5.7(a)), the large network of grain boundaries ensuing from the coating's nanocrystalline morphology resists the flow of current. This generates sufficient amount of heat to quickly evaporates the thin (<5 μm) coating. It is interesting to

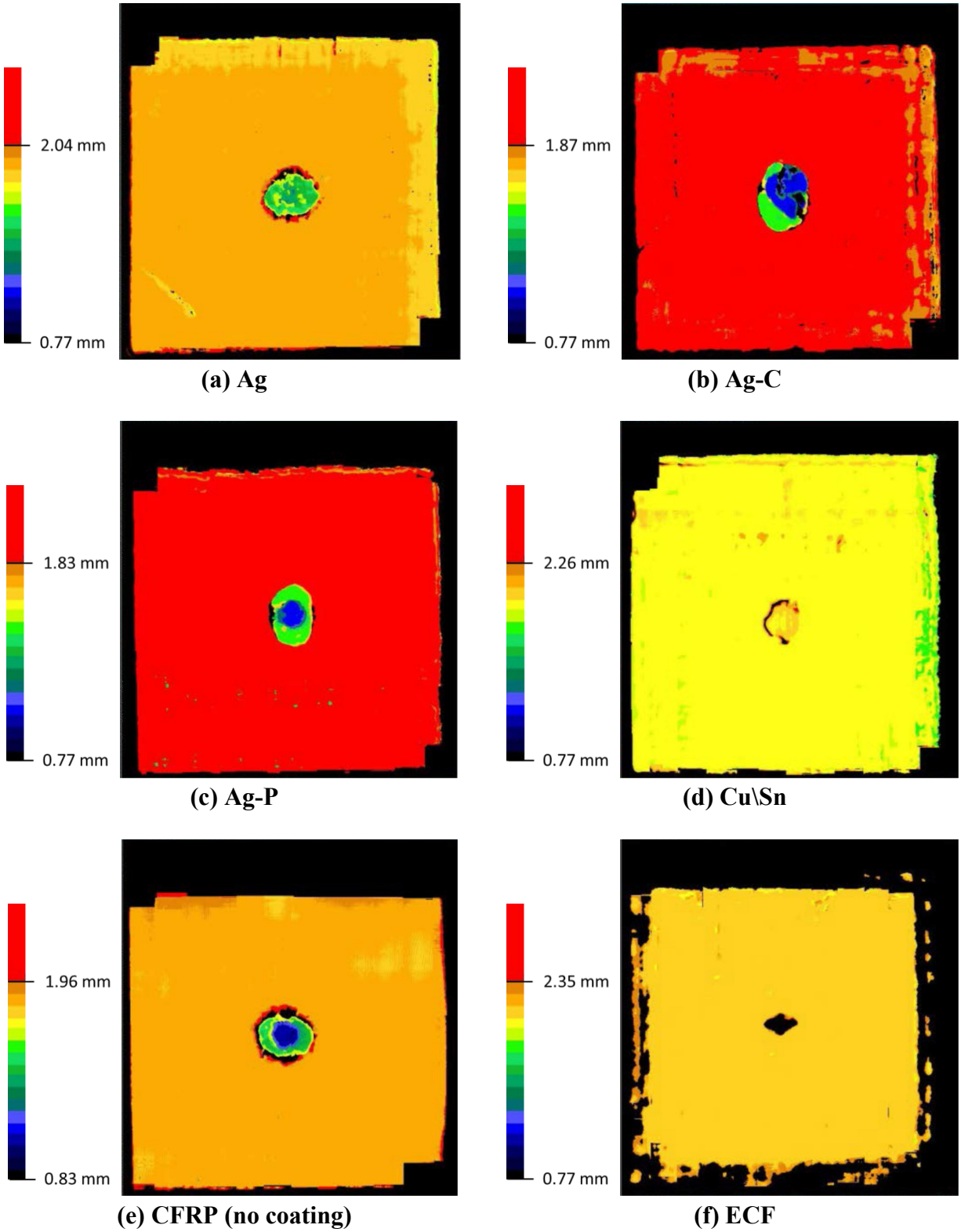

Figure 5.5: Ultrasonic C-scan (time of flight) images of the coated composite panels after undergoing 40 kA lightning impulse strike

observe from Figure 5.8(a) that the coating damage manifested in a Lichtenberg pattern [12]; a test with a multimeter (Fluke 87 V) found that this dark pattern was non-conducting. On the other hand, the continuous metal coating Cu\Sn even with a higher resistivity performed on par with ECF in protecting the underlying CFRP. Although tin (the matrix) has a relatively low melting point of 505 K compared to 1356 K of copper [13], and specific heat of 0.21-0.24 compared to 0.39 kJ·kg·K for copper [14], with at least 14 times higher mass of conducting material compared to the ECF, the copper-tin material could absorb the thermal energy before beginning to melt away. Moreover, with the addition of copper to tin, the net electrical and thermal properties of the composite could be expected to improve.

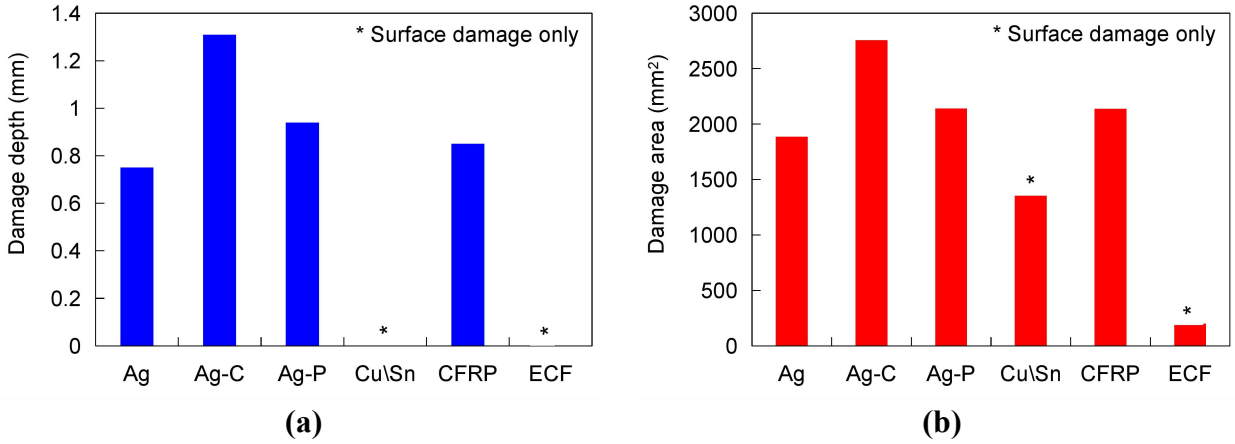

Figure 5.6: Damage characteristics of the samples derived from ultrasonic C-scans: (a) Maximum damage depth, and (b) Maximum damage depth

To summarize the earlier discussion, for a coating material to be employable as a LSP material, it must be able to withstand the high current densities without significant thermal damage. The tests and associated results discussed in the previous paragraphs are not intended to provide a holistic assessment of a design strategy but only to present the associated challenges and/or opportunities. It is reasonable to hypothesize that by varying loading, sintering parameters and/or modifying techniques to attain dispersion, percolation and/or changing the overall amount of conducting material, the performance extracted from each of these strategies could be largely enhanced.

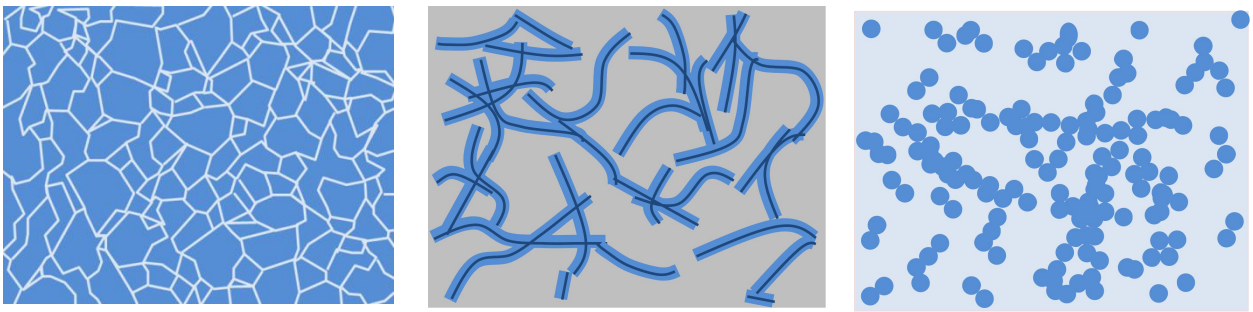

(a) **(b)** **(c)**

Figure 5.7: Schematics of material design at the microstructural level for the three silver-based LSP coatings: (a) Ag, (b) Ag-C and (c) Ag-P (The size and volume fraction of grain boundaries and conductive fillers are not representative of the true values)

Another difficult question pertains to why Ag-P and Ag-C are more damaged than baseline CFRP. Commencing the discussion with Ag-P, the use a thin coating with low-conductivity polymer PEDOT:PSS as the matrix can be assumed not to have a dramatic influence on the conducting/insulating properties of the composite surface. It must also be cautioned that maximum damage area and depth of Ag-P and CFRP are also close enough to be within the margin of experimental error. In the case of Ag-C specimen with silver coating on (graphitic) carbon nanofibers, it is reasonable to believe that this coating is indeed partially conducting with respect to the lightning currents. We hypothesize that the lightning currents are injected (distributed) into a composite over a larger area as the coating succumbs to Joule heating. This extends the boundaries of delamination resulting from resin deterioration and subsequent ejection of gases from the charring resin. On the other hand, the surfacing film possibly arrests the ejection of the gases forcing them broader and deeper into the composite. This could also explain the intriguing damage signature in the Ag-C specimen. It is believed that the extra-central regions of damage are indeed weak spots generated in the composite and/or surfacing film through which the gases vent out.

In order to test the hypotheses presented for the Ag-C sample, an equivalent surfacing film-clad CFRP specimen (SF) but without conducting material was prepared and tested with the same 40 kA impulse waveform employed throughout this study. Figure 5.8(b) shows that the SF specimen also demonstrated extra-central damage similar to the Ag-C specimen although these regions were closer to the center and less blemished. Concurrently, the damage to the center seemed

comparatively invasive in the SF specimen, which is expected because of the concentration of the current at the center. This damage signature supports that our hypothesis with regard to the Ag-C specimen was indeed plausible and that the surfacing film could add to the damage unless used in conjunction with a superior LSP material.

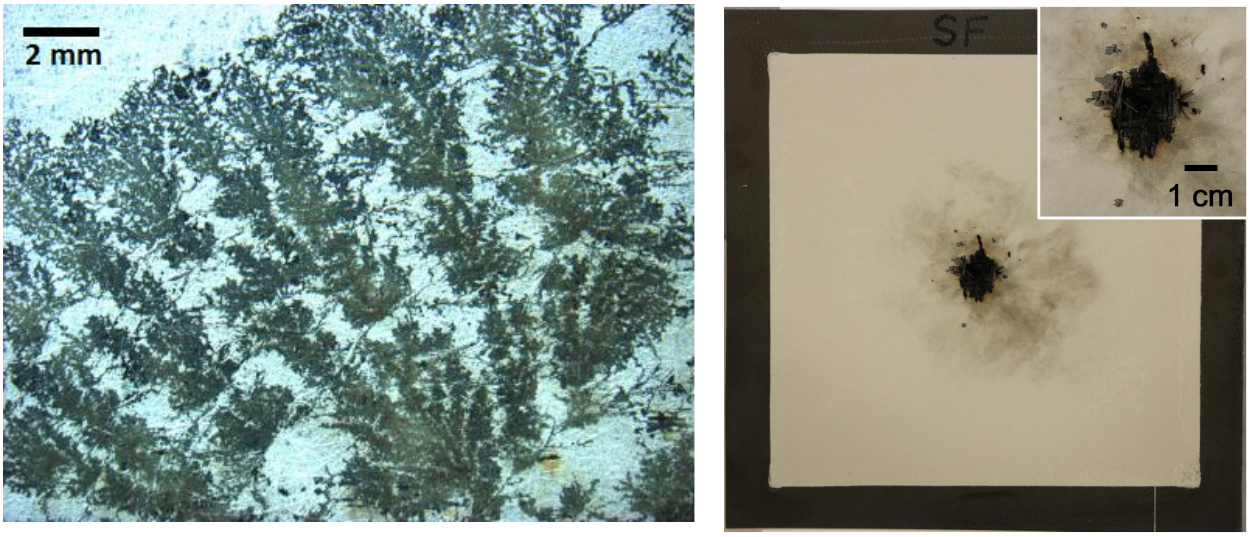

(a) **(b)**

Figure 5.8: Damage behavior of (a) Ag showing Lichtenberg pattern [12], and (b) SF showing extra-central damage; inset: magnified view of damage; sample size is 30 cm × 30 cm

Continuous metallic coatings, with exception to Ag, protected the composites from the emulated impulse strike. As Cu\Sn coating performed satisfactorily against light impulse currents with just 10 wt.% loading of copper, a tin-only coating (Sn) was also included into the test program for comparison. ECF, Cu\Sn and Sn specimens were subjected to continuous currents of 200 A for 1 s. The voltage response is shown in the Figure 5.9. ECF sample showed a low resistance of 0.17 $m\Omega \cdot cm^{-1}$. Sn, on the other hand, showed an even lower resistance of 0.12 $m\Omega \cdot cm^{-1}$. This could be explained by the large thickness of the coating which is also spread all over the entire surface specimen unlike the mesh-like copper foil. Cu\Sn was found to be more resistive 0.33 $m\Omega \cdot cm^{-1}$ than the Sn coating. This higher resistance is possibly because the Cu\Sn coating was discontinuous towards one of the edges (manufacturing defect), decreasing the effective area of cross-section of the coating. Adding to that, the coating of the Cu\Sn specimen was thinner than the Sn. It was found that the resistance of all the three materials marginally increased after current injection: ECF: 1.76%, Cu\Sn: 2.26%, and Sn:1.9%. In addition to the electrical measurements, real-time thermography was employed to provide the following information: (i) Specimen defects:

absence of Joule heating at the lower edge the Cu\Sn specimen (Figure 5.10(a)) allows for the identification of coating discontinuity through thermal snapshots presented; the photograph of the sample is also shown. (ii) Instrumental flaws: Figure 10(b) shows hot-spots in Sn specimen close to the electrodes possibly arising due to non-uniform clamping. (iii) Current distribution: It can be seen from the thermal reflections in the IR mirror, Figure 5.10(b), that the CFRP substrate of the Sn specimen actually heats up (due to thermal conduction) approximately 2 s after the current injection. This delayed heating (conducted through the composite) allows to conclude that the current is flowing through the coating and does not enter the CFRP, meaning that the Sn coating is indeed able to handle the current density.

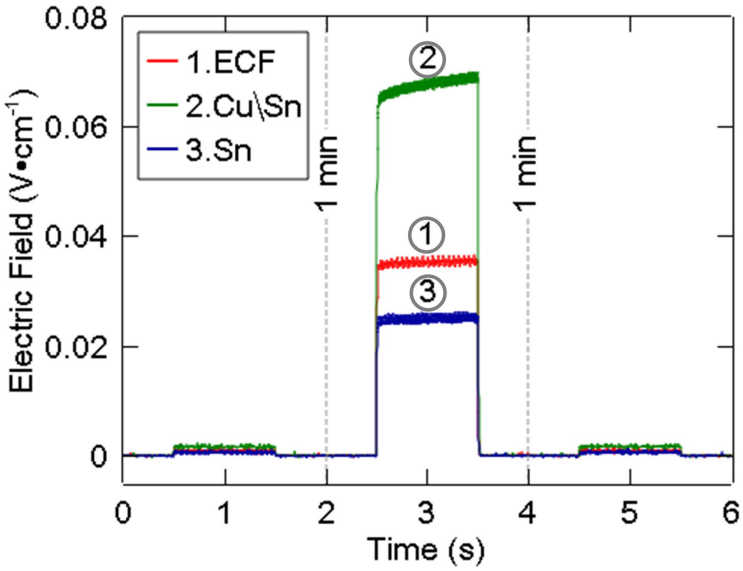

Figure 5.9: Voltage response of coated specimens to conducted continuous currents (charge transfer: 200 C)

Damage protection offered by the coatings to the underlying composites is an important criterion to recommend a conductive material for LSP purposes. Even so, it is also important to simultaneously study the physical aspects of the material –lightning interaction. Naturally, it is expected of any LSP candidate to sustain a lightning strike and continue to offer protection from multiple events. This would otherwise translate into a repair and maintenance burden for the airline. Cu\Sn and ECF offered protection to the underlying composites from lightning impulse strikes. High frame-rate photography employed during the lightning impulse test on Cu\Sn specimen (snap shots shown in Figure 5.11) showed hot metallic fragments flying away from the

strike zone. While such a behavior could also be expected from the Sn coating, it was not seen with ECF. It is anticipated that the combination of Joule heating in the coating softens the low-melting point coating which in parallel is shattered by the acoustic shockwave and the fragments of the coating are strewn away from the point of arc in an explosive fashion. A higher degree of damage may be expected with higher current amplitudes and must be viewed in terms of the

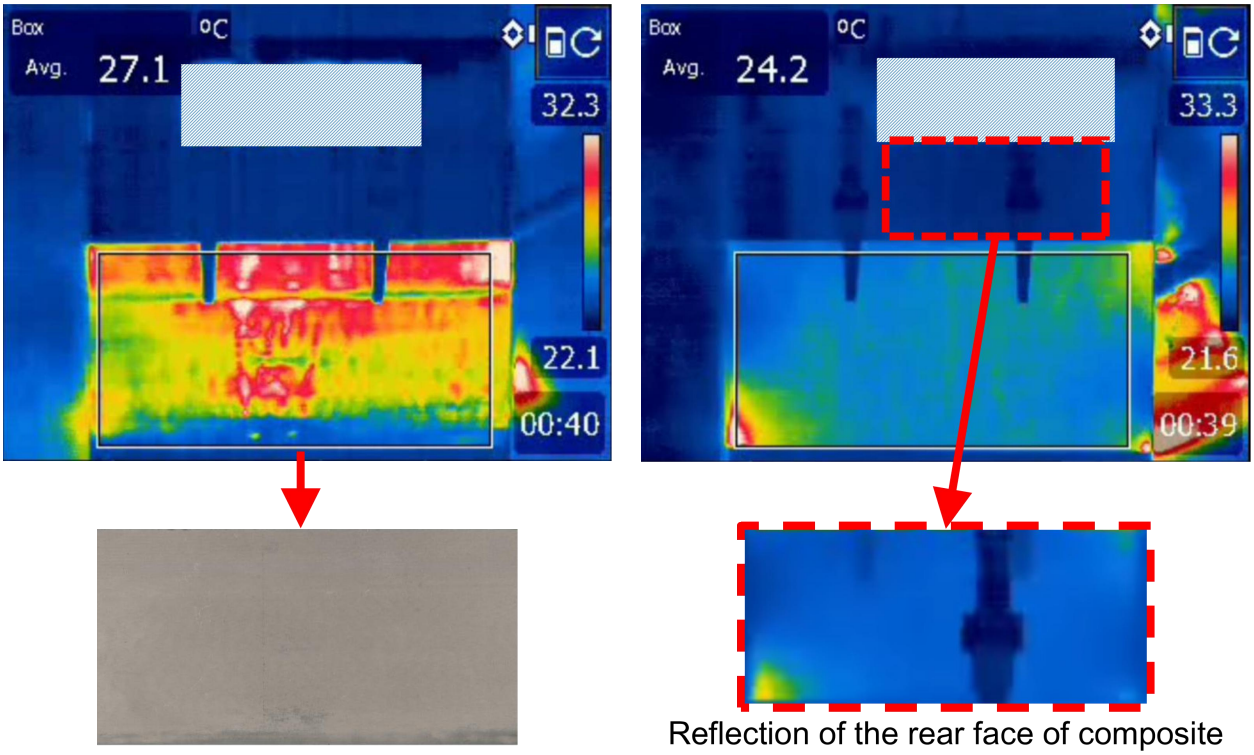

Figure 5.10: Thermal images (maximum temperature) during continuous current test of (a) Cu\Sn showing coating defects with a photograph of the specimen, and (b) Sn showing hot-spots near electrodes; The reflection from the composite rear which attained its maximum temperature approximately 2 s after the continuous current test is also shown. Specimen arrangement and scale are described in Figure 5.3 (Top- view of specimen holder). Part of the mirrors showing stray reflections has been masked for clarity

damage possible to adjacent structural and functional systems of the aircraft. This patch of evaporated metal also means that the coating would not be able to protect against the ensuing current components of a real strike such as the lightning C-component that is responsible for charge transfer or a re-strike.

Figure 5.11: Snapshots from 40 kA lightning impulse strike on Cu\Sn continuous coatings showing hot runaway coating fragments

Lastly, the different tests conducted in this study point towards ECF-protected CFRP as the superior material among the tested candidates. It is of interest to study how this material performs against a full-scale lightning test. Figure 5.12 show the photograph and ultrasonic C-scan image of a damaged 22.5 cm × 22.5 cm (total area) specimen of the ECF-clad CFRP subjected to Zone 2A Lightning (D, B and C* components) as described in SAE ARP5412 [6] at a commercial test facility. The test methods were in accordance with SAE ARP5416 [15]. A jet-diverting electrode with an initiating wire was used to produce a single discharge. As expected, photography and ultrasonic characterization indicate that the panel only suffered surface damage.

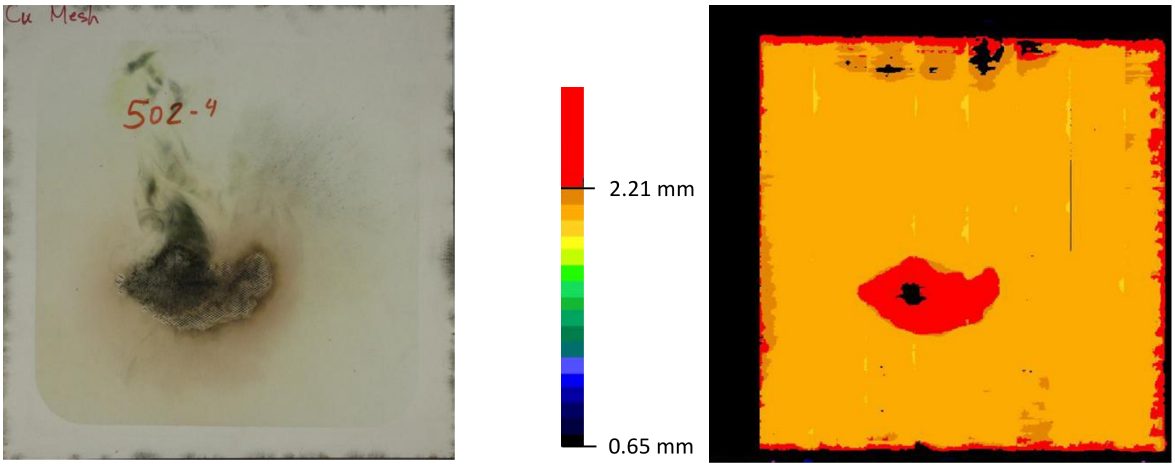

(a) **(b)**

Figure 5.12: (a) Photograph and (b) Ultrasonic C-scan of ECF-clad CFRP showing surface damage after subjection to zone II lightning [15]; sample size is 22.5 cm × 22.5 cm

The evaluation of different conductive coatings for LSP has led to ECF as a superior solution, which is also an industry-wide standard, establishing the applicability of the adopted test procedure. On the other hand, a clear lack of correlation was observed between the 4-point probe resistivity values (Table 5.1) and the damage characteristics ensued from the impulse strike

tests (Figure 5.6). As hypothesized in the technical discourse, thermal effects such as Joule heating could play a predominant role in the manifestation of damage. The regular 4-point probe measurements utilize currents on the order of tens of mA and do not produce substantial heat. Moreover, measurements are made over a relatively very small area which may not be fully representative of the entire specimen.To circumvent these disadvantages and arrive at more reliable values for this important electrical property, a relatively high current of 5 A was passed through coated coupons of size 12.7 cm ×1.27 cm (8.9 cm × 1.27 cm subtracting area under electrodes) and values of the sheet resistance were derived. This quantity is graphically represented in Figure 5.13 and is in better agreement with the quantified damage characteristics, but they still not fully representative. This deviation is witnessed because lightning strikes to a material is a multi-physics phenomenon, whose outcome is governed by many interacting properties. Modeling of such a complex phenomenon is a difficult and cumbersome process. This discussion demonstrates the deficiencies involved in generalizing electrical resistivity or sheet resistance values as an estimate for the degree of lightning protection and hence reinforces the need for emulated lightning strikes.

Ultimately, the material characteristics and lightning interaction with coatings studied through this test program call for two broad improvements on the materials front. For hybrid coatings, percolation and increased volume of conducting particles would need more attention. The metallic coatings, on the other hand require an improvement in resistance against melting effects. While manufacturing processes must ensure coating uniformity and repeatability, it is recommended that the samples are tested in the final configuration, i.e. with surfacing film and paint. With these revisions, the coated specimens may be tested again, with close monitoring of their real-time behavior using the supplementary methods such as high-speed videography and thermography. Furthermore, the following suggestions may be implemented when a sufficient number of samples are available: (i) Lightning impulse may be carried out in injection mode (as described in the Materials and Methods Section) in case the the coated specimens succumb to the arc-entry test. (ii) The behavior of the coated specimens against lightning continuous currents may be primarily tested in the current injection mode. (iii) As coating materials are upgraded, the lightning-material interactions must be seen as an integral part of the emulation tests, i.e., the satisfactory performance of the coating must ensure no damage to the coating in addition to the underlying composite substrate.

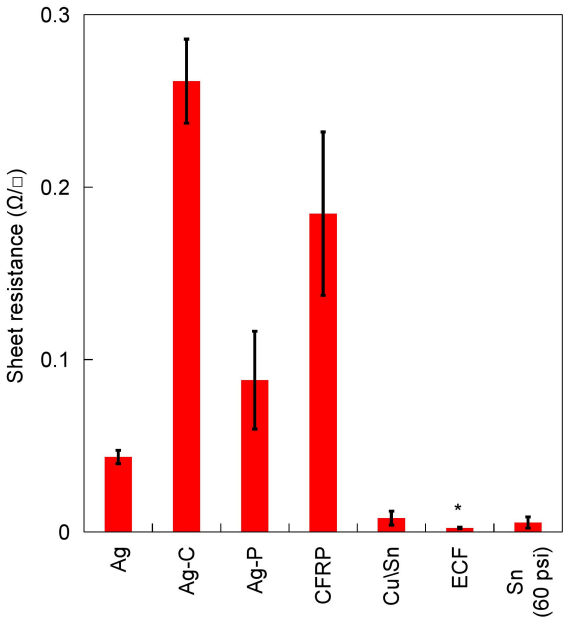

Figure 5.13: Sheet resistance of coated specimens from ambient current tests

5.5 Conclusion

Different conducting coatings for CFRP, each with their own material design, were subjected to lightning impulse strikes in the laboratory and the damage response studied via non-destructive evaluation. A cause-effect relationship was proposed for the different damage characteristics observed, signifying the different properties a LSP material must possess beyond electrical conductivity. These experiments suggest that attention must be paid to the uniformity and/or percolation characteristics of hybrid /composite coatings as these can severely limit the capacity of the coatings to support high current densities and associated phenomena arising from lightning strikes. Importantly, this study demonstrates the need for experimental lightning strike tests to estimate the protection offered by conducting materials and reiterates the superiority of the copper foil as a LSP solution.

5.6 Acknowledgments

CFRP coatings were developed and shared by: Rouhollah Farahani (Ag-P), Xavier Cauchy (Ag-C) from Ecole Polytechnique de Montreal and Hanqing Che (Cu\Sn and Sn) from McGill University. The CFRP and ECF-clad CFRP panels used in this study were provided by Bombardier Inc. Ultrasonic inspection of the samples was carried out at Centre Technologique en Aerospatiale, Montreal, Canada. This work was carried as a part of the CRIAQ NSERC COMP-502 project (grant number CRDPJ418046-11).

5.7 References

1. Federal Aviation Administration, *Aviation Maintenance Technician Handbook-Airframe*. Aviation Supplies & Academics Inc., 2012.
2. Gagné, M. and D. Therriault, *Lightning strike protection of composites.* Progress in Aerospace Sciences, 2014. **64**(0): p. 1-16.
3. Chakravarthi, D.K., et al., *Carbon Fiber–Bismaleimide Composites Filled with Nickel-Coated Single-Walled Carbon Nanotubes for Lightning-Strike Protection.* Advanced Functional Materials, 2011. **21**(13): p. 2527-2533.
4. Gou, J., et al., *Carbon nanofiber paper for lightning strike protection of composite materials.* Composites Part B: Engineering, 2010. **41**(2): p. 192-198.
5. *Shin, J.-H. and O.-Y. Kwon, AE Monitoring of Lightning-Damaged CRFP Laminates during Compression-After-Impact Test.* Journal of Acoustic Emission, 2011. **29**: p. 8.
6. *SAE ARP5412: Aircraft Lightning Environment and Related Test Waveforms.* SAE International, 2005. p. 57.
7. P S M Rajesh, *Response of composite panels with conductive coatings submitted to emulated lightning strikes.* Ph.D Thesis, University of Montreal, 2017 (submission in progress).
8. Cauchy, X., et al., Synthesis of highly conductive, uniformly silver coated carbon nanofibers by electroless deposition (Submitted to ACS Applied materials and interfaces; under review)
9. Dermanaki Farahani, R., et al., *Electrically Conductive Silver Nanoparticles-Filled Nanocomposite Materials as Surface Coatings of Composite Structures.* Advanced Engineering Materials, 2016. **18**(7): p. 1189-1199.
10. Martin Gagne, *Properties of lightning strike protection coatings.* MastersThesis, University of Montreal, 2016.
11. Che, H., et al., *Metallization of carbon cibre reinforced polymers by cold spray.* Surface & Coatings Technology, 2017. **313**: p. 236-247.
12. Yuzo Takahashi, *Two hundred years of lichtenberg figures*. Journal of Electrostatics, 1979. **6**: p. 1-13
13. Fran Cverna, *ASM Ready Reference: Thermal Properties of Metals.* ASM International, 2002.
14. Valencia, J. J. and Quested P. N., *Thermophysical Properties,* ASM Handbook, 2008. **15:** p. 468-481
15. *SAE ARP5416: Aircraft Lightning Test Methods.* SAE International, 2005. p.146 .

CHAPTER 6 ARTICLE 3: CONTINUOUS AND SELECTIVE-AREA COATING OF SILVER ON FIBER-REINFORCED POLYMER COMPOSITES FOR AEROSPACE APPLICATIONS

P S M Rajesh, Claire Delaroa[†], Martin Gagné, Jolanta E. Klemberg-Sapieha, Fréderic Sirois and Daniel Therriault[*]

Submitted to Langmuir, July 2017

Keywords: Aerospace, coating, composite, electrical conductivity, silver

6.1 Abstract

The ability to realize continuous and patterned coatings of pure metal on fiber-reinforced polymer in a cost-effective manner is of prospect for various conductive applications. Electroless plating by Tollen's process was adapted to produce silver coating on carbon fiber-reinforced polymer with an average coating surface density of 0.31×10^{-3} g·cm^{-2} and a sheet resistance as low as 1.7×10^{-1} Ω·□$^{-1}$. Electrical, metallographic, and mechanical characteristics of the coatings are presented. In order to extend the process to produce selective-area coatings of conductive architectures, we propose a direct-write-assisted method that confines the plating chemicals to specific locations on the composite substrates in the form of metalized channels and surfaces bordered by hydrophobic banks. Deposition with linear resolution on the order of hundreds of microns was achieved using this hybrid method. Conductive architectures for different applications such as electrical circuitry, electromagnetic interference shielding, sensing and communication (antennae) are illustrated to demonstrate the versatility of the selective-area coating method.

6.2 Introduction

The aircraft industry has been taking strides in the design, construction and operation of modern airplanes and helicopters including: (i) replacement of mechanical and hydro-mechanical flight control systems by wired control for aircraft control,[1] (ii) employment of lightweight fiber-reinforced polymers (FRP) for the structure,[2] covered with conductive foils/meshes for protection

from lightning and electromagnetic interference (EMI), (iii) implementation of communication devices to relay a wide variety of information,[3] and (iv) structural health monitoring (SHM) approaches via use of sensors.[4] The feature common to all these technologies is electrical conductivity which is usually realized via metallic materials. Although metals have a high density and can adversely affect the economy of weight, their usage for the discussed aerospace applications is presently indispensable given their application-critical electrical and thermal properties. Fabrication of conductive designs in the form of channels, patterns etc. directly at the required location on structural surfaces can help manage weight by cutting down on the insulation materials and substrates associated with the use of conductive materials. Such selective-area coatings can be very handy in small drones and micro-air vehicles where both power and space are constrained and could possibly be extended to larger aircraft.

Dip-pen lithography,[5] e-jet[6] and inkjet printing,[7] direct ink writing[8] and its laser-assisted variant,[9] physical[10] and chemical vapor deposition,[11] and other deposition methods can be used to produce conductive pathways on various substrates. Although, deposition with high resolution and reliability can be achieved using these methods, they require expensive equipment that may not always be compatible with aerospace materials (e.g., lasers with polymer composites) or scaled-up (e.g., vacuum systems used for vapor deposition) to the requirements of the industry. Moreover, many of the above listed methods utilize specially formulated inks containing a carrier (solvent or polymer) to achieve suitable rheological properties. The advantage of pure metals lies in their superior electrical conductivity required to achieve a high quality of signal transmission and increased ampacity. Silver has the highest conductivity amongst metals, is corrosion resistant and has superior thermal properties, making it an ideal candidate for a variety of electrical applications.

Electroless plating, also known as autocatalytic plating, is the method of using redox reaction(s) in a chemical bath to coat a metal on to a substrate.[12] In contrast to electroplating, the absence of external electric fields results in coatings of uniform thickness even along edges and corners[12]. The feasibility of the Tollen's approach to coat silver on carbon fiber-reinforced polymer (CFRP) was previously explored by the authors and a scope for improved properties and application was observed.[13] Given the facile nature of this method, electroless plating has been crossed with (pairs of) techniques such as microlithography and etching,[14] two-photon polymerization/

lithography and using a hydrophobic coating,[15] two-photon polymerization/lithography and plasma treatment,[16] photo-patterning and solvent vapor treatment,[17] and soft-lithography[18] among others to achieve selective-area coating. Three-dimensional (3D) printing has evolved into one of the most sought-after manufacturing genres in recent times due its additive and customizable nature. The direct-write method is an extrusion-based technique where the required fluidic material or solution is selectively deposited on a substrate using a programmable robot, and evaporation or curing are employed to solidify the printed material.[19] A hybrid method based on the fusion of direct-write, hydrophobic masking and electroless plating techniques is thus envisaged to realize selective-area coatings on FRP.

Here, we present our work on (i) producing highly conductive, continuous coating of silver on CFRP by investigating the optimal parameters for electroless Tollen's chemistry (henceforth referred to as electroless silver) and thermal sintering, and the microstructural, electrical and tribological characterization of the coating, and (ii) development of a method to produce selective-area coatings of electroless silver, and illustration of the potential applications based on the proposed method.

6.3 Experimental section

6.3.1 Materials

The following chemicals were used for the sensitization and silver coating process: tin chloride ($SnCl_2.2H_2O$, Sigma Aldrich), hydrochloric acid (HCl, Anachemia), silver nitrate ($AgNO_3$, Alfa Aesar), potassium hydroxide (KOH, Anachemia), ammonia solution (28% H_5NO, Alfa Aesar) and dextrose ($C_6H_{12}O_6$, Sigma Aldrich). The CFRP used in the study was fabricated from 4 plies of Cycom 5276-1 resin / 8HS carbon fiber weave arranged in a $(0/90)_{2S}$ fashion.

Polylactide (PLA 4032D, NatureWorks LLC), dichloromethane (CH_2Cl_2, Anachemia) and NeverWet®, a commercial product from Rust-Oleum® were used to create the hydrophobic masks in the study.

6.3.2 Silver coating of CFRP: Chemistry and sintering

Silver coating is traditionally carried out by a two-step bath process. The first step called sensitization (or pre-treatment) coats the sample with metal ions; tin chloride ($SnCl_2$) solution

was used for this purpose. These metal ions help reduce the silver ions from the bath to metallic silver thereby initiating the coating on the substrate.[20] The second step involves the reduction of the Tollen's reagent (ammonia complex of silver, $2[Ag(NH_3)_2]^+$) by dextrose ($C_6H_{12}O_6$) thereby coating the sample in the chemical bath. The preparation of the Tollen's reagent involves intermediate reactions between silver nitrate ($AgNO_3$), potassium hydroxide (KOH) and ammonia (NH_3). Additional details pertaining to the chemistry of the electroless process adopted in this study are presented in the Results and Discussion section. The optimization of electroless plating of silver on CFRP is considerably complicated given the dependence of the plating process on many open variables (e.g., time, concentration, molar ratios and quantities of chemicals). It was thus indispensable to fix certain variables to proceed with the optimization exercise. In this study, the concentration of $AgNO_3$ was set to 0.1 M and the coating time was limited to 15 min. In this work, the following parameters were studied: (i) $SnCl_2$ concentration and sensitization time, (ii) $AgNO_3$: KOH ratio, and (iii) sintering temperature and time.

Preparation of coating chemicals: The sensitization solution was prepared by mixing solid $SnCl_2$ into deionized (DI) water via stirring. 1M HCl was added drop-wise until complete dissolution of the salt was achieved. To prepare Tollen's reagent, $AgNO_3$ was mixed with DI water to prepare a 0.1 M solution. KOH was added to the silver nitrate solution in a 1:1 molar ratio, to begin with. This produced a brown precipitate of solid silver (I) oxide, Ag_2O. A gradual addition of 28% H_5NO solution was made until the precipitate completely dissolved. $C_6H_{12}O_6$ solution was prepared according to the stoichiometric molar ratio of 1:2 with respect to the silver complex but with an excess mass to achieve a complete reaction with the Tollen's reagent.

Sensitization and silver coating: CFRP coupons (size: 1.27 cm × 4.23 cm × 1.65 mm) were cleaned with acetone to remove dirt and grease. Both sensitization and coating were carried out by suspending a CFRP sample vertically in a beaker containing the freshly prepared chemical solutions. The ratio of the surface area of the samples to the volume of coating solutions was kept constant throughout the study. They were then left untouched in the sensitization solution for different durations of time as discussed in the Results and Discussion section. The sensitized coupons were then washed by dipping and gently swaying them in multiple baths of DI water. The Tollen's reagent and the reducing solution were mixed and the sensitized coupons were immediately transferred (before drying) into this new coating bath. The coating was allowed to

proceed for 15 min with occasional rocking of the bath. Thereafter, the samples were thoroughly washed in DI water and left for drying overnight. The change in the wet weight of the samples before and after coating was used to estimate the amount of deposited silver.

Choice of sintering parameters: To identify the sintering parameters that can lead to improved (lower) resistivity, the silver coated coupons were heated in vacuum (<63.5 mm of Hg) at 80, 100 and 120 °C each for 3, 6 and 12 h (StableTemp vacuum oven, model 282A). The temperature range was kept low keeping in view the glass transition temperature of the composite substrate. Decrease in resistivity of the samples were used to choose the optimal sintering parameters.

6.3.3 Selective-area coatings

Preparation of sacrificial polymer: 20 wt.% polylactide (PLA 4032D, NatureWorks LLC) was dissolved in dichloromethane (CH_2Cl_2, Anachemia) via sonication in an ultrasonic bath (Ultrasonic cleaner FS60H, Fisher Scientific) for 1 h to prepare the solution of sacrificial polymer.[21]

Printing of sacrificial polymer: PLA solution was filled into a 3 mL syringe and fitted with a nozzle of 510 μm inner diameter. This syringe was inserted into a pneumatic dispenser (HP-7X, EFD) and placed in a robotic arm (I&J2200-4, I&J Fisnar Inc.). Printing was executed by moving (speed: 0.5-30 $mm \cdot s^{-1}$) the syringe over a set of coordinates input via the computer while the desired value of pressure (0.5-1 MPa) was applied using the dispenser. Required patterns were generated by extruding the PLA on FRP.

6.3.4 Coating characterization

Electrical resistivity and temperature coefficient: A 4-point probe (Jandel) was used for resistivity measurements. The currents were injected through the exterior points of the probe using a programmable current source (Keithley 220), while the voltage was measured across the interior points using a multimeter (Hewlett Packard 34401A). Measurements were made on three different locations for each of the three samples tested. For each location, 10 measurements ranging from 10 mA to 100 mA with a 10 mA step were conducted. The measurement locations were center-aligned along the sample's longitudinal axis. The resistance was estimated by applying the Ohm's law, and was subsequently converted into resistivity depending on the dimensional characteristics of the probe and the sample.

The estimation of the temperature coefficient of resistance was carried out using the same system described in the previous paragraph except that the sample was heated in flowing nitrogen gas between approximately 20 and 120 °C at a linear rate with a step-size of 1°C. A resistivity test rig (A. & M. Fell Ltd.) with a temperature controller (Temptronic Corporation, TP3000) was utilized for this purpose. The voltage was recorded after a 3 s stabilization time at every temperature step. Three samples, each of size 12.7 mm × 19.05 mm, were tested and an average of three readings was taken at every temperature step to obtain a reliable result.

Electron microscopy and energy-dispersive X-ray spectroscopy: A field emission electron microscope (FESEM, JOEL JSM7600F) equipped with an energy dispersive x-ray spectroscopy (EDS) detector was used for studying the homogeneity, morphology and thickness of the silver coating. The secondary electron images were obtained at a magnification of 50 000×; the accelerating potential for the electron gun was 5 kV.

X-ray diffraction studies: Two silver-coated CFRP samples, one sintered and the other as-coated, were subjected to X-ray diffractometry (Philips X'pert diffractometer) at room temperature with a copper target; K_α radiation at 50 kV and 40 mA. The samples were scanned at rate of ~0.17 °s^{-1} and a step size of 0.016 ° in the range of 30-90 °.

High current characteristics: A Lambda EMS 150-33-D-RSTL, 5000 W power supply was utilized to inject a 5 A rectangular current pulse into test coupons of size 12.7 mm × 1.27 mm for 1 s. A National Instruments multifunction data acquisition (DAQ, USB-6211) module was used to record the voltage and current (PR 430 probe) data while a LabVIEW® 2013 program both controlled the power supply and logged the electrical data.

Mechanical properties: Nanoindentation was carried out using a Hysitron TriboIndenter® with a Berkovich diamond tip. The hardness and Young's modulus were obtained using the Oliver & Pharr technique[22] applying loads ranging from 100 μN to 5000 μN at a linear rate. The loading and unloading time was 5 s each while the holding time at maximal load was 2 s.

Adhesion tests were conducted and evaluated according to ASTM D3359 – 09 standard, method B. A cross-hatch pattern with two sets of normal cuts was produced on the silver coated CFRP substrate with a multi-tooth cutter. While eleven equally-spaced cuts were inscribed in each

direction; the size of the pattern itself was 12.7 mm × 12.7 mm. A pressure-sensitive tape (Gardco, model P-A-T paint adhesion test kit) was manually applied over the pattern and peeled off at a 180° angle to the tape direction with a constant pull. The adhesion of the coatings was graded on a scale of 0 to 5 where 0B indicated 65% of coating removal (poor adhesion) and 5B indicated 0% of coating removal (excellent adhesion).

6.4 Results and discussion

Sensitization (pre-treatment) was found to greatly improve the quality of the coatings, although not imperative for silver deposition on CFRP. Figure 6.1(a) shows the effect of different concentrations of $SnCl_2$ (0.01 M, 0.05 M and 0.10 M) and sensitization times (1, 5 and 10 min) on the mass of silver and specific resistivity of the deposited coating. It can be seen that this investigation did not represent any confident trend and were ridden with high standard deviations. Thus, sensitization with 0.05 M $SnCl_2$ for 5 min, the same values employed in our previous work[11] were used for the rest of this study.

After sensitization, the second step of the silver coating is the Tollen's reaction and deposition. The Tollen's reaction is set up between two components – the Tollen's reagent and the reducing agent. Many different procedures exist for both the preparation of the Tollen's reagent and for the choice of the reducing agent.[23] The reactions depicted in Equations 1 and 2 are adopted in this study for the preparation of the Tollen's reagent,[24] which is an ammonia complex of silver, $2[Ag(NH_3)_2]^+$ in an aqueous solution, written as $2[Ag(NH_3)_2]OH$. Thereafter, silver is coated on the sensitized sample in the bath as per Equation 3.[25]

$$2AgNO_3 + 2XOH \rightarrow Ag_2O + 2XNO_3 + H_2O \quad (6.1)$$

$$Ag_2O + 4NH_4OH \rightarrow 2[Ag(NH_3)_2]OH + 3H_2O \quad (6.2)$$

$$2[Ag(NH_3)_2]OH + RCHO \rightarrow 2Ag + 4NH_3 + RCOOH + H_2O \quad (6.3)$$

where, X in the alkali metal oxide was potassium, and the aldehyde was dextrose (R: $C_5H_{11}O_5$) in our case.

For the preparation of Tollen's reagent, the optimal ratio of $AgNO_3$ to KOH (Equation 1) for silver deposition was investigated between 1:0.6 and 1:1.4 with an interval of 0.2. Based on the results plotted in Figure 6.1(b), a $AgNO_3$ to KOH ratio of 1:1.2 was chosen for the study as it

resulted in the highest average weight deposited and was only marginally behind in terms of specific resistivity of the samples produced with a molar ratio of 1:1.4. Moreover, the molar ratio of 1:1.2 was also the best choice for process consistency (lower standard deviation) observed in both the average weight of deposit and specific resistivity. The amount of ammonia used in Equation 2 was adjusted to obtain a complete dissolution of the Ag_2O formed in the earlier step (Equation 1). For the final step, the Tollen's reagent was mixed with excess dextrose solution in order to reduce the complex to produce metallic silver, thereby producing a coating on the CFRP sample.

Sintering helps in reducing the amount of resistive grain boundaries,[26] thereby decreasing the overall resistance of a coating. Thermal energy can drive the grains of a metal to coalesce. Grain boundaries are high energy sites; this phenomenon is predominant when grain to grain boundary (volume:surface area) ratio is low, i.e., smaller grains are present. Figure 6.1(c) shows the results obtained by sintering the coatings for different time-temperature combinations. Increased temperatures always resulted in larger changes in resistivity, although the effect of time was less apparent at higher temperatures. The difference between change in resistivity after 3 and 6 h of sintering decreased with increasing temperature and stagnated at 12 h. It is believed that the specimens are inadvertently subjected to possible oven contamination which competes against sintering and becomes apparent when specimens are aged for longer duration (12 h). The graph shows that the combination of 120 °C and 6 h has resulted in the greatest decrease in resistivity and so these sintering parameters were applied to all the samples prepared for characterization and testing. Ultimately, a coating as shown in Figure 6,1(d) with an average specific resistivity of 5.6×10^{-5} $\Omega\cdot g\cdot cm^{-2}$ was obtained. This representative SEM image shows that the coating is homogenous on the surface with a 100 nm grain size, while an average thickness of 4.1 μm for the coating was deduced from the EDS map (inset) of the sample cross-section. The coating is not uniformly continuous; this may be largely attributed to the surface condition of the CFRP substrate.

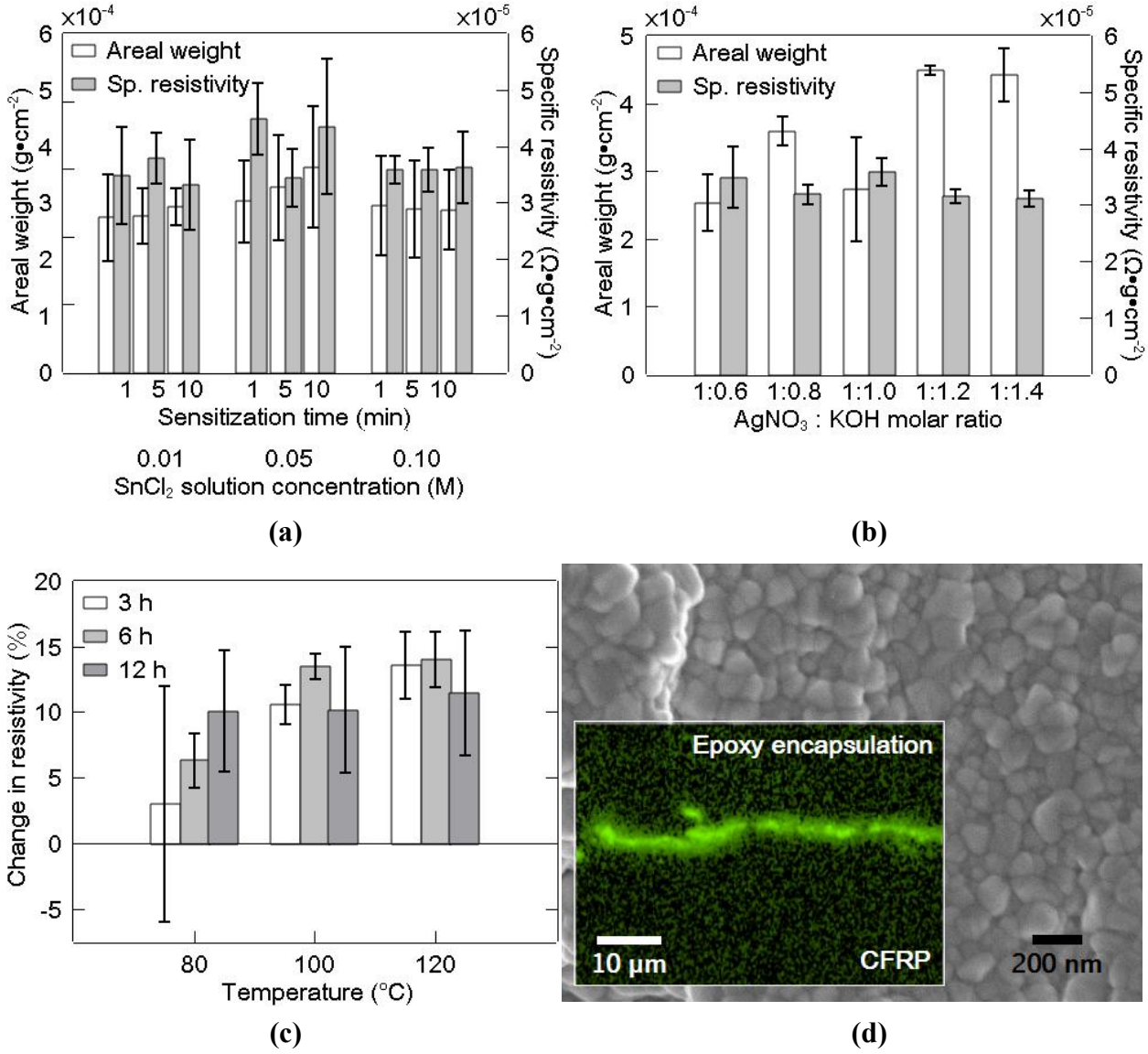

Figure 6.1: (a) Effect of sensitization parameters on silver deposition (molar ratio of AgNO3:KOH is 1:1; no sintering), (b) Effect of AgNO3:KOH molar ratio on silver deposition (SnCl2 concentration: 0.05M, sensitization time: 5 min; no sintering), (c) Effect of sintering parameters on resistivity of silver coatings (SnCl2 concentration: 0.05M, sensitization time: 5 min; AgNO3:KOH molar ratio is 1:1.2), and (d) Final microstructure of silver coating (secondary electron image of coating top view); inset: EDS map of coating cross-section (Ag L-series). Error bar equals 1 standard deviation (1σ)

Phase analysis of the coatings was carried out using X-ray diffraction (XRD). In the XRD spectra, Figure 6.2(a), the 38.1°, 44.3°, 64.6°, 77.6° and 81.6° peaks belong to the (111), (200), (220), (311) and (222) planes,[27] respectively, and represent a face-centered cubic (FCC) structure. Given

the pronounced peak of the (111) lattice plane, it may be deduced that the orientation of the grains was predominantly parallel to the CFRP substrate.[28] The narrow peaks in the sintered sample suggest an improvement in crystallinity and corroborate the diminished values of specific resistivity (improved conductivity) obtained upon sintering.

Although the electrical resistivity of the coating was highly satisfactory, it is well-known that metals can demonstrate Joule heating especially while carrying current of higher amplitudes and for extended duration. It is thus important to characterize how the coating resistivity varied with sample temperature and test for the current-carrying ability of the coating. To obtain the temperature coefficient of resistivity, three samples cut from a larger coupon were subjected to two temperature ramps (~ 20-120 °C) each, which showed that the resistance data from the ramps overlapped (Figure 6.2(b)); this implies that the heat from the temperature cycling did not alter the previously sintered microstructure of the coating. From these temperature ramp measurements, the average temperature coefficient of resistivity was computed as 1.79×10^{-3} $°C^{-1}$ (std. deviation: ~5%); this value is in the same order of magnitude as reported for pure silver, 4.1×10^{-3} $°C^{-1}$, in literature.[29] Additionally, current injection tests were performed, where current pulses with 5A amplitude were injected into rectangular coupons of coated CFRP for 1 s. Typical test results are shown in Figure 6.2(c). The recorded voltage response was invariant with respect to time during current injection. During the same test, the pre- and post-test resistance showed almost no change. These observations establish the absence of significant Joule heating at the tested current values. A superior 0% coating removal after peel-adhesion test as shown in Figure 6.2(d) led to a corresponding 5B classification. The mechanical properties of the silver coating were: hardness of 0.6±0.3 GPa, elastic modulus of 10±4 GPa, coefficient of friction of 0.2. These results are highly satisfactory as evinced from their comparison with those of the surfacing film (Surface Master 905C, Cytec Engineered Materials): hardness of 0.3±0.05 GPa, elastic modulus of 6.9±0.6 GPa, and coefficient of friction of 0.5.

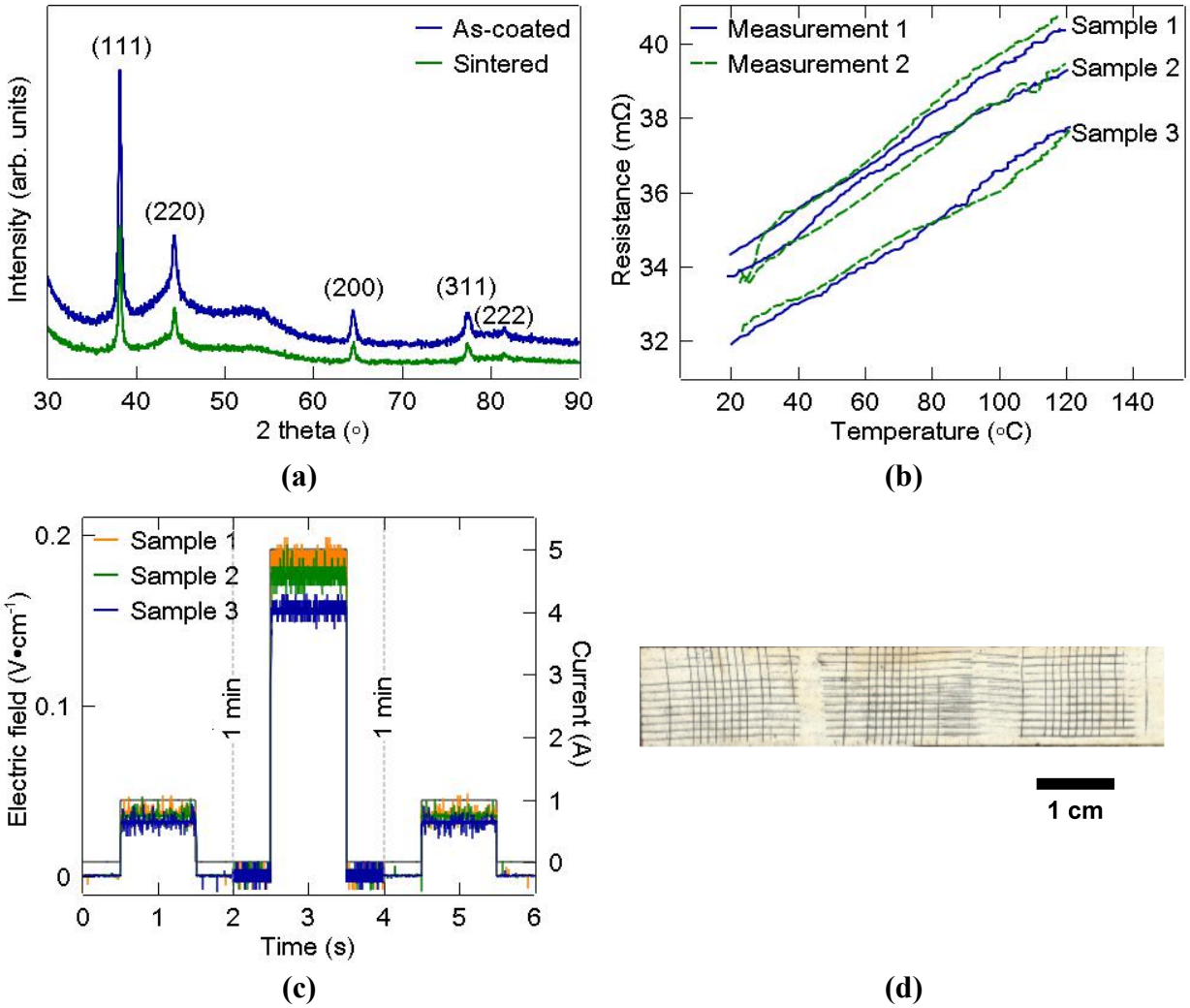

Figure 6.2: (a) X-ray spectra of the silver coatings; sintering parameters: 120 °C, 6 h, (b) Dependence of the silver coating resistance on temperature, (c) Typical results from current injection tests on silver coated CFRP, and (d) Silver-coated CFRP specimen after peel adhesion tests

The next goal was to achieve selective deposition of silver to produce coatings of application-specific designs. This was realized by creating a hydrophobic mask to selectively confine the silvering solution thereby coating regions of interest. The process of producing the hydrophobic mask and selective-area coating thereof is illustrated in Figure 6.3. The requisite design for the final coating was first printed using the sacrificial polymer PLA on a cleaned substrate (Figure 6.3(a)). Once the sacrificial polymer had dried sufficiently, a commercial "two-step" hydrophobic coating was applied (Figure 6,3(b)); the time between the first and the second coat was limited to 1 min. Then, the sacrificial polymer was peeled off immediately along with the hydrophobic

coating present over it (Figure 6.3(c)). It is important to peel off the sacrificial polymer before the hydrophobic material dries and forms a continuous layer. The hydrophobic coating was left undisturbed for at least 1 h. To produce silver coatings, two methods are available: one, the samples could be dipped into the silvering solution (Figure 6.3(d, i)) or two, the silvering solution could be introduced into the open channels using a pipette (Figure 6.3(d, ii)). After leaving the samples undisturbed for 30 min the remnant solution was disposed and the sample carefully rinsed (Figure 6.3(e)). Note that annealing the samples can further improve conductivity.

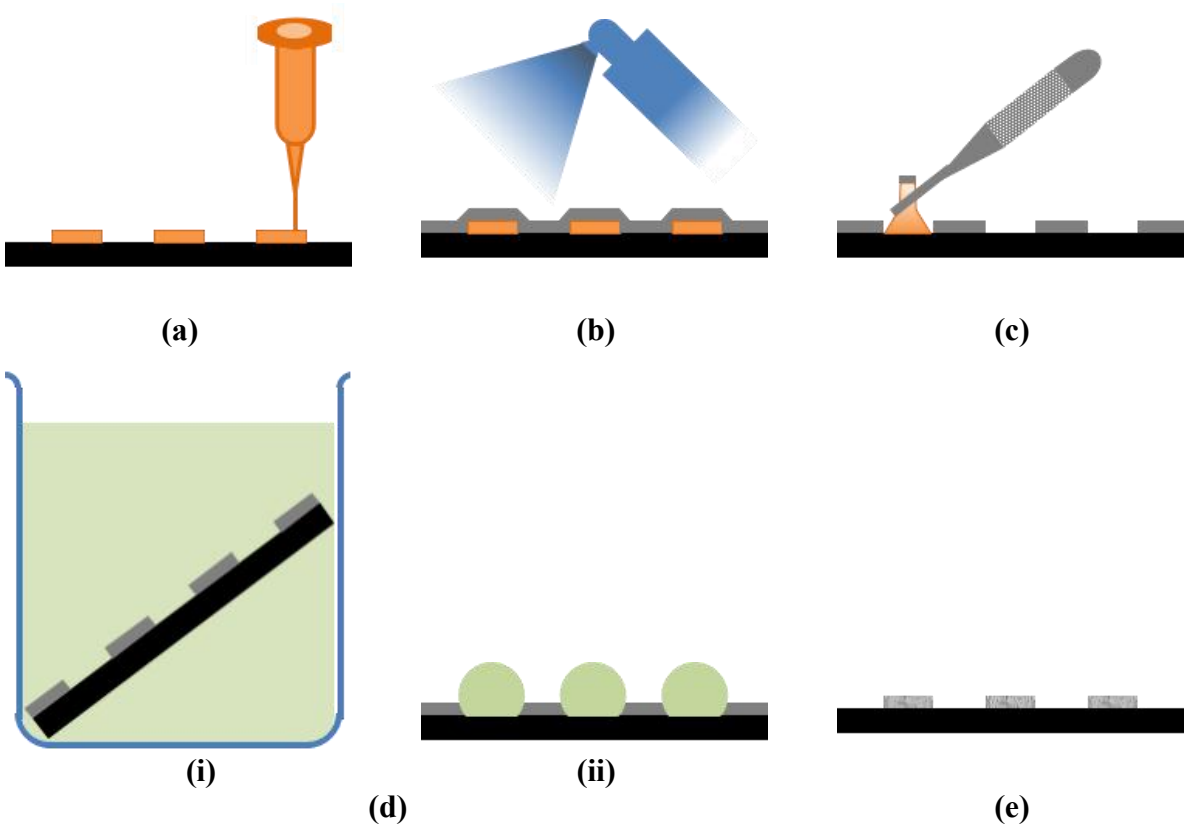

Figure 6.3: Schematic of the process for producing selective area coatings of electroless silver (cross-sectional view): (a) Print sacrificial polymer design/ affix masking screen, (b) Apply hydrophobic coating, (c) Remove sacrificial polymer/ masking screen, (d) Undertake electroless deposition via: (i) Dip substrate in silvering solution, or (ii) Introduce silvering solution at required locations, (e) Dispose deposition chemicals, rinse and dry; If required, peel away/clean hydrophobic coating and/or sinter

An area of application, small aircraft and drones being increasingly used for rescue, reconnaissance, medical assistance, surveying and even recreational use. Four pertinent

conductive applications from this aerospace sector were chosen and requisite designs for their operation were replicated with the proposed direct write-assisted selective-area electroless silver deposition technique to demonstrate the versatility of the method (Figure 6.4(a-d)).

(i) Electrical connections and circuitry: The importance of this application is better visualized in the context of fly-by-wire technology, where the miles length of cables are becoming increasingly difficult to manage[30] and maintain.[31] Figure 6.4(a) demonstrates the ability to produce channels with a resolution on the order of hundreds of microns which can be employed either for electrical circuitry or for any or all of the three following applications. Replacing wires altogether by laying conductive paths directly on the structural surfaces has two advantages – reduced weight of polymer insulation and associated maintenance, and effective management of electrical connections via reduction in cable clutter. If electrical insulation is desired, it could be provided by polymer paint for low-voltage applications.

(ii) EMI shielding: Figure 6.4(b) shows CFRP with a grid-shaped silver coating. Akin to presently used copper meshes/foils, such coatings can find application in EMI shielding[32] and possibly extended to lightning protection[33] due to their high electrical conductivity. Moreover, silver coatings overcome the challenges ensuing from the use of copper mesh/foil, such as the weight from isolation plies[34] for protection against galvanic corrosion.[35] Surface application also eases repair of the coatings as the electrical continuity between the site of repair and the remainder of the structure can be easily verified.[36] When desired, 3D printing can be replaced by manual intervention so as to allow for the realization of repetitive or simple designs. In the present application, a pre-fabricated mask was used to play the role of the sacrificial polymer, while in the next application (antenna), an adhesive tape was used for the same.

(iii) Antennae: Electrical conductivity is imperative for communication systems. Fabricating antennae on existing aircraft parts as opposed to separate structures again provides weight and cost advantage. Figure 6.4(c) shows a patch antenna coated on glass fiber-reinforced polymer (GFRP: FR4) designed based on transmission line model[37] to function as a WiFi antenna around the 2.4 GHz range. This example demonstrates that the proposed method could be adapted to different polymer or composite substrates.

(iv) Strain sensors: Figure 6.4(d) shows a simple coated strain gauge that could be used for structural health monitoring (SHM). A particular advantage of such strain gauges is the absence of the glue and plastic sheeting usually used with conventional gauges. For example, an application of such plated sensors is for SHM of flapping wing aircraft where decreased interference with the modal characteristics of the thin wings could be expected.

(a)

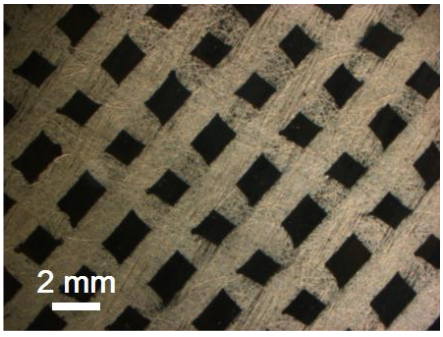

(b)

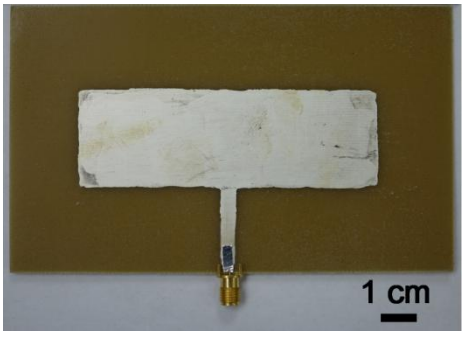

(c)

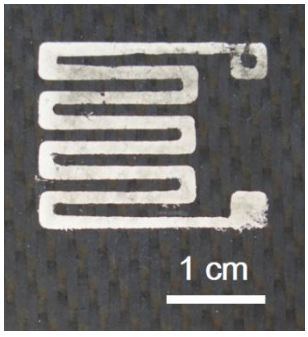

(d)

Figure 6.4: Design illustrations for potential aerospace applications of continuous and selective area coatings; Substrate is CFRP unless mentioned otherwise (a) Silver channels for electrical connections on a model wing with port-side navigation light; Inset: Silver channel with sub-millimeter resolution silver channel on a separate substrate, (b) Conductive grid-shaped coatings for protection against lightning strikes and EMI, (c) Communication antennae – rectangular microstrip patch on GFRP, (d) Strain sensor for structural health monitoring

6.5 Conclusion

A method of producing continuous and selective area coatings of silver was devised to produce lightweight, custom-shaped conductive designs on FRP. The coating protocol was optimized to achieve a high degree of conductivity and characterized for use in different conditions. An

average specific resistivity of 5.6×10^{-5} $\Omega\cdot g\cdot cm^{-2}$ was obtained for the coating produced on CFRP with the following parameters: $SnCl_2$ concentration and time for sensitization: 0.5 M and 5 min. and $AgNO_3$:KOH molar ratio for silver metallization and coating time: 1:1.2 and 15 min, respectively. Mechanical properties were also found to be comparable or exceeding those of the epoxy surfacing film. Various conducting applications pertinent to the aerospace industry were illustrated to showcase the scope and applicability of the method. In summary, the proposed method is an economical way to to produce conductive selective area coatings by leveraging the availability of 3D printers and CNC machines in laboratories and manufacturing facilities. While it has already been shown that different substrate materials can be coated using this method, future work is aimed at an extension of the method to adapt to different electroless and electro-plated metals. However, before this can be realized, further optimization of the process will be required in order to produce coatings with greater uniformity and repeatability.

6.6 Author information

Corresponding Author

*E-mail: daniel.therriault@polymtl.ca

Present Addresses

† Present address: Department of Materials Science and Engineering, Institut National des Sciences Appliquées de Lyon, 20 Avenue Albert Einstein, 69100 Villeurbanne, France

Author Contributions

The manuscript was written through contributions of all authors. All authors have given their approval to the final version of the manuscript.

Funding Sources

This work was funded under the NSERC CRIAQ COMP-502 project. The authors declare no competing financial interests.

6.7 Acknowledgment

The authors appreciate the assistance of Sampada Bodkhe from the Laboratory for Multiscale Mechanics (Mechanical Engineering), for obtaining the X-ray diffraction spectra, and assistance in 3D printing. The authors also thank Michael Leberge from the Functional Coating and

Surface Engineering Laboratory (Physics Engineering), for carrying out the nano-indentation on the coatings. The CFRP panels used in this study were provided by Bombardier Inc., Montreal, Canada.

6.8 Abbreviations

FBW, fly-by-wire; CFRP, carbon-fiber reinforced polymer; EDS, energy-dispersive X-ray spectroscopy; EMI, electromagnetic interference; FRP, fiber reinforced polymer; GFRP, glass-fiber reinforced polymer; SEM, scanning electron microscopy; SHM, structural health monitoring; XRD, X-ray diffraction.

6.9 References

1. Schmitt, V. R.; Morris, J. W.; Jenney, G. D., *Fly-by-wire: A Historical and Design Perspective*. Society of Automotive Engineers: 1998.
2. (a) Baker, A. A. B.; Kelly, D. W., *Composite Materials for Aircraft Structures*. American Institute of Aeronautics & Astronautics: 2004; (b) Mouritz, A. P., *Introduction to Aerospace Materials*. Elsevier Science: 2012.
3. Brady, C., *The Boeing 737 Technical Guide*. 2016.
4. (a) Ostachowicz, W.; Güemes, A., *New Trends in Structural Health Monitoring*. Springer Vienna: 2013; (b) Yuan, F. G., *Structural Health Monitoring (SHM) in Aerospace Structures*. Elsevier Science: 2016.
5. Hung, S.-C.; Nafday, O. A.; Haaheim, J. R.; Ren, F.; Chi, G. C.; Pearton, S. J., Dip Pen Nanolithography of Conductive Silver Traces. *The Journal of Physical Chemistry C* **2010**, 114 (21), 9672-9677.
6. Wei, C.; Qin, H.; Chiu, C.-P.; Lee, Y.-S.; Dong, J., Drop-on-demand E-jet printing of continuous interconnects with AC-pulse modulation on highly insulating substrates. *Journal of Manufacturing Systems* **2015**, 37, Part 2, 505-510.
7. Finn, D. J.; Lotya, M.; Coleman, J. N., Inkjet Printing of Silver Nanowire Networks. ACS *Applied Materials & Interfaces* **2015**, 7 (17), 9254-9261.
8. Russo, A.; Ahn, B. Y.; Adams, J. J.; Duoss, E. B.; Bernhard, J. T.; Lewis, J. A., Pen-on-Paper Flexible Electronics. *Advanced Materials* **2011**, 23 (30), 3426-3430; (b) Ahn, B. Y.; Walker, S. B.; Slimmer, S. C.; Russo, A.; Gupta, A.; Kranz, S.; Duoss, E. B.; Malkowski, T.

F.; Lewis, J. A., Planar and Three-Dimensional Printing of Conductive Inks. *Journal of Visualized Experiments: JoVE* **2011**, (58), 3189.

9. Skylar-Scott, M. A.; Gunasekaran, S.; Lewis, J. A., Laser-assisted direct ink writing of planar and 3D metal architectures. *Proceedings of the National Academy of Sciences* **2016**, 113 (22), 6137-6142.
10. Rossnagel, S. M.; Powell, R.; Ulman, A., *PVD for Microelectronics: Sputter Desposition to Semiconductor Manufacturing*. Elsevier Science: 1998.
11. Baum, T. H.; Comita, P. B., Chemical Vapor Deposition of Gold and Silver. In *The Chemistry of Metal CVD*, Wiley-VCH Verlag GmbH: 2007; pp 303-327.
12. Henry, J. R., Electroless (autocatalytic) plating. *Metal Finishing* **2002**, 100, 409-420.
13. P S M, R.; Cauchy, X.; Gagne, M.; E Klemberg-Sapieha, J.; Sirois, F.; Therriault, D., Wet Chemical Metallization of Aerospace Composites as a Lightning Protection Strategy. In *Engineering Solutions for Sustainability*, John Wiley & Sons, Inc.: 2015; pp 187-192.
14. Miyoshi, K.; Aoki, Y.; Kunitake, T.; Fujikawa, S., Facile Fabrication of Silver Nanofin Array via Electroless Plating. *Langmuir* **2008**, 24 (8), 4205-4208.
15. Formanek, F.; Takeyasu, N.; Tanaka, T.; Chiyoda, K.; Ishikawa, A.; Kawata, S., Selective electroless plating to fabricate complex three-dimensional metallic micro/nanostructures. *Applied Physics Letters* **2006**, 88 (8), 083110.
16. Yan, Y.; Rashad, M. I.; Teo, E. J.; Tanoto, H.; Teng, J.; Bettiol, A. A., Selective electroless silver plating of three dimensional SU-8 microstructures on silicon for metamaterials applications. *Optical Material Express* **2011**, 1 (8), 1548-1554.
17. Nakanishi, T.; Hirai, Y.; Kojima, M.; Yabu, H.; Shimomura, M., Patterned metallic honeycomb films prepared by photo-patterning and electroless plating. *Journal of Materials Chemistry* **2010**, 20 (32), 6741-6745.
18. Tvingstedt, K.; Inganäs, O., Electrode Grids for ITO Free Organic Photovoltaic Devices. *Advanced Materials* **2007**, 19 (19), 2893-2897.
19. (a) Hon, K. K. B.; Li, L.; Hutchings, I. M., Direct writing technology—Advances and developments. *CIRP Annals - Manufacturing Technology* **2008**, 57 (2), 601-620; (b) Lewis, J. A.; Gratson, G. M., Direct writing in three dimensions. *Materials Today* **2004**, 7 (7–8), 32-39.

20. Mallory, G. O.; Hajdu, J. B., Electroless Plating: Fundamentals and Applications. *American Electroplaters and Surface Finishers Society* **1990**.
21. Guo, S.-Z., Heuzey; M.-C., and Therriault, D., Properties of Polylactide Inks for Solvent-Cast Printing of Three-Dimensional Freeform Microstructures. *Langmuir* **2014,** 30 (4), 1142-1150.
22. Fischer-Cripps, A. C., *Nanoindentation 3 ed.* Springer-Verlag New York: 2011.
23. (a) Mallory, G. O.; Hajdu, J. B., Electroless Plating: Fundamentals and Applications. *American Electroplaters and Surface Finishers Society* **1990**; (b) Schlesinger, M.; Paunovic, M., *Modern Electroplating*. Wiley: 2011; (c) Heber, D. C., Methods of Silvering Mirrors. *Publications of the Astronomical Society of the Pacific* **1911,** 23 (135), 13.
24. Zienkiewicz-Strzałka, M.; Pasieczna-Patkowska, S.; Kozak, M.; Pikus, S., Silver nanoparticles incorporated onto ordered mesoporous silica from Tollen's reagent. *Applied Surface Science* **2013,** 266, 337-343.
25. Sangsuk, S., Preparation of high surface area silver powder via Tollens process under sonication. *Materials Letters* **2010,** *64* (6), 775-777.
26. Yoon, S. H.; Lee, J. H.; Lee, P. C.; Nam, J. D.; Jung, H.-C.; Oh, Y. S.; Kim, T. S.; Lee, Y. k., Sintering and consolidation of silver nanoparticles printed on polyimide substrate films. *Macromolecular Research* **2009**, 17 (8), 568-574.
27. Singh, N.; Khanna, P. K., In situ synthesis of silver nano-particles in polymethylmethacrylate. *Materials Chemistry and Physics* **2007**, 104 (2–3), 367-372.
28. Ghorbani, H. R. Biological coating of paper using silver nanoparticles. *IET Nanobiotechnology [Online]* **2014**, p. 263-266.
29. Smithells, C. J., *Metals Reference Book*. Elsevier Science: 2013.
30. Dinh-Khanh, D.; Mifdaoui, A.; Gayraud, T. In Fly-By-Wireless for next generation aircraft: Challenges and potential solutions, Wireless Days (WD), 2012 IFIP, 21-23 Nov. 2012; 2012; pp 1-8.
31. Furse, C.; Haupt, R., Down to the Wire. *IEEE Spectrum* **2001**.
32. Ersoy, M. S.; Onder, E., Electroless silver coating on glass stitched fabrics for electromagnetic shielding applications. *Textile Research Journal* **2014,** *84* (19), 2103-2114.

33. Ha, M. S.; Kwon, O. Y. K.; Choi, H. S., Improved Electrical Conductivity of CFRP by Conductive Silver Nano-particles Coating for Lightning Strike Protection. In *17th International Conference on Composite Materials*, Edinburgh, 2009.
34. Gagné, M.; Therriault, D., Lightning strike protection of composites. *Progress in Aerospace Sciences* **2014**, 64, 1-16.
35. Zhang, B.; Patlolla, V. R.; Chiao, D.; Kalla, D. K.; Misak, H.; Asmatulu, R., Galvanic corrosion of Al/Cu meshes with carbon fibers and graphene and ITO-based nanocomposite coatings as alternative approaches for lightning strikes. *International Journal of Advanced Manufucturing Technology* **2013**, 67 (5-8), 1317-1323.
36. Kawakami, H.; Feraboli, P., Lightning strike damage resistance and tolerance of scarf-repaired mesh-protected carbon fiber composites. *Composites Part A: Applied Science and Manufacturing* **2011**, 42 (9), 1247-1262.
37. Balanis, C. A., *Antenna Theory: Analysis and Design 4 ed.* John Wiley & Sons: 2015.

CHAPTER 7 GENERAL DISCUSSION

The goal of the thesis is intertwined with the responsibility of the ELE group, which is the identification of the most promising surface material(s) for the purpose of lightning protection of aircraft structures by performing experimental lightning strikes in the laboratory. By delivering on the following, this goal is said to have been accomplished: (i) lightning emulation facilities for LSP testing, (ii) procedure for systematic evaluation of conductive coatings, and (iii) test results and observations. Ultimately, recommendations are made on the conductive coating technologies developed within the scope of the COMP-502 project for further research.

7.1 Lightning emulation facilities and their application to LSP testing

A lightning impulse emulator, capable of producing current waveforms with a peak amplitude of 40 kA conforming to those described in the SAE aerospace recommended practices [38], has been realized. Arc-entry, injection and conduction test modes are available. Provisions made for waveform control enable the testing of different specimens with wide-ranging electrical properties. The functional aspects of the emulator are described in Chapter 4.

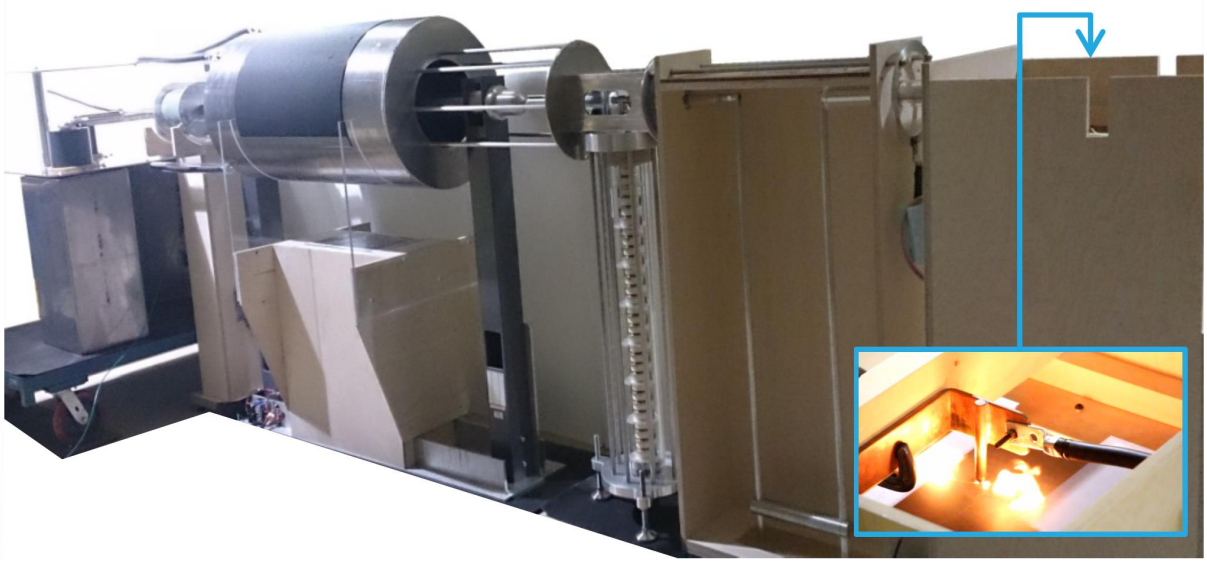

Figure 7.1: The Impulse strike emulator

Figure 7.2 shows the effect of variable inductance on the waveform of the current impulse.

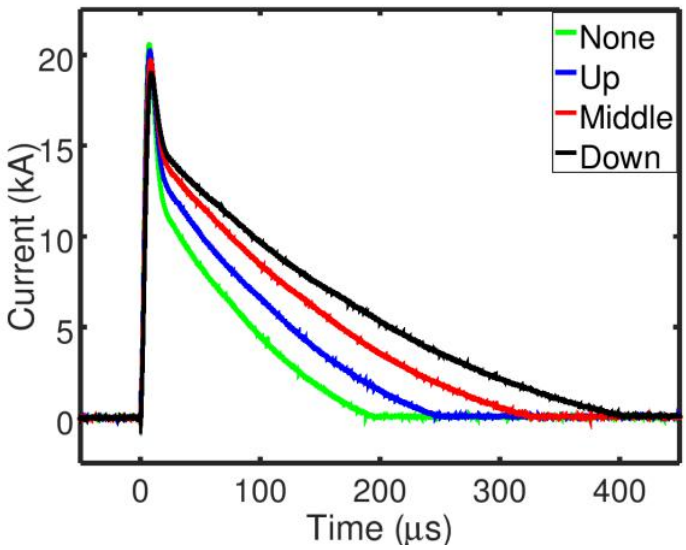

Figure 7.2: Effect of variable inductance on impulse waveform

Commercial power supplies were used for lightning continuous current tests and ambient-current resistance/resistivity measurements. The basic test setup is shown in Figure 7.3

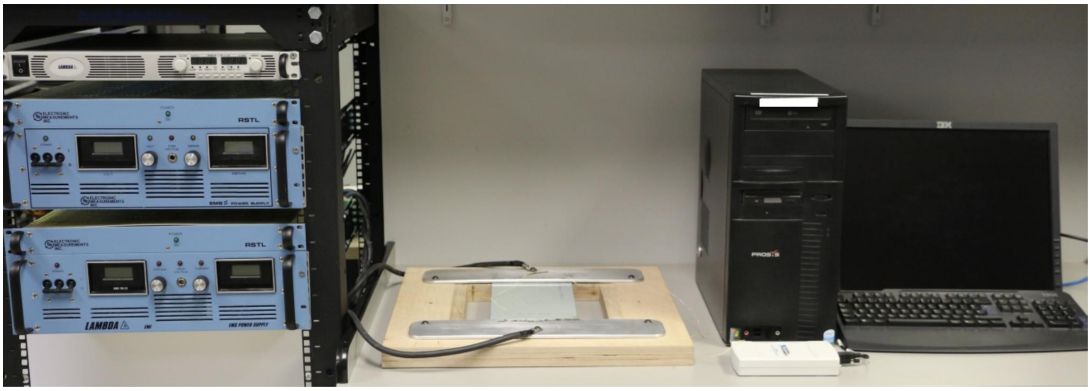

Figure 7.3: Key electrical equipment for continuous current emulation

7.2 Procedure for systematic evaluation of conductive coatings for LSP applications

The flow chart in Figure 7.4 describes a plausible test plan for preliminary evaluation of conductive coatings for LSP when using separate impulse (A or D component) and continuous current (C-component) emulators capable of producing peak current intensities lower than those prescribed in the SAE standards.

The procedure relies on three test modes to subject the coated specimens to the current waveforms. The arc-entry mode is the most severe as it also encompasses the effect of the high-arc temperatures and shock waves resulting from dielectric breakdown of the air-gap. On the other hand the conducted current mode is moderate as the currents are distributed through the entire coating cross-section. Intermediate to these is current injection which is envisaged as a balanced test mode to be realized with a narrow cylindrical positive electrode in contact with specimen center.

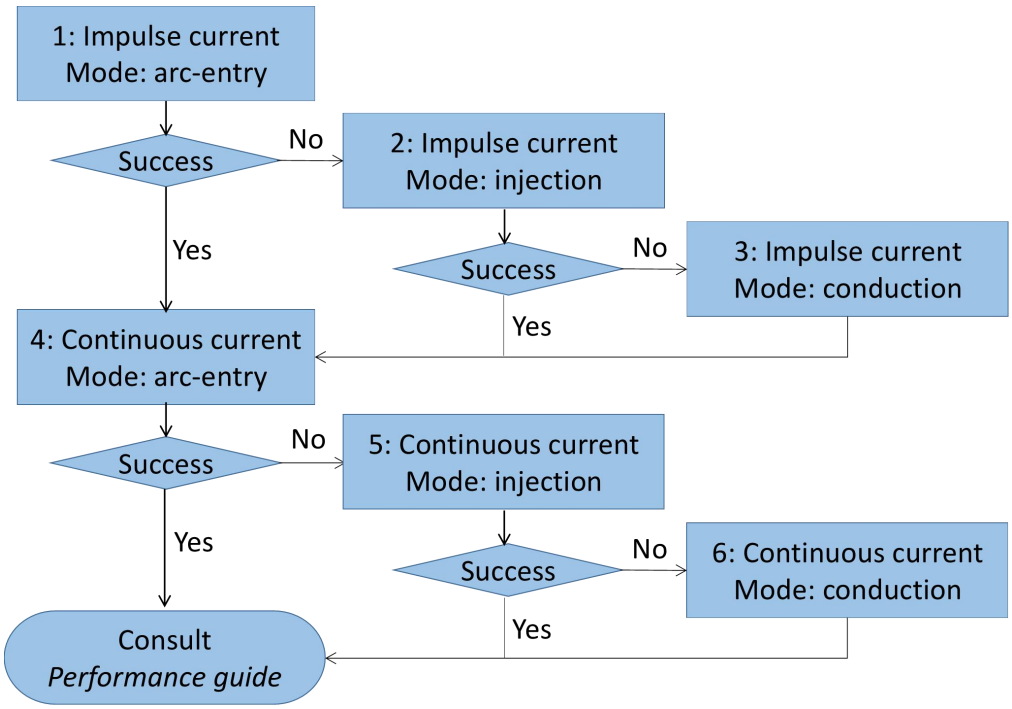

Figure 7.4: Procedure for LSP testing with separate impulse and continuous current emulators

The test procedure is designed to be followed as an iterative loop until the following success criteria are satisfied with the harshest test mode (arc-entry): (i) Composite substrate must not be damaged, and (ii) conductive coating must not be damaged; electrical conductivity must also be maintained. Damage may be assessed via non-destructive and destructive testing.

7.3 Lightning test results and observations

A modified version of this flowchart was employed in Chapter 5 as insufficient number of specimens were available for testing. The lightning impulse and continuous current tests were performed in arc-entry and conduction mode, respectively. Photography and ultrasonic testing

for arc-entry, and real-time electrical measurements and thermography for continuous currents tests were respectively used to study the performance of the coatings. The resistance of the coupon samples and damage suffered by the specimens is quantified in Figure 7.5. The results show that metallic coatings outperformed their hybrid counterparts. Among the different coatings produced within the scope of the project, Cu\Sn specimens suffered the least damage from lightning impulse tests, the tin coating showed better performance against continuous current emulation.

Table 7.1: 'Performance guide' for use in conjunction with procedure for LSP testing

Success with test #	***Next step***
1, 4	Retest (same) specimen to assess re-strike capability*. If success with tests 1 and 4 again, follow A, else follow B. A: Test sufficient (user-determined) number of specimens for confidence (repeatability) and proceed to tests with chopped waveform tests of increased amplitude or complete waveform of standard or decreased amplitude. B: Follow steps below as applicable *Damage accumulation via re-strikes may be used as means to anticipate specimen behavior at higher amplitudes
Others	Review composition, processing, volume and/or manufacturing steps with focus on either or all of shock waves, rapid electromagnetic changes melting effects etc. based on damage characteristics. Prepare new specimen and retest.
None	Review composition, processing, volume and/or manufacturing steps to lower sheet resistance. Prepare new specimen and retest.

During the course of testing certain observations were made that may limit the understanding of the coatings' performance and reliable comparison. The surfacing film has a strong influence on the damage manifestation of tested specimens, and hence a common strategy is necessary for all the specimens for comparison purposes. Manufacturing discrepancies such as incomplete or non-uniform coating observed respectively in Cu\Sn and Al specimens must be addressed.

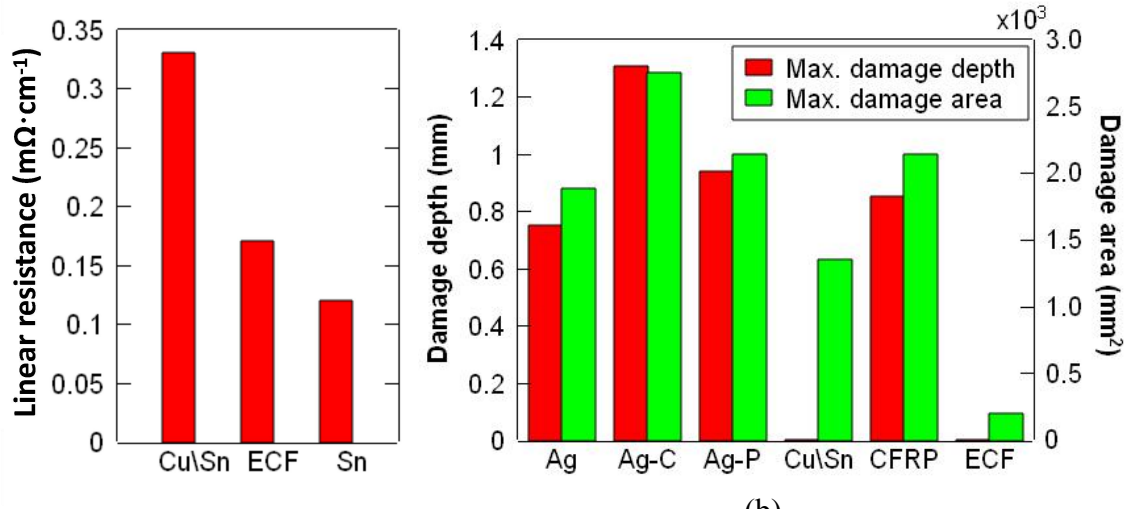

Figure 7.5: (a) Specimen resistances measured during continuous current emulation, and (b) Quantification of damage suffered by test specimens subjected to lightning impulse currents with a peak amplitude of 40 kA

7.4 Performance evaluation and identification of promising conductive coatings

A single, incomplete iteration of lightning strikes was performed on the coated specimens due to constraints on number of specimens available. None of the materials satisfied the success criteria and thus the identification of a single promising material has not been possible. However it may be anticipated that with further iterations, useful coating technologies may be conceived. Thus, the following brief set of recommendations covering materials, dimensional and manufacturing aspects of the coatings are provided for consideration by the materials groups for improvement of coating performance.

The specimens produced within the scope of the COMP-502 project may be divided into two categories:

Silver-based hybrid coatings: Although the hybrid coatings use some smart, ingenious materials designs, it is highly possible that the optimization of processing parameters to achieve satisfactory dispersion and percolation of the conductive fillers was carried out via 4-point probe tests. The limitations of this technique are discussed in Chapter 5. It is recommended to utilize ambient-current tests on larger coupons for this purpose.

Tin-based metallic coatings: These coatings could benefit by increasing the fraction of high-conductivity material. Before going for changes in terms of the coating composition, it is important to lower the resistivity of the present system of particles. Deoxidation of the particles can lead to better cold welding and decrease the net resistance of the coating. Similarly, when higher melting point metals are added, it may be necessary to use dual spray guns or sandwich spray techniques in order to maintain an ambient temperature to allow for physical bonding among the particles. This would be a prerequisite for sintering even at higher temperatures.

Given the presence of two silver-based hybrid materials, specimens of CFRP completely coated in silver were also produced as a reference material. Electroless plating cannot be used to reliably produce thick coatings. In fact, techniques such as this, utilizing wet chemistry on composites structures may not be amicable to the industrial setting of composite aircraft manufacture. Such limitations of the manufacturing techniques must be looked into and alternatives considered. On the other hand, the remaining manufacturing techniques have a good scope to cater to the aerospace sector especially because of their ability to produce coatings over large areas and/or similarity to existing technologies employed by the industry, leading to easy implementation.

CHAPTER 8 CONCLUSION AND RECOMMENDATIONS

Three objectives, tied to the goal of identifying promising conductive coatings developed within the scope of the COMP-502 project, were set up at the commencement of this thesis work. They pertained to building lightning emulation facilities, devising test protocols and applying them to evaluate different conductive coatings for LSP and extend the application of research efforts put into this thesis. These objectives have been achieved and the primary research findings from this work discussed. This helps conclude the COMP-502 project. The following paragraphs present an overview of said objectives and associated recommendations.

Separate lightning impulse and continuous current emulators, capable of producing a peak current of 40 kA and sustained currents of up to 500 A were realized. While the impulse emulator was powered by capacitive storage and the waveform controlled by variable inductance, the continuous current emulator was based on commercial power supplies. Arc-entry (impulse emulator only), current injection and distributed current tests can be realized with the emulators. The waveforms have been shown to conform to the SAE standards. It is possible to upgrade the emulator to incorporate a practical degree of automation: (i) a computer program/application approach to shut-down the capacitor charging operation on reaching an input voltage, subsequent trigger of lightning strike and recording of test waveform, and (ii) motorized variable inductance control. The possibility to trim down the physical length of the structure may be reviewed so as to further improve the performance of the emulator. The continuous current emulator, based on a commercial power supply, is limited to a maximum voltage of 10 V although it can deliver 500 A of current. The limitation in voltage restricts the materials that could be tested. Higher voltage limits could make the emulator more versatile even at the expense of current amplitude.

Various conductive coatings: silver nanoparticles in PEDOT:PSS, silver-coated carbon nanofibers, silver, tin, copper-tin were tested as potential candidates for aircraft LSP, with unprotected CFRP and ECF-protected CFRP as reference materials. Non-destructive testing via ultrasonic inspection, electrical measurements, thermography and photography/videography were employed to study the protection offered by the coatings. While none of the materials withstood the lightning impulse emulation, the metallic coatings performed satisfactorily against lightning

continuous currents. Recommendations provided for improvement of coatings fall into two broad categories. For silver-based hybrid coatings, increased filler volume and improved percolation must be considered. Tin-based metallic coatings would benefit from the incorporation of a larger fraction of high conductivity particles in the coatings. Such a coating may be produced either as a composite or with a multi-layered architecture. Increased coating density may be considered for the silver coating. Two other materials were also studied in the COMP-502 project but not provided for testing. Scale-up challenges with Magnetron-sputtered aluminum coatings may be addressed by optimizing the deposition protocol and/or using larger deposition chambers. One approach to bypass fabrication challenges and promote materials such silver nanorod-functionalized graphene to the test phase is via use of adhesives/binding agents (containing the conducting particles) for applying the coating or having the conducting particles sandwiched between the the composite and an epoxy surfacing film analogous to the strategy employed with silver-coated carbon nanofiber.

Furthermore, in order to reap more benefits from the research efforts, applications, strategies and developments to extend the test equipment, methods and materials were considered. The lightning emulators developed can not only be applied to research of new conducting materials for LSP but also for studies to better understand the performance of existing materials under different simulated scenarios. Such a test campaign was carried out for one of the industrial partners to test a LSP technology under repeated lightning strikes. Various target applications such as testing for EMI shielding and calibration of lightning sensors are listed in the thesis. Multi-functional technologies are the present trend in the scientific world. With a similar line of thought, a strategy was devised to have thermography play the dual roles of a non-destructive technique to study coating behavior against continuous lightning currents as well as a facilitator for examining the flaws associated with the materials, manufacturing methods and test equipment. Lastly, the know-how garnered from the preparation of silver coatings by electroless plating were extended to produce selective-area coatings of desired designs. The said technique was a fusion of extrusion-based printing, hydrophobic masking and electroless plating. Different conductive designs for application in electrical circuits, EMI shielding, sensors and antennae were demonstrated.

It is anticipated that the developed test equipment and methods will find application in the future phases of the project, and recommendations made for improvements of materials will lead to better coatings, and ultimately transform into a practical LSP technology for aircraft, while the philosophy of holistic and sustainable research will guide the co-development many other useful technologies.

REFERENCES

1. Uman, M.A. and V.A. Rakov, The interaction of lightning with airborne vehicles. Progress in Aerospace Sciences, 2003. 39(1): p. 61-81.

2. Rupke, E., Lightning Direct Effects Handbook. 2002, AGATE: Advanced General Aviation Transport Experiments.

3. Zhang, B., et al., Galvanic corrosion of Al/Cu meshes with carbon fibers and graphene and ITO-based nanocomposite coatings as alternative approaches for lightning strikes. The International Journal of Advanced Manufacturing Technology, 2013. 67(5-8): p. 1317-1323.

4. Miracle, D.B. and S.L. Donaldson, ASM Handbook, Volume 21 - Composites. 2001, ASM International.

5. F.A.A., Aviation Maintenance Technician Handbook-Airframe. 2012: Aviation Supplies & Academics, Incorporated.

6. Boeing 787 Dreamliner Specs. Available from: http://www.modernairliners.com/boeing-787-dreamliner/boeing-787-dreamliner-specs/.

7. Gerlach, J.C., V. Mazur, and B.D. Fisher, Lightning strikes to an airplane in a thunderstorm. Journal of Aircraft, 1984. 21(8): p. 607-611.

8. McCormick, D., Global Warming: Soon with 50% More Lightning, in IEEE Spectrum. 2014.

9. Punekar, G.S. and C. Kandasamy, Indirect Effects of Lightning Discharges. Serbian Journal of Electrical Engineering, 2011. 8(3): p. 245-262.

10. Volland, H., Handbook of Atmospheric Electrodynamics. 1995: Taylor & Francis.

11. Uman, A.M., The Lightning Discharge. Dover Books on Physics. 2012, USA: Courier Dover Publications.

12. Wilson, C.T.R., A Theory of Thundercloud Electricity. Proceedings of the Royal Society of London. Series A. Mathematical and Physical Sciences, 1956. 236(1206): p. 297-317.

13. Rakov, V.A. and M.A. Uman, Lightning: Physics and Effects. 2007: Cambridge University Press.

14. Soula, S., Electrical Environment in a Storm Cloud. Aerospace Lab, 2012. Lightning Hazards to Aircraft and Launchers(5): p. 10.

15. Schonland, B. and D. Malan, The distribution of electricity in thunderclouds. Meteorology and Atmospheric Physics, 1950. 3(1): p. 64-69.

16. Uman, M.A., Lightning. 2012: Dover Publications.

17. Wessel-Berg, T., A proposed theory of the phenomenon of ball lightning. Physica D: Nonlinear Phenomena, 2003. 182(3): p. 223-253.

18. Clieford, D.W. and H.W. Kasemir, Triggered Lightning. Electromagnetic Compatibility, IEEE Transactions on, 1982. EMC-24(2): p. 112-122.

19. O'Loughlin, J.B. and S.R. Skinner, General Aviation Lightning Strike Report and Protection Level Study. 2004, National Institute for Aviation Research: USA.

20. Uman, M.A., The Art and Science of Lightning Protection. 2008: Cambridge University Press.

21. Kind, D. and K. Feser, High-voltage Test Techniques. 2001: Newnes.

22. Plumer, J.A. and J.D. Robb, The Direct Effects of Lightning on Aircraft. Electromagnetic Compatibility, IEEE Transactions on, 1982. EMC-24(2): p. 158-172.

23. Carpenter Jr., R.B. and M.N. Drabkin Lightning Strike Protection. 28.

24. SAE ARP5412: Aircraft Lightning Environment and Related Test Waveforms. 1999, SAE International. p. 53.

25. Kutz, M., Handbook of Materials Selection. 2002: Wiley.

26. International, A., Standard Test Method for Dielectric Breakdown Voltage and Dielectric Strength of Solid Electrical Insulating Materials Using Impulse Waves. 2012.

27. Hexcel, Hexforce (R) Reinforcements: Technical Fabrics Handbook. 2010.

28. Textile Products, I. Products. Available from: http://www.textileproducts.com/.

29. Shin, J.-H. and O.-Y. Kwon, AE Monitoring of Lightning-Damaged CRFP Laminates during Compression-After-Impact Test. Journal of Acoustic Emission, 2011. 29: p. 8.

30. Chakravarthi, D.K., et al., Carbon Fiber–Bismaleimide Composites Filled with Nickel-Coated Single-Walled Carbon Nanotubes for Lightning-Strike Protection. Advanced Functional Materials, 2011. 21(13): p. 2527-2533.

31. Wu, C., et al. Study of carbon nanotubes/short carbon fiber nanocomposites for lightning strike protection. in Behavior and Mechanics of Multifunctional Materials and Composites. 2010. SPIE.

32. Shah, T., et al. Carbon Nanostructures for electromagnetic shielding and lightning strike protection applications in aircraft. in Aerospace EMC, 2012 Proceedings ESA Workshop on. 2012.

33. Zhao, W., et al., EMI shielding effectiveness of silver nanoparticle-decorated multi-walled carbon nanotube sheets. International Journal of Smart and Nano Materials, 2010. 1(4): p. 249-260.

34. Inc., M., General Technical Data Sheet for Nickel-coated Carbon Fiber.

35. Cline, J.D.F.L., FL), Lightning diverter strip. 1980, Dayton-Granger, Inc. (Fort Lauderdale, FL): United States.

36. Mahapatra, P., et al., Aviation Weather Surveillance Systems: Advanced Radar and Surface Sensors for Flight Safety and Air Traffic Management. 1999: Institution of Electrical Engineers.

37. Ellis, R.E. and A.J. Mason, The in-service flight testing of some carbon fibre-reinforced plastic components. Composites, 1983. 14(3): p. 233-236.

38. International, S., ARP 5412 Aircraft lightning environment and relative test waveforms. 2005.

39. International, S., ARP5414 Aircraft lightning zoning. 2005.

40. International, S., ARP5416 Aircraft lightning test methods. 2005.

41. Warren, C., et al. Design and implementation of a portable lightning current simulator. in Plasma Science, 2000. ICOPS 2000. IEEE Conference Record - Abstracts. The 27th IEEE International Conference on. 2000.

42. Haryono, T., et al. The Design of A High Amplitude Impulse Current Generator. in High Voltage Engineering and Application, 2008. ICHVE 2008. International Conference on. 2008.

43. Walko, L.C., et al. Full scale lightning generation techniques for aircraft susceptibility evaluations. in Energy Conversion Engineering Conference, 1997. IECEC-97., Proceedings of the 32nd Intersociety. 1997.

44. Meppelink, J. and E.G. Jordan, Complex lightning current simulation in laboratory, in International Conference on Pulsed Power Applications 2001. p. 6.

45. Heidler, F., et al., Parameters of Lightning Current Given in IEC 62305 - Background, Experience and Outlook, in 29th International Conference on Lightning Protection. 2008. p. 22.

46. Rao, P.N.A.P., K.N. Shamanna, and G.R. Nagabhushana. Lightning test facility for light combat aircraft. in Electromagnetic Interference and Compatibility '97. Proceedings of the International Conference on. 1997.

47. Baksht, R., et al. Explosion of thin aluminum foils in air. in Pulsed Power Conference, 2003. Digest of Technical Papers. PPC-2003. 14th IEEE International. 2003.

48. White, R.A., Full-System Tests Using the Sandia Lightning Simulator. 1983, Sandia National Labs: New Mexico. p. 65: 1-17.

49. Madsen, S.F. and K. Bertelsen Mobile impulse current generator for verifying the lightning protection of wind turbines according to IEC 61400-24 (CDV)

50. Zantout, A.E. and O.I. Zhupanska, On the electrical resistance of carbon fiber polymer matrix composites. Composites Part A: Applied Science and Manufacturing, 2010. 41(11): p. 1719-1727.

51. Featherston, C.A., et al., Development of a Methodology to Assess Mechanical Impulse Effects Resulting from Lightning Attachment to Lightweight Aircraft Structures. Applied Mechanics and Materials, 2010. 24-25: p. 6.

52. Hirano, Y., et al., Artificial lightning testing on graphite/epoxy composite laminate. Composites Part A: Applied Science and Manufacturing, 2010. 41(10): p. 1461-1470.

53. Feraboli, P. and H. Kawakami, Damage of Carbon/Epoxy Composite Plates Subjected to Mechanical Impact and Simulated Lightning. Journal of Aircraft, 2010. 47(3): p. 999-1012.

54. Baldacim, S.A., et al. Lightning Effects in Aircraft of the Composite Material. in 17th CBECIMat - Congresso Brasileiro de Engenharia e Ciência dos Materiais. 2006. Brasil.

55. Morgan, A., Additives, Nanocomposites, and Barrier Coatings, in Long-Term Durability of Polymeric Matrix Composites, K.V. Pochiraju, G.P. Tandon, and G.A. Schoeppner, Editors. 2012, Springer US. p. 39-75.

56. Mouritz, A.P., Z. Mathys, and A.G. Gibson, Heat release of polymer composites in fire. Composites Part A: Applied Science and Manufacturing, 2006. 37(7): p. 1040-1054.

57. Gandhi, S., R. Lyon, and L. Speitel, Potential Health Hazards from Burning Aircraft Composites. Journal of Fire Sciences, 1999. 17(1): p. 20-41.

58. Fisher, F.A., J.A. Plumer, and R.A. Perala, Aircraft Lightning Protection Handbook. 1989: Federal Aviation Administration.

59. O'Driscoll, D., et al., Lightning Strike of Perforated Carbon Fiber Epoxy Laminar Flow Panels. Journal of Composites Technology & Research, 2000. 22(2).

60. Kwon, O.Y. and J.H. Shin, Acoustic Emission Monitoring of Lightning-Damaged CFRP Laminates during Compression-after-Impact. Journal of the Korean Society for Nondestructive Testing, 2012. 32(3): p. 7.

61. Mall, S., B.L. Ouper, and J.C. Fielding, Compression Strength Degradation of Nanocomposites after Lightning Strike. Journal of Composite Materials, 2009. 43(24): p. 2987-3001.

62. Feraboli, P. and M. Miller, Damage resistance and tolerance of carbon/epoxy composite coupons subjected to simulated lightning strike. Composites Part A: Applied Science and Manufacturing, 2009. 40(6-7): p. 954-967.

63. Ming-Shing, L., et al. Simulated lightning tests on external fuel tank of aircraft. in Electromagnetic Compatibility, 1994. Symposium Record. Compatibility in the Loop., IEEE International Symposium on. 1994.

64. Research and Innovation, E.C. Lightning Protection for Structures and Systems on Light Aircraft Using Lightweight Composites. 2012; Available from: http://ec.europa.eu/research/transport/projects/items/lightning_en.htm.

65. Huadong, W. and M. Siegel. Correlation of accelerometer and microphone data in the “coin tap test&rdquo. in Instrumentation and Measurement Technology Conference, 1999. IMTC/99. Proceedings of the 16th IEEE. 1999.

66. Kijvev, V.V. and N.A. Orlov. Implementation of artificial intelligence methods in NDT: expert systems approach. in 13th World Conference on Non-Destructive Testing. 1992. Sao Paulo, Brazil: Elsevier Science.

67. Kataoka, S., et al. The development of an expert system for defect identification and its assessment. in 9th International conference on nondestructive evaluation in the nuclear industry. 1988. Tokyo, Japan: American Society for Metals.

68. Ogi, T., et al., A Neural Network Applied to Crack Type Recognition, in Review of Progress in Quantitative Nondestructive Evaluation, D. Thompson and D. Chimenti, Editors. 1990, Springer US. p. 689-696.

69. Gros, X.E., An eddy current approach to the detection of damage caused by low-energy impacts on carbon fibre reinforced materials. Materials & Design, 1995. 16(3): p. 167-173.

70. Hillmann, S., et al., Characterization of wet conductive coatings using eddy current techniques. AIP Conference Proceedings, 2012. 1430(1): p. 441-448.

71. Shin, J.-H. and O.-Y. Kwon, AE Monitoring of Lightning-Damaged CFRP Laminates During Compression-After-Impact Test. J. Acoustic Emission, 2011. 29.

72. Buynak, C.F., T.J. Moran, and S. Donaldson, Characterization of impact damage in composites. SAMPE Journal, 1988. 24(2): p. 4.

73. Gou, J., et al., Carbon nanofiber paper for lightning strike protection of composite materials. Composites Part B: Engineering, 2010. 41(2): p. 192-198.

74. Geng, D.B., H.J. Guo, and S.Q. Zhang, The Effect of Lightning Strikes on Bismaleimide Composites by Dynamic Mechanical Analysis. Advanced Materials Research, 2011. 179-180: p. 6.

75. Chen, X., G. Liu, and H. Wang, The Residual Strength Test And Analysis of Composite Rudder After Lightning Strike, in 18th International Conference on Composite Materials. 2011: Korea.

76. Azamian, P., et al. The high-current carrying capacity of CNT enhanced composites. in The 18th International Conference on Composite Materials. 2011. Korea.